Aerodynamic Loss Modelling in Transonic Turbines

XiuQuan Yang

A Thesis

in

The Department

of

Mechanical and Industrial Engineering

Presented in Partial Fulfilment of the Requirements
for the Degree of Master of Applied Science at
Concordia University
Montreal, Quebec, Canada

April 2003

ABSTRACT

Aerodynamic Loss Modelling in Transonic Turbines

XiuQuan Yang

The aerodynamic design of a turbine stage starts with a mean line aerodynamic calculation that gives the stage main geometric features. A key element in that calculation is the aerodynamic loss system. The AMDCKO (Ainley and Mathieson, Dunham and Came, and Kacker and Okapuu) loss system, after being tested on hundreds of modern axial turbines over a wide design point operating range, was found lacking in its ability to predict reasonably well the aerodynamic turbine efficiency at higher than optimum reaction. Based on a better understanding of the loss mechanisms at high Mach number at blade exit and given a good base of test data, modifications are made to the trailing edge loss, tip-clearance loss and secondary loss models to reflect recent design practices. The modified AMDCKO loss system is validated against the known efficiencies of 46 turbine stages of varied engine applications. It is believed that this new model improves significantly the predictive capability of the mean line design program and provides a better assessment of compressibility effect on the different loss components.

Acknowledgements

I would like to thank my supervisor, Dr. Wahid Ghaly, for his supervision and guidance during the project and for his very constructive remarks on the writing of this thesis.

I would like to thank Pratt & Whitney Canada (P&WC), for their giving me such a privileged opportunity and for their financial support and resources. Many thanks go to all the members of P&WC's Turbine Aero group for their support and help; in particular to the chief of that group, Sami Girgis. Special thanks go to Edward Vlasic, for his technical expertise and guidance in this project.

I would also like to thank our librarians, secretaries, computer lab technicians, and all those who have given me support and help in this undertaking.

The most important acknowledgement goes to my wife Yan Li and my daughter FuYao, for their consistent and unfailing support and help.

Also, I would like to express thanks to my extended family in China, my parents, my brothers, and all my relatives, for their care, understanding, support, and help.

I dedicate this modest work to my great family.

Table of Contents

List of Figures viii

List of Tables xi

Nomenclature xii

1. Introduction 1

2. Review of Axial Turbine Performance Prediction Methods 5

2.1 Classification of Losses and Their Mechanisms 5

2.1.1 Profile Loss 6

2.1.2 Trailing Edge Loss 8

2.1.3 Secondary Loss 8

2.1.4 Annular Loss 11

2.1.5 Tip Clearance Loss 12

2.1.6 Shock Loss 14

2.2 Categories of Loss Prediction Models 18

2.2.1 Correlation and Calculation Methods 18

2.2.2 Overall Stage Method and Loss Component Analysis Methods 18

2.2.3 Design and Off-Design Methods 20

2.2.4 Individual Loss Component Model 20

2.3 Turbine Mean-Line Loss Systems 22

2.4 AM+DC+KO Loss System 23

2.4.1 Structure of Loss System 23

2.4.2 Profile Loss Correlation 24

2.4.3 Secondary Loss Correlation 28

2.4.4 Tip-Clearance (Tip Leakage) Loss Correlation 31

2.4.5 Trailing Edge Loss Correlation 33

2.5 Present Work 36

3. Evaluation of the AMDCKO Loss System 37

3.1 Problem Statement 37

3.2 Performance Prediction Using the AMDCKO Method 38

3.2.1 Effect of Reaction on the loss Component 39

3.2.2 Effect of Reaction on the Aerodynamic and Geometric Parameters 40

3.3 Assessment of the AMDCKO Loss System 44

3.3.1 Trailing Edge Loss 45

3.3.2 Tip-Clearance Loss 47

3.3.3 Secondary Loss 47

4. Modification and Validation of AMDCKO Loss System 49

4.1 Modification of Trailing Edge Loss Correlation 49

4.2 Modification of Tip Clearance Loss Correlation 53

4.3 Modification of Secondary Loss Correlation 55

4.4 Optimum Exit Mach Number and Optimum Delta Mach Number 57

4.5 Validation 61

4.6 Concluding Remarks 61

5. Conclusion, Suggestions, and Future Work 65

5.1 Conclusion 65

5.2 Suggestions and Future Work 66

References 68

Appendices 73

Appendix I: Terminology and Definitions 74

I.1 Blade Section Terminology 74

I.2 Velocity Triangle 76

I.3 Isentropic Efficiency 77

I.4 Loss Coefficient 78

I.5 Reaction 80

Appendix II: Turbine Stage Aerodynamic and Geometric Data 81

Appendix III: Result Curves of Efficiency with Reaction 88

List of Figures

Figure 1.1	Typical structure of a design system for axial flow turbine	2
Figure 2.1	Flow structure in a turbine cascade	5
Figure 2.2	Boundary layer and separation bubble	7
Figure 2.3	Boundary layer and wake at the trailing edge of a turbine blade	8
Figure 2.4	Secondary flow in a turbine blade passage	9
Figure 2.5	Flow over the tip gap for an unshrouded blade	12
Figure 2.6	Visualisation of fluid path lines in the clearance gap of an unshrouded turbine blade	13
Figure 2.7	Flow over a shrouded tip seal	13
Figure 2.8	Trailing edge shock system for a turbine blade, with suction surface coolant ejection	14
Figure 2.9	Schematic diagram of a shock-boundary layer interaction	14
Figure 2.10	Schlieren photographs showing the development of shock waves at exit Mach numbers	16
Figure 2.11	Distribution of Mach number around the blade surface for the blade shown in figure 2.10	17
Figure 2.12	Variation of loss coefficient with exit Mach number	17
Figure 2.13	Classification of turbine performance prediction methods and loss models	21
Figure 2.14	Profile loss coefficient, nozzle blades	24
Figure 2.15	Profile loss coefficient, impulse blades	24
Figure 2.16	Ainley's loading factor Z	29

Figure 2.17	Trailing edge loss coefficient	34
Figure 3.1	Turbine stage efficiency Vs reaction	38
Figure 3.2	Loss component variation with reaction	39
Figure 3.3	Loss component variation with reaction, area charts	40
Figure 3.4	Aerodynamic and geometric parameter variation with reaction	41
Figure 3.5	Vane and blade profiles	42
Figure 3.6	Velocity triangle diagram	43
Figure 3.7	Structure of supersonic trailing edge flow	45
Figure 3.8	Loss Vs Mach number for a turbine cascade	46
Figure 3.9	Variation of the two-dimensional loss components with Mach number for a turbine cascade	46
Figure 3.10	Trailing edge loss Vs Mach number	46
Figure 3.11	Effect of reaction and tip-clearance on efficiency	47
Figure 4.1	Profile loss variation with exit Mach number obtained experimentally by different investigators	50
Figure 4.2	Profile loss comparison between AMDCKO and experimental data	52
Figure 4.3	Correction to trailing edge loss	53
Figure 4.4	Comparison and correction of tip-clearance loss correlation with Roelke data	54
Figure 4.5	Correction to secondary loss	56
Figure 4.6	Effects of trailing edge loss, tip-clearance loss and secondary loss corrections	56

Figure 4.7	Comparison of loss component variation with reaction before and after modification	58
Figure 4.8	Loss component variation with reaction after modification, area charts	59
Figure 4.9	Optimum exit Mach number Vs pressure ratio	60
Figure 4.10	Optimum delta Mach number Vs pressure ratio	60
Figure 4.11	Comparison of predicted optimum efficiencies of 46 turbine stages	63
Figure 4.12	Optimum reaction Vs pressure ratio	63
Figure I.1	Blade section terminology	74
Figure I.2	Axial flow turbine stage and velocity triangles	76
Figure I.3	T-s diagram for a reaction stage	77
Figure III.1	Result curves of efficiency with reaction	89

List of Tables

Table 4.1	Cascade experimental data	50
Table 4.2	Cascade parameters for profile loss experimental data	51
Table 4.3	Results of validation against 46 turbines of 17 engines	62
Table II.1	Aerodynamic and geometric data, T2	82
Table II.2	Aerodynamic and geometric data, T45	84
Table II.3	Aerodynamic and geometric data, T9	86

NOMENCLATURE

A	Annulus Area
B	Constant in AMDCKO Eqs. for Tip-Clearance Loss Coefficient
b_x	Axial Chord
c or C	True Chord
C	Absolute Velocity
C_L	Airfoil Lift Coefficient
c_p	Specific Heat Capacity (at Constant Pressure)
f	Correction Factor
$f_{(AR)}$	Aspect Ratio Function
$f_{(Re)}$	Reynolds Number Correction Factor
h	Blade or Vane Height (Span)
H or h	Enthalpy
ΔH	Enthalpy Drop
i	Incidence
k	Tip Clearance
k'	Equivalent Tip Clearance for Shrouded Blade
K_1, K_2, K_3, K_p, K_s	Correction Factors Defined in Text
M	Mach Number
o	Throat Opening
P	Total Pressure

p	Static Pressure
PR	Pressure Ratio for a Turbine Stage
q	Dynamic Head (P- p)
R	Reaction, Pressure-Based
Rvt	Velocity-Based Reaction at Blade Tip
R (or r)	Radius
Re (Re c)	Reynolds Number Based on True Chord and Exit Gas Conditions
REFAC	Reynolds Number Correction Factor for AMDC Loss System
s	Pitch
Δs	Entropy Increase through a Cascade Blade Row
U	Blade Velocity at Mid Height
V	Relative Velocity for Rotor
W_S	Specific Work for a Turbine Stage
t (or tet)	Trailing Edge Thickness
t_{MAX}	Blade Maximum Thickness
x	Distance along Chord from Trailing Edge
Y	Loss coefficient $\Delta P / q$ where q is (generally) taken at blade exit
Y_T	Total Loss Coefficient for a Blade Row
Y_P	Profile Loss Coefficient
Y_S	Secondary Loss Coefficient
Y_{SHOCK}	Component of Profile Loss Coefficient due to Leading Edge Shock
Y_{TE}	Trailing Edge Loss Coefficient

Y_{TET}	Trailing Edge Loss Multiplier, in AMDC Loss System
Y'_{TET}	Trailing Edge Loss Coefficient in KO Loss System
Y_{TC} or Y_{CL}	Tip Clearance Loss Coefficient
Z	Ainley's Loading Parameter defined by Eq. 2.19
α	Gas Flow Angle for Cascade Blades
α_m	Mean Gas Angle Defined in Equation 2.21
β	Metal (Blade) Angle for Cascade Blades
β	Relative Flow Angle for Rotor Blade Row
δ	Flow Deviation
δ_1^*	Inlet Endwall Boundary Layer Displacement Thickness
ε	Flow Turning (Deflection)
γ	Ratio of Specific Heats
λ	Stagger Angle
λ	An Empirical Function, Fig. 8 of reference [2]
Λ	Enthalpy-Based Reaction
θ	Blade Camber Angle
ρ	Density
ξ	Energy (Enthalpy) Loss Coefficient referred to the Isentropic Velocity
$\Delta\phi^2_{TET}$	Trailing Edge K. E. Loss Coefficient
η	Isentropic Efficiency

η_{tt}	Turbine Efficiency (Total to Total)
η_0	η_{tt} at Zero Tip Clearance
ϕ^2	Kinetic Energy Coefficient
	= (actual gas exit velocity/ideal gas exit velocity)^2
ζ	Energy (Enthalpy) Loss Coefficient
ζ_s	Entropy Loss Coefficient, defined by Eq. 1.15

Subscripts

AR	Aspect Ratio
ex	Exit Condition
H	Hub
in	Inlet Condition
MEAN	Mid Span
N (V)	Nozzle (Vane)
opt	Optimum
p	Pressure Side
R (B)	Rotor (Blade)
Re	Reynolds' Number
ref	Reference
rel	Relative Condition
s	Isentropic Process
s	Suction Side

ss	Static-to-Static
T	Tip
te	Trailing Edge
ts	Total-to-Static
tt	Total-to-Total
u	Circumferential
x	Axial
0	Total
1, 2	Inlet and Exit Conditions for Cascades
1, 2, 3	Turbine Stage Sections (1-Inlet for Nozzle, 2-Exit for Nozzle and Inlet for Rotor, 3-Exit for Rotor)

AMDC	as per Ainley, Mathieson, Dunham, and Came
AMDCKO	as per Ainley, Mathieson, Dunham, Came, Kacker, and Okapuu
DK, RD, DN	Thick, Standard, and Thin Trailing Edge respectively, described in reference [42]
P&WC	Pratt & Whitney Canada

1. Introduction

The design procedure of the turbine component of a gas turbine engine is a very complex engineering operation, involving thermodynamic and aerodynamic design, stress design, and many mechanical and electrical designs etc. The turbine aerodynamic design is a fundamental part in this process. It usually consists of many iterative steps in which the previously assumed or computed values are progressively modified according to the results of more refined flow calculations. A schematic of the design system for an axial flow turbine is presented in Fig. 1.1.

The designs are usually performed by starting from the so-called "mean-line" design (as shown by the dotted line rectangle in Fig. 1.1). This assumes that the thermodynamic processes experienced by the working fluid can be represented by blade mid-span quantities, e.g., velocity triangles. In this procedure, conservation of mass, momentum and energy laws as well as other thermodynamic, aerodynamic, and gas dynamic relations etc. are applied at mid-span. However, in order to predict accurately the turbine aerodynamic efficiency, and then to optimize the various design parameters such as gaspath shape, number of blades etc, and designers have to specify losses in the various parts of the stage. This is the crux in mean-line design. Despite the development in computational methods to simulate the flow field in turbine blade passages, the estimation of stage performance is still a matter of considerable difficulty. This is because flows through a turbine blade passage are many and varied, hence extremely complex (as will be discussed in the next chapter). Well-developed Computational Fluid Dynamics

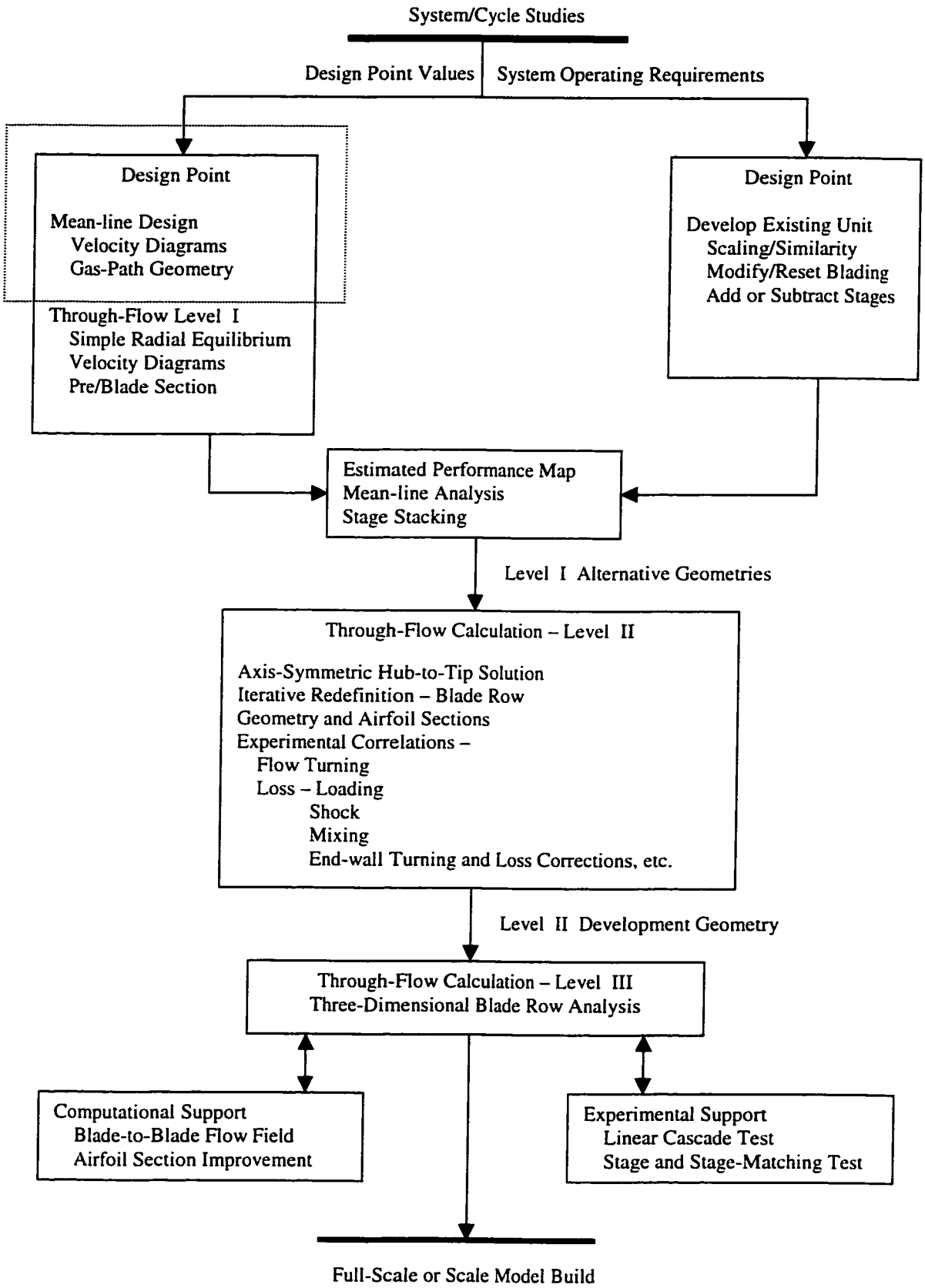

Fig. 1.1 Typical structure of a design system for axial flow turbine.

(CFD) methods, which provide a solution of the full 3-D Navier-Stokes equations, are able to predict with confidence the relative performance of different blades geometry, however, they can not be used as design tools, i.e., they can not predict the geometry that would accomplish a given task. Moreover, they cannot provide quantitative estimates of the relative effects of the different loss components. To solve this problem, designers still rely on the accumulated data, obtained from experimental testing. Since many efforts have been expended in testing turbine blades, from these measurements it has been possible to relate the blade performance to its geometry and to the flow parameters such as Mach and Reynolds numbers. This began as an empirical process, and then progressed to include a series of loss models. The excellence of theses models is ultimately judged by their ability to predict accurately the turbine aerodynamic efficiency. This requires that the loss models reflect the latest knowledge and design practices, and therefore, should be constantly reviewed and updated as new test data or methods become available.

In this work, efforts are firstly made to review and assess the analytical and experimental studies on losses and loss models for axial gas turbines. Then, after investigating, analyzing and comparing a number of turbine performance prediction methods, it was found that the AMDCKO (Ainley & Mathieson [1], Dunham & Came [15], and Kacker & Okapuu [20]) mean line loss system is one of the more widely adopted loss systems in axial turbine design. An evaluation of the AMDCKO loss system showed that it is lacking in its ability to predict reasonably well the aerodynamic efficiency when it is applied to a stage of higher than optimum reaction, which corresponds to transonic blade exit Mach number. The physical implication of high Mach number flow on each of the loss components was then evaluated, and the AMDCKO loss system was modified to

reflect these implications. The modified AMDCKO loss system was then validated against experimental data and its ability to predict the aerodynamic efficiency in a large modern turbine design range was demonstrated for 46 turbine stages where the design point expected optimum reaction and efficiency were predicted to within 1% error.

2. Review of Axial Turbine Performance Prediction Methods

In this chapter, the previous work related to loss prediction methods for axial turbines will be thoroughly reviewed, special attention will be given to the AMDCKO loss system, and the outline of the current work will also be given.

2.1 Classification of Losses and Their Mechanisms

The flow processes that occur in turbine stages are always very complicated. They are always three dimensional, viscous, and unsteady. They may be incompressible or compressible, with subsonic, transonic, and supersonic regimes that may be present simultaneously in different regions. In addition to the primary flow through the blade passages, there are secondary flows which move fluid across the passages under the action of centrifugal and Coriolis forces; blade loading effects causing incidence and deviation; leakage between the moving blade tips and the stationary shroud; boundary layers and wakes shed by blades; and, for transonic and supersonic blades, shock waves

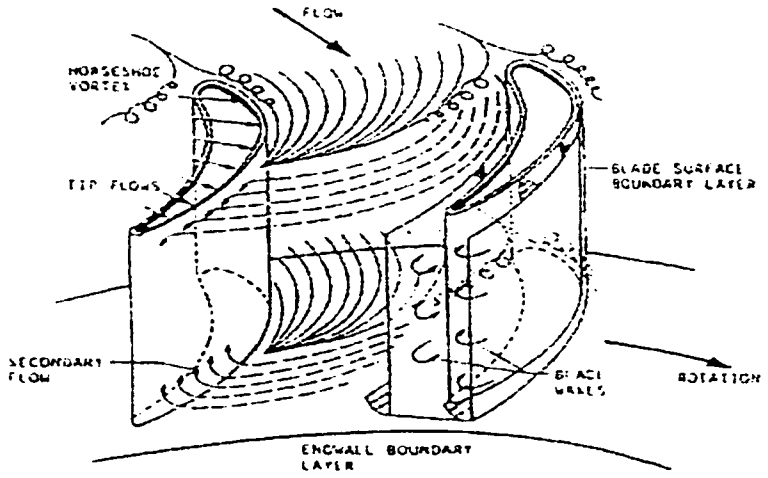

Fig. 2.1 Flow structure in a turbine cascade[40].

and shock-boundary layer interaction in the passage and at the trailing edges. Another class of effects is unsteady, generated mainly by the interaction of adjacent blade rows. A schematic representation of the flow field through an axial turbine blade passage is shown in Fig. 2.1.

In the open literature, from the 1940's, when the explosion of research on aircraft engines started, to the present, classification of losses was never treated in an identical manner. Different ways to divide the various loss-generating mechanisms have been proposed. These differences arise largely because the various effects are interrelated, and the choice of categories often depends on the experimental data available rather than pure theoretical grounds. A common classification is as follows:

Profile loss

Trailing edge loss

Secondary loss

Annulus loss

Tip clearance loss

Shock loss

2.1.1 Profile Loss

Profile loss is the loss arising from the growth of the blade surface boundary layers, and the attendant surface friction and blockage effects. It includes separation loss under adverse condition of extreme angles of incidence or high inlet Mach number. The blade boundary layers assumed are well away from the end walls and the flow is often thought

two-dimensional so that the loss may be based on two-dimensional cascade tests or boundary layer calculations.

When the flow on a turbine blade surface is laminar, transitional flows often occur. An understanding of transition and its effect on aerodynamics is important in turbines. Laminar flows with laminar separation bubbles are often encountered in the turbine with accelerating flows. Turbine flow with a laminar separation bubble is illustrated in Fig.2.2. The laminar flow separates because of the local adverse pressure gradient. This separation bubble will reattach, and this may in turn initiate the transition to turbulent flow downstream.

The profile loss from this type of boundary layer buildup is due to a loss of stagnation pressure, which in turn is caused by a loss of momentum in the viscous fluid. The mechanical energy is dissipated into heat and entropy is increased. The magnitude of the profile loss mainly depends on the blade shape, the pressure gradient to which the flow is subjected, roughness of the blade surfaces, and Reynolds number. The difficulty of predicting transition of the boundary layer remains a major limitation to accurate prediction of this loss.

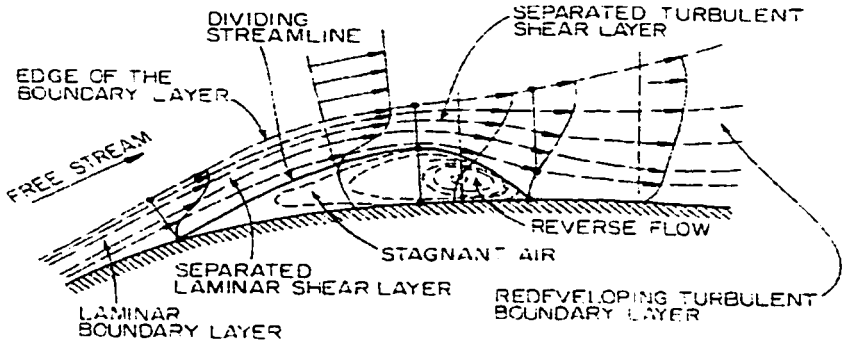

Fig. 2.2 Boundary layer and separation bubble [22].

2.1.2 Trailing Edge Loss

The trailing edge loss is caused by a finite thickness of the trailing edge and the wake shed from it. Fig. 2.3 shows boundary layers and wake at the trailing edge of a turbine blade. Because of the finite trailing edge thickness, the flow separates at two points on both sides of the trailing edge. Between these points there is a region, called the base region, where the pressure is significantly lower than that of the freestream. Downstream of the trailing edge, the region merges with the boundary layers shed from the two sides of the blade to form a single wake, which then gradually dissipates through shear with the freestream. Therefore, the trailing edge loss basically is due to the low base pressure acting on the trailing edge, the mixing out and dissipation in the base region and wake, and the combined blockage of the trailing edge and the boundary layers.

2.1.3 Secondary Loss

Secondary loss is caused by the distortion of the fluid due to viscous effects during the turning process in the blade passage including end-wall boundary layers (the boundary layers on the hub and shroud surfaces of the blade rows).

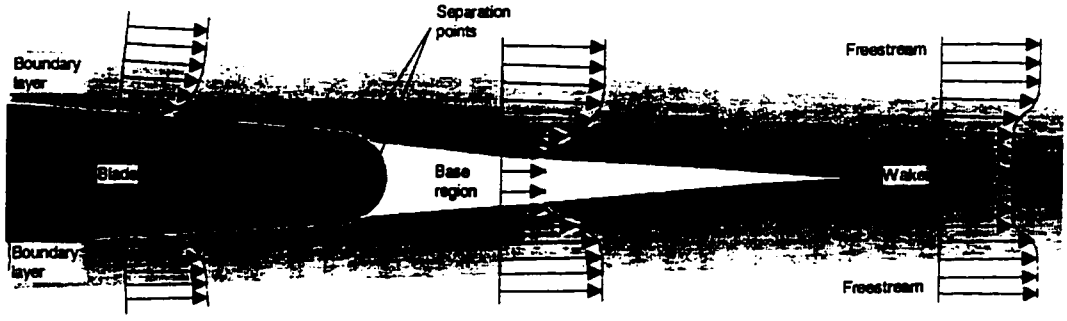

Fig. 2.3 Boundary layers and wake at the trailing edge of a turbine blade [18].

Secondary flow is a generic term for cross-stream velocities, which in a turbine have two principal sources. The first is the turning of the fluid through the blade passage. This sets up a pressure gradient across the passage normal to the streamlines of a magnitude given by the Euler-n equation:

$$\frac{\partial p}{\partial n} = \rho \frac{C^2}{r} \tag{2.1}$$

Where r is the local radius of curvature in the normal n direction.

Since the velocity C is larger in the middle of the passage than in the boundary layers on the end walls, the local radius of curvature must also be larger to equalize the pressure gradients, and the difference in turning in the center of the passage and near the end walls causes the twin circulations, termed the *passage vortex*, to form (Fig. 2.4a). Additionally, the inlet end wall boundary layer itself rolls up into a vortex at the leading edge of the blade, which then spreads around the two sides of the blade (Fig. 2.4b). This is often

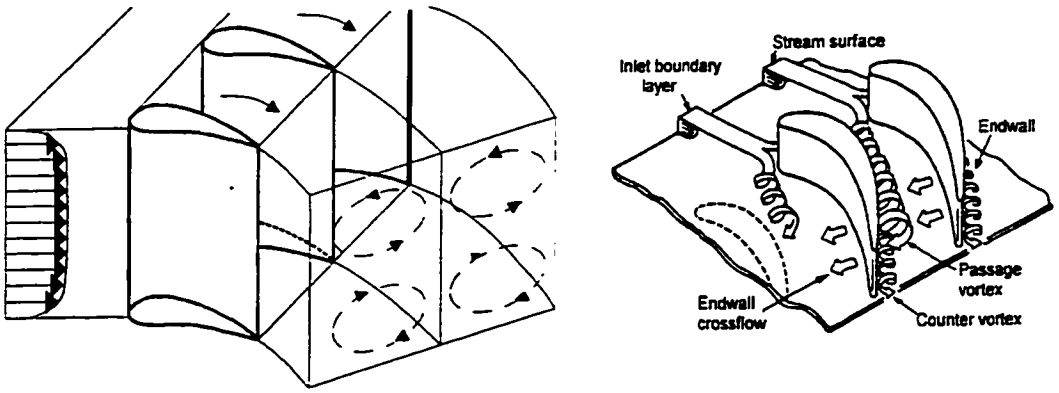

(a) Passage vortex

(b) Horseshoe vortex after Langston [23]

Fig. 2.4 Secondary flow in a turbine blade passage.

known as the *horseshoe vortex*, after its shape in plan view. On the pressure surface of the blade, this amplifies the passage vortex, but on the suction surface it rotates in the opposite direction to the passage vortex, and is thus constrained to a *counter vortex* in the suction surface corner. Secondary flows are an important source of loss, not so much because of their own kinetic energies, which are usually small, but because they redistribute low momentum boundary layer fluid throughout the passage and produce subsequent mixing losses, which may be appreciable. Also, they create flow distortion for subsequent stages which in turn suffer further losses.

Sieverding [33] gives a full discussion of the secondary flows in turbines. Dunham [14] reviews a large number of proposed secondary flow loss correlations. Most secondary loss models include some or all of the following influence factors.

- *Blade shape (turning).* The secondary flow, and the passage vortex in particular, is a function of the turning, or deflection, in the passage, and hence of the shape of the blade. The secondary flow deflects the fluid on the end wall much more in the case of the high-turning blade. Most correlations include the turning angle, or a combination of inlet and exit angle. Often it is assumed that the influence is similar in nature to that of blade shape on profile loss.

- *Pitch-chord ratio.* The pitch-chord ratio (or solidity, chord-pitch ratio) affects the loading of the blade, and it might be expected that this influences the secondary flow in a similar way to the blade shape. However, its influence appears to be limited, and Sieverding [33] speculates that the change in magnitude of blade loading with pitch-chord ratio may be partly offset by a change in the loading pattern.

- *Aspect ratio (height/chord).* Secondary flow losses occur mainly near the end walls of the blade passage and would be expected to have less influence in blades of large aspect ratio. Horlock [17] showed a strong influence for aspect ratios below about 3, but little influence above this value. Some early correlations were based on aspect ratio alone, but this is a considerable oversimplification.

- *Mach number.* Analytically, the secondary loss appears to decrease with increasing Mach number. High exit Mach numbers imply a rapid acceleration to the throat and a strongly favorable streamwise pressure gradient, which tends to limit the growth of the boundary layers in which the secondary flows originate. At transonic and supersonic conditions, the influence of Mach number on secondary loss is very uncertain.

- *Inlet boundary layer thickness.* There appears to be a critical displacement thickness of the inlet boundary layer, above which secondary flow loss is not further influenced. Dunham and Came [15] considered that most turbines were above this critical value.

2.1.4 Annulus Loss

Annulus loss is due to the surface friction of the hub and shroud boundary layers between blade rows. It is closely related to the secondary flow and sometimes is incorporated into secondary loss category. Denton and Cumpsty [11] show that more entropy is generated in those regions of the end wall which are exposed to a high velocity relative to the wall. Between stages this velocity is generally small, and the loss is unlikely to be great. Between the stator and rotor, however, the velocity is high, and this gap should be kept small to reduce the annulus loss.

2.1.5 Tip Clearance Loss

Tip clearance loss is due to the leakage of flow through the gap between the rotor blade tip and the shroud. This leakage causes turbulence, a pressure drop and interferes with the mainstream flow and the outer wall boundary layer. The detailed loss mechanisms depend on blade tip geometry and on whether the blades are shrouded or unshrouded.

The leakage flow over unshrouded blades has been much more intensively studied than that over shrouded blades. The flow over the tip gap for an unshrouded blade is sketched in Fig. 2.5 (a. thick blade, b. thin blade). The flow entering the tip gap from the pressure side of the blade separates from the blade tip and contracts to a jet, with a contraction coefficient of about 0.6. If the blade thickness is more than about four times the tip gap (Fig. 2.5a), as is usually the case for turbines, the jet mixes out above the blade tip with a resultant increase in static pressure and in entropy. The leakage of fluid and its subsequent mixing also affect the mean exit angle of flow from the blade. As the leakage flow is ejected from the tip gap into the blade passage, it rolls up into a vortex which can be seen in Fig. 2.6. This vortex interacts with the secondary flow passage vortex to form a region of complex flow and further loss generation.

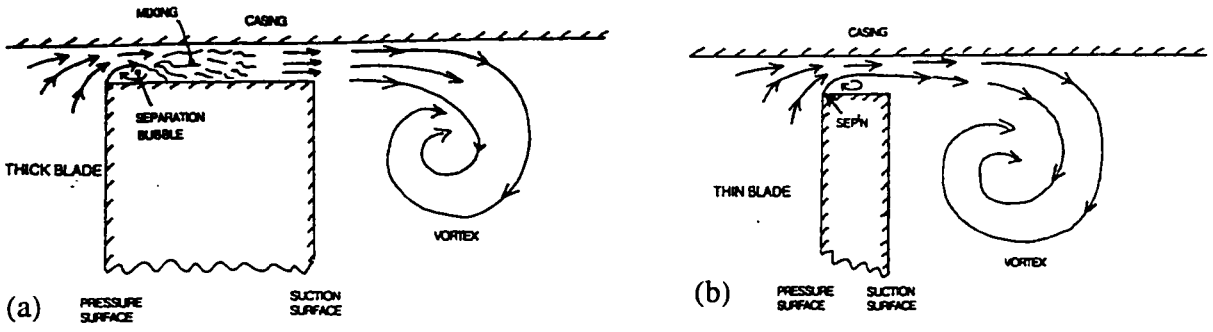

Fig. 2.5 Flow over the tip gap for an unshrouded blade [10].

The flow over the shrouded turbine blade with a single tip seal is illustrated in Fig. 2.7. The leakage flow contracts to a jet as it passes through the seal and the jet mixes out firstly in the clearance space. Then the leakage flow must be re-injected into the main flow where the difference in both the meridional velocity and the swirl velocity of the two flows will generate further mixing. Generally, for both shrouded and unshrouded blades, entropy (or loss) creation due to tip leakage flows is associated with the mixing processes that take place between the leakage flow and the mainstream. In case of unshrouded blades, this interaction is much stronger.

There are two important influencing factors to tip clearance losses: tip clearance height and the blade loading. Most turbines show a linear decrease in efficiency with increasing clearance gap size, although this line would not pass through the origin, and therefore the relation is presumably nonlinear at very small gaps (less than about 1% chord)--- see, for example, Bindon [4]. The rate of decrease varies considerably with the degree of reaction. The degree of reaction influences the pressure difference across the gap. For zero reaction, or impulse blades, the change in static pressure through the rotor is ideally

Fig. 2.6 Visualization of fluid path lines in the clearance gap of an unshrouded turbine blade [4].

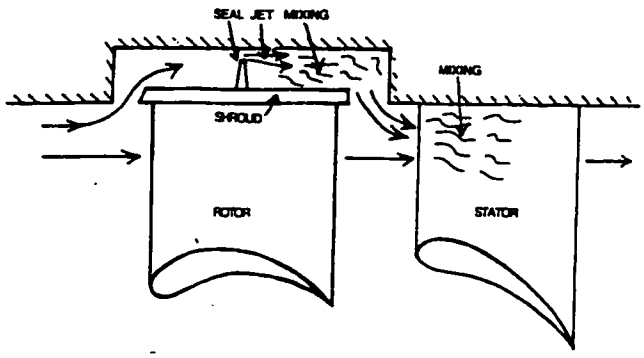

Fig. 2.7 Flow over a shrouded tip seal [10].

zero, and in reality small, so that the pressure difference between suction and pressure surfaces, and hence across the gap, is also small. The leakage flow is therefore smaller than it would be for a comparable reaction turbine, which has a much larger pressure change and pressure difference across the blade.

2.1.6 Shock Loss

Shock loss is due to the formation of shock waves within, or at the trailing edge of, blade rows. The shocks within the blade passage are usually oblique so that $\Delta p / p$ is small and they generate little direct loss. The most serious consequence of transonic flow in turbines is the shock system at the trailing edge, as shown in Fig. 2.8. The low base pressure formed immediately behind the trailing edge can generate a large trailing edge loss. The flow expands around the trailing edge to this low pressure and is then recompressed by a strong shock wave at the point where the suction and pressure side

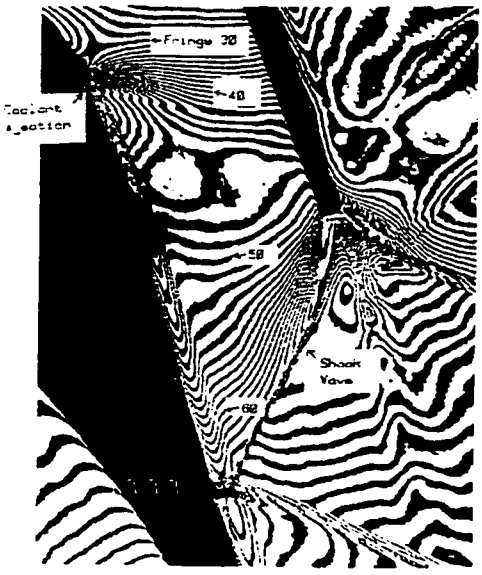

Fig. 2.8 Trailing edge shock system for a turbine blade, with suction surface coolant ejection [10].

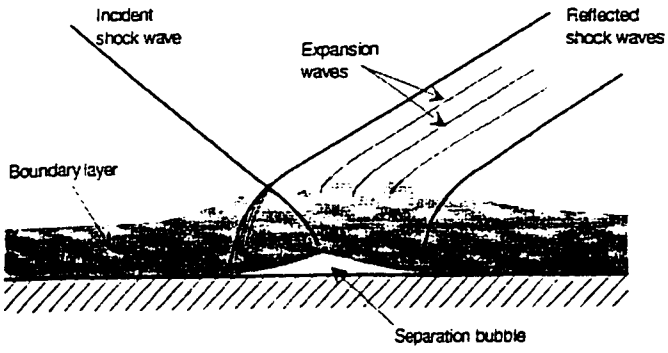

Fig. 2.9 Schematic diagram of a shock-boundary layer interaction, [18].

flows meet. The entropy generation comes from the intense viscous dissipation at the edges of the separated region immediately behind the trailing edge and from the strong shock formed in the vicinity of this region. For cooled turbine blades with thick trailing edges this may be the largest single source of loss in the machine.

Another mechanism of increased trailing edge loss under transonic condition is the shock - boundary layer interaction. The principal mechanisms of such shock-boundary layer interactions are introduced in the textbook by Japikse [18], and Fig. 2.9 shows the basic effects. The incident shock wave is a sudden recompression, so that the boundary layer is locally subject to a strong pressure gradient increasing in the flow direction. Such a pressure gradient tends to decelerate, stagnate, and ultimately separate the boundary layer. This pressure field cannot travel upstream in a supersonic flow and so cannot influence the mainstream upstream of the shock. Deep within the boundary layer close to the wall the flow is subsonic, however, and the pressure field can travel upstream here and cause the boundary layer to separate some small distance before the shock impinges. Depending on the flow velocity upstream and downstream of the shock, the state of the boundary layer (whether it is laminar or turbulent, and if laminar, it will be turbulent after the separation bubble formed by the shock), and the local curvature of the blade, the boundary layer may reattach downstream of the shock or it may separate entirely into a large, stagnant region with a significant increase in profile loss. Two reflected shocks from the surface are formed at the points where the flow separates and reattaches, and close observation will often reveal weak expansion waves between them.

Figure 2.10 shows the development of shock waves and shock-boundary layer interaction for a turbine blade row at different exit Mach numbers. Figure 2.11 shows the

corresponding distribution of Mach number around the blade surface. From these figures we can see that at an exit Mach number just below unity a near-normal shock stands across the passage (Fig. 2.10a). The blade surface Mach number distribution shows decelerations corresponding to this shock ($x/c \approx 0.6$) and the shock wave position at the trailing edge ($x/c \approx 0.98$). As the exit Mach number increases, the shock waves become more oblique, and close inspection of Figs. 2.10b and 2.10c shows that the boundary layer on the blade suction surface separates from that surface at the point where the shock wave impinges and then reattaches. At the highest Mach number (Fig. 2.10d), the

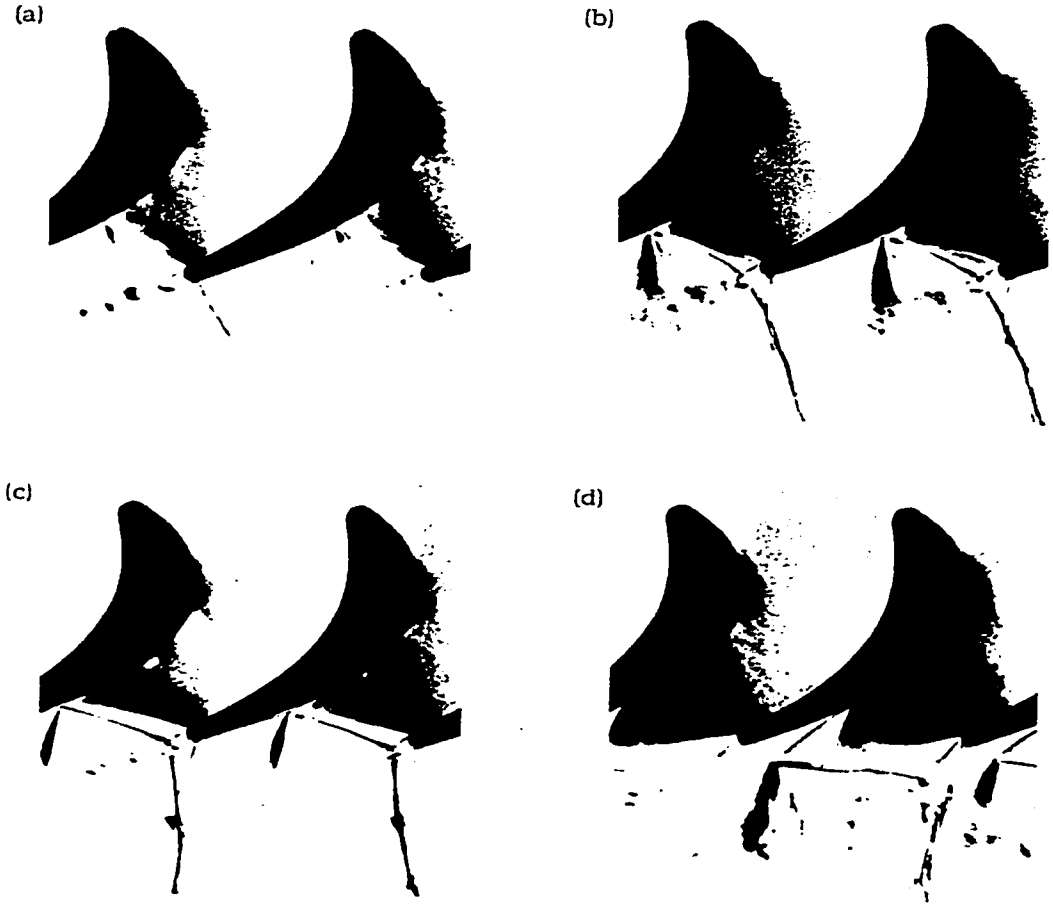

Fig. 2.10 Schlieren photographs showing the development of shock waves at exit Mach numbers: (a) 0.67, (b) 0.89, (c) 1.05, and (d) 1.33 [18].

separation no longer reattaches but extends beyond the trailing edge, forming a large, low-momentum shear layer. In this area of the blade surface, Figure 2.11 shows a region of constant Mach number from $x/c \approx 0.7$ onwards, indicative of a separated region of low static pressure.

The effect of the shock waves and the shock wave-boundary layer interactions on the stage performance can be seen clearly in Fig. 2.12, in which the measured loss is plotted against exit Mach number for the same turbine blade as shown in Fig. 2.10. The loss is very nearly constant until past the critical Mach number (the critical Mach number is the Mach number at the exit at which the velocity at the throat of the blade becomes sonic---in this example, about 0.87). Once separation occurs, the thickening of the suction surface boundary layer at this point gives rise to a large increase in loss, and because of the unsteadiness of the separation itself, the measured loss can vary widely even under nominally equilibrium conditions.

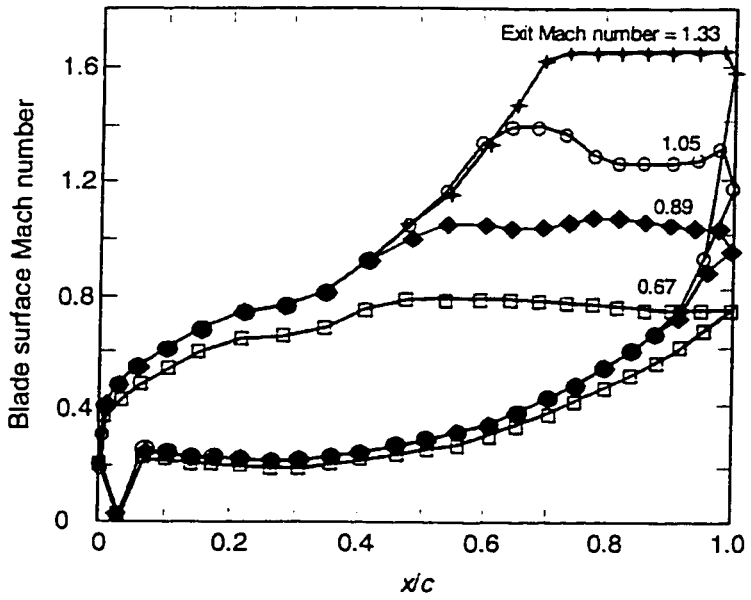

Fig. 2.11 Distribution of Mach number around the blade surface for the blade shown in Fig. 2.10 [18].

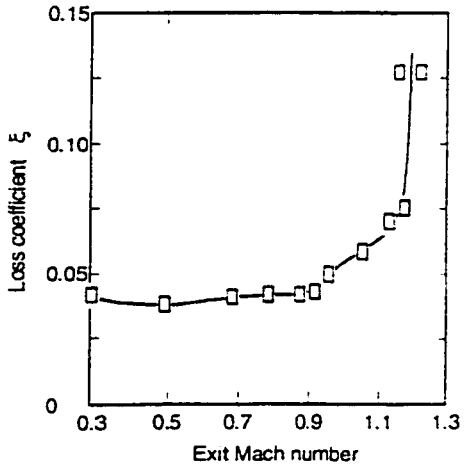

Fig. 2.12 Variation of loss coefficient with exit Mach number [18].

2.2 Categories of Loss Prediction Methods

2.2.1 Correlation and Calculation Methods

Surveys on various loss prediction methods were reported by many authors. As classified by Denton [9], there are two types of loss prediction methods referred to as correlation and calculation methods. The former is concerned with the method that predicts losses using simple blade geometry and flow condition as parameters. This method is often used in the initial stages of turbine design (and is referred to as preliminary mean-line design) to obtain optimum stage geometry. It also has been used for parametric studies of turbine performance due to changes in geometry and flow conditions. On the other hand, the calculation method refers to the detailed velocity distribution and boundary layer growth calculations. This method may be used for the blade profile optimization or in the CFD-based computer codes for the simulation of 3-D viscous compressible flow and other complex phenomena in actual turbine engines. Such a method, however, requires the knowledge of blade surface coordinates, and also must solve the problems of boundary layer transition, shock-boundary layer interaction and flow separation for which much progress is yet to be made for a complete understanding of the phenomena. However, calculation methods do not provide an insight as to how a particular design variable affects the performance.

2.2.2 Overall Stage Method and Loss Component Analysis Method

Another way of classifying the turbine performance prediction methods is proposed by Sieverding [32]. He divided all the methods into two major categories. The first category groups together the so-called *overall stage performance methods*. The use of these methods generally does not require any details of the blading, and the complex flow

patterns in the turbine are deliberately ignored. These methods are in general derived from overall performance measurements of a number of turbines with similar characteristics e.g., same range of reaction, same aspect ratio, or same family of blade profiles. The most widely known of this method includes Smith's [26] and Soderberg's [13] correlations. These methods are usually used in the initial design phase to obtain quick selection of the turbine design parameters and estimates of efficiency. However, the optimization of a turbine for a given duty requires a deep understanding of the flow, and only very refined performance prediction methods, that take into account details of the blading and of the meridional flow channel, can be of real help. This is done, to a certain extent by the second category of performance estimation methods called *loss component analysis methods*. These methods evaluate the total losses through the individual loss components each of which is influenced by more or less a large number of geometric and aerodynamic parameters. This requires defining clearly the important influence parameters and making certain that the influence of each parameter can be studied separately. Generally, such systematic variation of the various influence parameters can only be done on simplified models. There exist, however, limitations to the degree of simplification beyond which the loss model becomes irrelavant. A constant effort has therefore to be made to simulate the real flow conditions as closely as possible. The degree of the differences remaining, between the real turbine flow and the model flow, determines whether the model test results can be applied to the turbine without any corrections or whether the model predictions indicate only the correct tendencies while the absolute loss level needs more detailed correction factors.

2.2.3 Design and Off-Design Methods

Turbine performance prediction methods are also divided into design point and off-design point ones. Operating at the design point condition usually means that the blade metal angle at the airfoil leading edge equals the inlet flow angle, i.e., the incidence is zero. It can also imply an incidence equal to minimum loss operation. Turbine aerodynamic losses at design point operation are usually at a minimum. Off-design performance prediction methods are used to evaluate turbine performance at conditions such as starting, idle, and variable power or speed. At these off-design conditions, the inlet flow velocity vectors are mismatched with the leading edge angle of the blades causing additional losses, commonly referred to as incidence losses. The methods for predicting off-design performance in turbines are usually based on empirical correlations because of the difficulty in calculating analytically the more complicated flows at off-design conditions.

2.2.4 Individual Loss Component Model

There are many experimental and/or analytical studies found in the literature, on specific categories of flows in turbines such as secondary flow, tip-clearance flow etc. Several of these studies detail the loss mechanism and propose a loss model that can be used for further prediction. Examples of these models can be seen in Fig. 2.13.

In summary, Fig. 2.13 shows the classification of the performance prediction methods and loss models for axial turbine blades and some examples in each category.

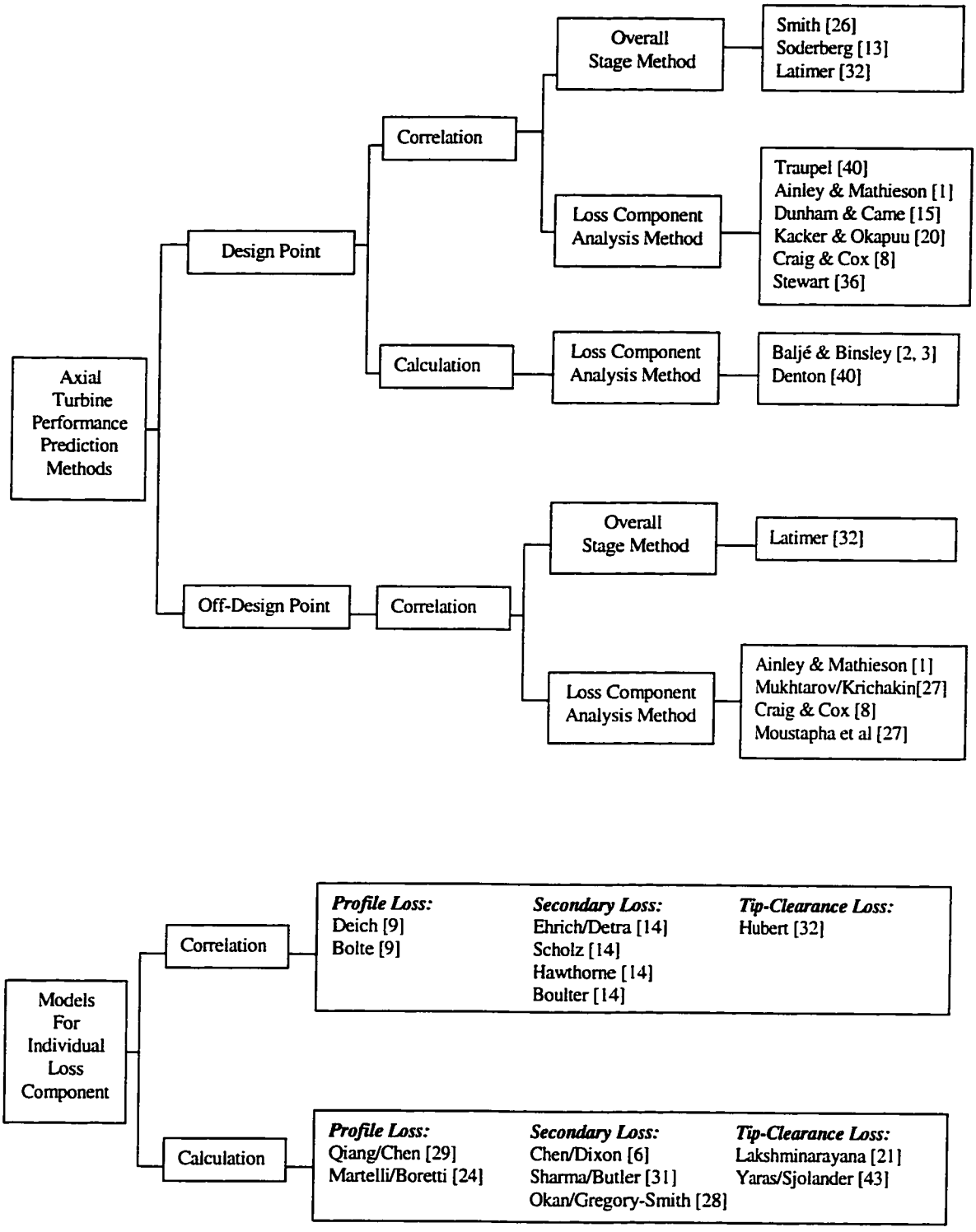

Fig. 2.13 Classification of turbine performance prediction methods and individual loss models

2.3 Turbine Mean-line Loss Systems

Since the objective of this thesis is to improve on the loss system used in predicting mean-line aerodynamic design performance, the focus is on the design point correlation methods that predict total airfoil loss for the blades (corresponding to the loss component analysis methods categorized by Sieverding [32]). Over the past 50 years, a number of such turbine mean-line loss systems have been described in the open literature, Traupel [40], Craig and Cox [8], and Stewart [36], however the best known and most widely used of these is that due to Ainley and Mathieson [1] (abbreviated as AM in the following). The AM system is a complete system in that it includes correlations for all loss components, for both design and off-design conditions. Their original scheme and correlations have been modified several times to suit other families of turbine stage designs, or as more comprehensive experimental test data became available. Notable modifications were made by Dunham and Came [15] (abbreviated as DC in the following) and Kacker and Okapuu [20] (abbreviated as KO in the following), so that this is now referred to herein as the AMDCKO scheme. DC's modification reflected the improved understanding of some aspects of the flow, most importantly the secondary flow. KO restructured the loss system and introduced the compressibility effects and shock losses into the calculation of profile and secondary loss coefficients. Detailed introduction and comparison of the AM+DC+KO loss correlations will be made in Section 2.4.

Similar to AM's scheme, Craig and Cox's correlations [8] were developed for the design of steam turbines but were acclaimed by workers in the gas-turbine as well as the steam-turbine industry. Later, data confirming and extending their method were published by

the Institution of Mechanical Engineers in extensive discussions of the Craig and Cox approach. Wilson [41] reviewed some of these data and thought they appear to agree well with the method by KO.

It is also worth mentioning that in Wei's [40] studies, loss prediction models by AM, DC, KO, Craig and Cox, and Moustapha and Kacker [27] predict turbine performance trends of his experimental results. These models were used in the simulation of mean-line performances on five different turbine stages. These stages reflect varied geometrical parameters, varied reactions and untwisted and free vortex bladings, work at different flow conditions, in subsonic and supersonic flow, and with and without cooling. These loss models were also used in the analysis of the optimum pitch/chord ratio, and it was found that there is no significant difference among them when they are employed to obtain the optimum pitch/chord ratio in the turbine optimization process.

2.4 AM+DC+KO Loss System

2.4.1 Structure of Loss System

In the AMDCKO system, the total pressure loss in a cascade of blades, expressed in terms of cascade exit dynamic pressure, consists of profile, secondary, trailing edge and tip leakage losses as in AMDC, but the overall structure is somewhat different.

AM: $$Y_T = (Y_P + Y_S + Y_{TC})Y_{TET} \tag{2.2}$$

DC: $$Y_T = [(Y_P + Y_S)REFAC + Y_{TC}]Y_{TET} \tag{2.3}$$

KO: $$Y_T = Y_p f_{(\mathrm{Re})} + Y_s + Y'_{TET} + Y_{TC} \tag{2.4}$$

Where Y_{TET} in Eqs 2.2 and 2.3 is a multiplier, not a loss coefficient.

In Eq 2.4, the blade Reynolds number is taken to affect the profile loss coefficient only, and the trailing edge loss coefficient is separated from the other loss terms. This would appear to be a more logical arrangement, since it is difficult to justify a connection between trailing edge losses and tip clearance losses, for example.

2.4.2 Profile Loss

AM: This model is based on cascade tests as well as on losses derived from overall tests on a variety of turbine stages. The data refer to blade profiles designed prior to 1950, i.e., either blade profiles with contours composed of circular arcs and straight lines or blades which make use of the British blade profile series with circular or parabolic camber lines. The maximum blade thickness varies between t_{MAX}/c = 0.15 to 0.25. The correlation is based on a series of graphs of total pressure losses versus s/c for nozzle ($\beta_1 = 0$) and impulse ($\beta_1 = \alpha_2$) blades (Figs. 2.14 and 2.15). For these plots, the incidence i =0, t_{MAX}/C=0.2, $R_e = 2\times10^5$, M<0.6.

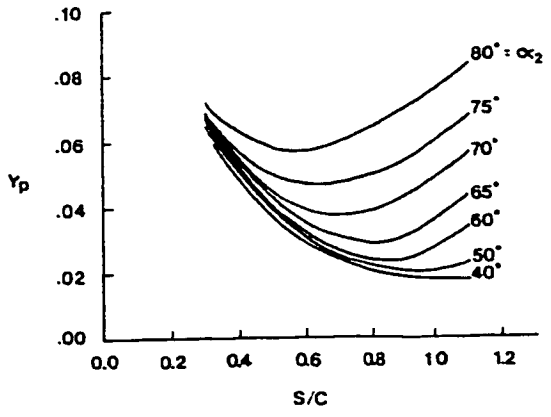

Fig. 2.14 Profile loss coefficient for $\beta_1 = 0$, $t_{MAX}/c = 0.2$ after Ainley and Mathieson [1].

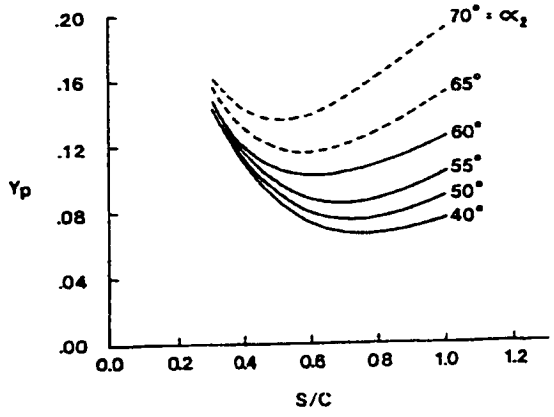

Fig. 2.15 Profile loss coefficient for, $\beta_1 = \alpha_2$, $t_{MAX}/c = 0.2$ after Ainley and Mathieson [1].

For other combinations of angles, the losses are calculated as

$$Y_P = \left\{ Y_{P(\beta_1=0)} + \left(\frac{\beta_1}{\alpha_2} \right)^2 \left[Y_{P(\beta_1=\alpha_2)} - Y_{P(\beta_1=0)} \right] \right\} \left(\frac{t_{MAX}/c}{0.2} \right)^{\frac{\beta_1}{\alpha_2}} \tag{2.5}$$

There is no Reynolds number correction to profile loss, but a Reynolds number correction to overall efficiency was recommended for $R_e < 2\times10^5$

$$(1-\eta_{corrected}) = (1-\eta) \left(\frac{R_{e.mean}}{2\times10^5} \right)^{-0.2} \tag{2.6}$$

DC: The DC model handles profile losses thusly:

- Mach number correction:

$$Y_p = Y_{p.AM} \left[1 + 60(M_2 - 1)^2 \right] \quad \text{for } M_2 > 1 \tag{2.7}$$

this is referred to by KO as *supersonic drag rise.*

- Reynolds Number correction:

$$Y_p = Y_{p.AM} \left(\frac{R_e}{2\times10^5} \right)^{-0.2} \tag{2.8}$$

KO: The KO model makes the following changes for profile loss:

$$Y_{P.AMDC} = \left\{ Y_{P(\beta_1=0)} + \left| \frac{\beta_1}{\alpha_2} \right| \left(\frac{\beta_1}{\alpha_2} \right) \left[Y_{P(\beta_1=\alpha_2)} - Y_{P(\beta_1=0)} \right] \right\} \left(\frac{t_{MAX}/c}{0.2} \right)^{\frac{\beta_1}{\alpha_2}} \tag{2.9}$$

Term $\left| \frac{\beta_1}{\alpha_2} \right|$ allows for negative gas inlet angle.

- Mach number correction:

$$Y_p = 0.914\left(\frac{2}{3}Y_{p.AMDC}K_p + Y_{SHOCK}\right) \tag{2.10}$$

where $K_p = 1 - K_2(1 - K_1)$ (2.11)

$$K_1 = 1 - 1.25(M_2 - 0.2),\ M_2 > 0.2 \tag{2.12}$$

$$K_2 = (M_1 / M_2)^2 \tag{2.13}$$

$$\left(\frac{\Delta P}{q_2}\right)_{SHOCK} \equiv Y_{SHOCK} = \left(\frac{\Delta p}{q_1}\right)_{SHOCK}\left(\frac{p_1}{p_2}\right)\cdot\frac{1-\left(1+\frac{\gamma-1}{2}M_1^{\,2}\right)^{\frac{\gamma}{\gamma-1}}}{1-\left(1+\frac{\gamma-1}{2}M_2^{\,2}\right)^{\frac{\gamma}{\gamma-1}}} \tag{2.14}$$

$$\left(\frac{\Delta P}{q_1}\right)_{SHOCK} = \left(\frac{R_H}{R_T}\right)\left(\frac{\Delta p}{q_1}\right)_H \tag{2.15}$$

$$\left(\frac{\Delta P}{q_1}\right)_H = 0.75(M_{1.H} - 0.4)^{1.75} \tag{2.16}$$

We can see that $Y_{shock} = f(M_{1,hub}, R_H/R_T, P_1/P_2, \gamma, M_1, M_2)$

Reynolds number correction:

$$\left.\begin{aligned} f_{(\mathrm{Re})} &= \left(\frac{\mathrm{Re}\,c}{2\times10^5}\right)^{-0.4} \quad \text{for} \quad \mathrm{Re}\,c \le 2\times10^5 \\ &= 1.0 \quad \text{for} \quad 2\times10^5 < \mathrm{Re}\,c < 10^6 \\ &= \left(\frac{\mathrm{Re}\,c}{10^6}\right)^{-0.2} \quad \text{for} \quad \mathrm{Re}\,c > 10^6 \end{aligned}\right\} \tag{2.17}$$

In summary, in the AMDCKO system, AM developed the profile loss model which depends on the pitch/chord ratio, inlet and outlet flow angles, blade maximum thickness and trailing edge thickness. This model was modified by DC with adding the terms related to Mach number and Reynolds number. KO developed finally this model by restructuring it and adding a Mach number correction factor which is mainly a function of the inlet and outlet Mach numbers.

Traupel's [40] and Craig and Cox's [8] correlations are also presented by using a series of graphs. Traupel correlated his profile loss with blade inlet and outlet angles, pitch, roughness, trailing edge thickness, Mach and Reynolds numbers, while Craig and Cox correlated with the inlet and outlet flow angles, ratio of pitch to camber line length, pitch to blade back radius ratio, contraction ratio of blade channel, trailing edge thickness, Mach and Reynolds numbers.

Comparing these different models, it can be seen that blade inlet and outlet angles have been taken into account in all models, blade surface roughness was only considered in the Traupel model, and the blade maximum thickness was only used by AMDCKO. Craig and Cox [8] used the geometrical parameters of the pitch to camber line length ratio in place of pitch to chord ratio and the contraction ratio of blade channel, which were not applied in the other models. The use of pitch to camber ratio has the advantage of being closely related to the boundary layer development, but it is more difficult to handle than the pitch to chord ratio.

2.4.3 Secondary Loss

AM: Ainley and Mathieson gave the secondary loss coefficient based on the blade loading or deflection.

$$Y_S = \lambda \cdot Z \tag{2.18}$$

where

$$\lambda = f\left(\frac{A_2^2 / A_1^2}{1 + D_H / D_T}\right) \tag{2.19}$$

$$Z = \left(\frac{C_l}{s/c}\right)^2 \cdot \frac{\cos^2 \alpha_2}{\cos^3 \alpha_m} \tag{2.20}$$

$$\frac{C_L}{s/c} = 2(\tan\alpha_1 + \tan\alpha_2)\cos\alpha_m \tag{2.21}$$

$$\alpha_m = \tan^{-1}\left[\frac{1}{2}(\tan\alpha_1 - \tan\alpha_2)\right] \tag{2.22}$$

Z is called Ainley's loading factor, which depends on inlet and outlet flow angles α_1 and α_2 only. The function $Z = f(\alpha_1, \alpha_2)$ is shown in Fig. 2.16.

DC: DC modified Ainley's basic equation as follow:

$$Y_S = \frac{c}{h} \cdot Z \cdot \frac{\cos\alpha_2}{\cos\beta_1} \cdot f\left(\frac{\delta_1^*}{c}\right) \tag{2.23}$$

Where $f\left(\frac{\delta_1^*}{c}\right)$ represents inlet end-wall boundary layer effect.

$f\left(\frac{\delta_1^*}{c}\right) = 0.0334$ is a constant, which implies that δ_1^*/c in turbines assumes a value for which losses asymptote to a max fixed value.

- Reynolds number correction:

$$Y_{S.corrected} = Y_S\left(\frac{R_e}{2\times10^5}\right)^{-0.2} \tag{2.24}$$

- No Mach number correction

KO: KO modified DC's correlation by proposing a new aspect ratio correction factor in place of DC's simple aspect ratio factor.

$$Y_{S.AMDC} = 0.0334 f_{(AR)}\left(\frac{\cos\alpha_2}{\cos\beta_1}\right)\left(\frac{C_L}{s/c}\right)^2 \frac{\cos^2\alpha_2}{\cos^3\alpha_m} \tag{2.25}$$

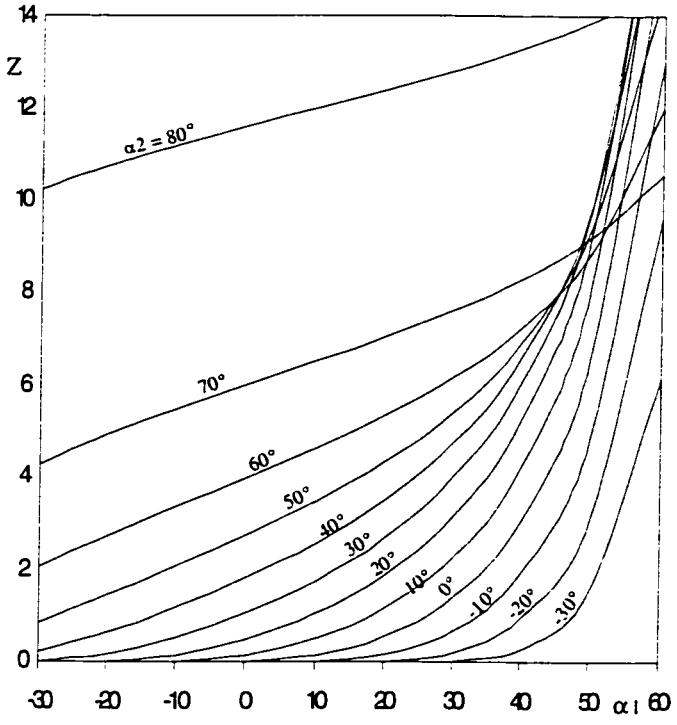

Fig. 2.16 Ainley's loading factor Z

- Aspect ratio modification

$$\left.\begin{aligned} f_{(AR)} &= \frac{1-0.25\sqrt{2-h/c}}{h/c} \quad \text{for } h/c \le 2 \\ &= \frac{1}{h/c} \quad \text{for } h/c > 2 \end{aligned}\right\} \tag{2.26}$$

- Mach number correction:

$$Y_S = 1.2 Y_{S,AMDC} K_s \tag{2.27}$$

$$K_s = 1 - K_3(1 - K_p) \tag{2.28}$$

$$K_3 = \left(\frac{1}{h/bx}\right)^2 \tag{2.29}$$

this is similar to the correction for the profile loss.

- No Reynolds number correction

KO stated that there is little evidence in the literature that secondary loss is affected by Reynolds number.

In summary, AM calculated the secondary loss with a loading factor that is a function of inlet and outlet flow angles only. From the review of new secondary loss data, DC modified this model by adding a dependence on aspect ratio and upstream boundary layer, which is simplified as a constant. KO developed the DC model by modifying the aspect ratio term and adding a Mach number correction factor, which is a function of the inlet and outlet Mach numbers. In this system, the secondary losses were assumed to be proportional to the strength of the secondary vortex. The derivation of the relation between the secondary vorticity and the secondary loss coefficient was given by

Lakshminarayana [22]. In such calculations, the secondary loss coefficient is a function of flow angles which implies the velocity triangles will significantly affect the losses.

Traupel [40] and Craig and Cox [8] established their secondary loss models using more parameters. Traupel structured the secondary loss as a function of blade pitch to span ratio, blade pitch to chord ratio, profile loss, inlet and outlet flow angles, and the ratio of inlet and outlet flow velocity, which implies that the correlation does account for compressibility effects. Craig and Cox model calculates the secondary loss as a product of basic secondary loss and two factors: a Reynolds number factor and a aspect ratio factor. The basic secondary loss was correlated with blade pitch/chord ratio, ratio of inlet and outlet flow velocities and the lift parameter, which is a function of the inlet blade angle and outlet flow angle.

Comparing these two groups of loss models, we can see that the pitch to chord ratio has not been taken into account in the AMDCKO loss model, while the influence of the upstream flow boundary layer on the secondary loss is not considered in the Traupel and Craig and Cox models. Unlike the Traupel model, there is not direct relationship between the profile and secondary losses in the Craig and Cox model as well as in the AMDCKO scheme.

2.4.4 Tip Clearance (Tip Leakage) Loss

AM: Similar to secondary loss correlation, tip clearance loss coefficient is a function of blade loading and the ratio of tip clearance to the blade height.

$$Y_k = B \cdot \frac{k}{h} \cdot Z \tag{2.30}$$

Where B = 0.5/0.25 for unshrouded/shrouded blades

DC: In this model, tip-clearance loss is handled thusly:

$$Y_k = B \cdot \frac{c}{h} \cdot \left(\frac{k}{c}\right)^{0.78} \cdot Z \tag{2.31}$$

Where B = 0.47/0.37 for unshrouded/shrouded blades.

And, for multiple seals

$$k = (geometrical\ k) \times (number\ of\ seals)^{-0.42}$$

KO: In this model, the following segregation in loss is made

For unshrouded blades:

$$\frac{\Delta\eta}{\eta} = 0.93 \frac{k}{h\cos\alpha_2} \cdot \frac{R_T}{R_{Meun}} \tag{2.32}$$

Then Y_{TC} is computed from $\Delta\eta$ by iteration method.

For a shrouded blade, the KO model is the same as the DC model given in Eq. 2.31.

In summary, the AMDCKO tip leakage loss models are generally based on simulating the tip leakage vortex and determining its induced drag on the blade assuming inviscid and incompressible flows. It was firstly done by AM to adapt the model for secondary loss calculation with influence of tip clearance. The loss becomes a function of the flow inlet and outlet angles and the ratio of tip clearance to blade height (see Eq. 2.30). Then DC modified this model in the light of some later cascade data, which suggested a non-linear variation of tip leakage losses with the ratio of tip clearance to blade height (see Eq. 2.31). KO kept using the DC model for shrouded blades but modified the structure of the model for unshrouded blades according to their new test data (see Eq. 2.32).

Traupel [40] developed a model for calculating the tip clearance loss for shrouded blades as a function of the velocity ratio and the ratio of leakage jet to the main flow through the passage. In this model, flow angles are not considered, which implies that the part of loss caused by the different directions of the leakage and the main flow is neglected. The model for calculating tip leakage loss for unshrouded blades given by Traupel assumes a linear variation of the cascade efficiency with tip clearance. This model is based on turbine test results and is similar to the tip leakage loss model given by KO (Eq.2.32).

Craig and Cox [8] thought the AM model for unshrouded blades is reasonable, provided that the axial velocity ratio remains approximately constant, and that the relative velocities are well below sonic value. They expressed the tip leakage losses for shrouded blades as an efficiency deduction caused by the tip leakage loss, which is a function of the leakage coefficient, the ratio of clearance area to throat area, and the efficiency when the clearance is zero. The leakage coefficient is mainly a function of the gap inlet and outlet velocity ratio, which is also related to the static pressure drop through the blade row. This model is based on turbine test results.

2.4.5 Trailing Edge Loss

AM: AM's consideration on trailing edge loss is reflected by the total loss coefficient equation,

$$Y_T = (Y_P + Y_S + Y_{TC})Y_{TET} \tag{2.33}$$

where Y_{TET} is a multiplier, not a loss coefficient.

DC: This model made the following rearrangement and addition:

$$Y_T = [(Y_p + Y_s)REFAC + Y_{TC}]Y_{TET} \tag{2.34}$$

DC did not modify the AM trailing edge loss correlation.

KO: This model made a significant rearrangement as follows:

$$Y_T = Y_p f_{(Re)} + Y_s + Y'_{TET} + Y_{TC} \tag{2.35}$$

The trailing edge loss coefficient Y'_{TET} is separated from the other loss terms. Y'_{TET} is calculated the same way as for profile loss coefficient: curves of trailing edge loss (energy) coefficient are given versus the ratio of trailing edge thickness to throat opening (te/o) for nozzle ($\alpha_1 = 0$) and impulse blading ($\beta_1 = \alpha_2$). These curves are shown in Fig. 2.17. For blades other than the two basic types, trailing edge losses are interpolated by

$$\Delta\phi^2_{TET} = \Delta\phi^2_{TET(\beta_1=0)} + \left|\frac{\beta_1}{\alpha_2}\right|\left(\frac{\beta_1}{\alpha_2}\right)\left[\Delta\phi^2_{TET(\beta_1=\alpha_2)} - \Delta\phi^2_{TET(\beta_1=0)}\right] \tag{2.36}$$

The conversion equation from $\Delta\phi^2_{TET}$ to Y'_{TET} is given by Eq. I.13.

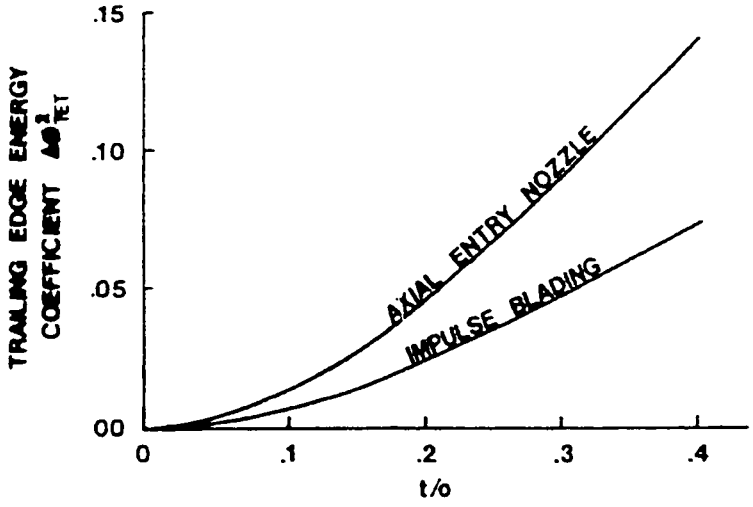

Fig. 2.17 Trailing edge loss (energy) coefficient correlated against te/o [20].

In summary, AM and DC considered the effect of trailing-edge thickness on blade loss in the same fashion. They concluded that there is a marked reduction in efficiency as a result of increasing trailing-edge thickness on either nozzle or rotor blades. However, they did not calculate a separate trailing-edge loss but multiplied the total loss coefficient by a trailing edge loss factor to account for the effect of trailing-edge thickness on blade loss. The multiplier is a function of trailing-edge thickness to pitch ratio. KO changed the way to correlate the trailing-edge loss and separated the trailing-edge loss coefficient from the other loss terms. They thought this is a more logical arrangement because it is difficult to justify a connection between trailing-edge losses and tip clearance losses, for example. For the nozzle blades ($\alpha_1 = 0$) and impulse blades ($\beta_1 = \alpha_2$), KO's trailing-edge loss coefficient is only a function of the ratio of trailing-edge thickness to the throat distance of the blade passage. For blades other than these two types, flow inlet and outlet angles are also taken into account.

Traupel [40] treated the trailing edge loss as a part of the profile loss, and correlated it as a function of the trailing edge thickness, outlet flow angle, basic profile loss, Reynolds and Mach number corrections. Craig and Cox [8] also grouped the trailing edge loss into the profile loss and correlated it by using flow outlet angle and the ratio of trailing edge thickness to pitch.

2.5 Present Work

This work is about the study of the loss models used in aerodynamic mean-line design to predict the turbine aerodynamic efficiency and optimize the gas-path. The AMDCKO loss system is believed to be one of the best known and most completely documented and therefore was chosen as a base model. However, this model fails to predict the qualitative

and quantitative behavior of the loss versus reaction at high values of reaction (which correspond to high subsonic to transonic exit Mach numbers), therefore, special emphasis is put in this work on the effect of high Mach number on the different types of losses. The AMDCKO model is first assessed for the available P&WC test data for 46 turbine stages that cover the full operation range, and each loss component is evaluated and analyzed. The literature is also explored for the most recent and relevant work on loss models for axial turbines. The physical implication of high Mach number flow on the loss components provided a qualitative assessment of trends in loss components and the most recent available data was then used to the components of loss in the AMDCKO model to reflect the physical implication of high Mach number flow, and the modifications are assessed with the P&WC available results for the 46 turbine stages. A discussion of each type of loss and the rational in modifying it are also given. The results obtained with the modified model demonstrate the ability and the robustness of the new model to predict the turbine stage efficiency to within $\pm 1\%$.

3. Evaluation of AMDCKO Loss System

3.1 Problem Statement

The AMDCKO system is one of the most widely used axial turbine performance prediction methods, and it is claimed that it is able to predict the efficiencies of a wide range of axial turbines of conventional stage loading to within ±1.5% [20]. Basically, the loss correlations in AMDCKO system are based on low subsonic cascade tests and do not account for high subsonic and transonic Mach number effects. This was adequate for low stage loading where the turbine stage is operating at lower Mach number. However, the modern trend in gas turbine design is to choose higher and higher stage loading to increase specific work (currently $\Delta H/U^2$ and C_x/U are chosen close to 2.5 and 1.0 [39,7]). This results in turbine stages that are very often designed to operate in the transonic range. Hence when used to predict the efficiency of transonic flow stage, the existing AMDCKO loss system appears not to be accurate and even not applicable when the Mach number is further increased. Studies on the relation between stage efficiency and reaction show that AMDCKO system predicts that stage efficiency increases almost continuously with increasing reaction values from 20% to 70%. However, experimental data for different types of engine stages shows that there is an optimum reaction beyond which the efficiency decreases (efficiency penalty due to non-optimum reaction) [38]. It is believed that the optimum reaction is a function of turbine stage pressure ratio. Based on these data, an expected stage efficiency versus reaction curve can be generated and the comparison between this curve and a curve generated by AMDCKO for a typical engine stage is shown in Fig. 3.1. It is observed that, below the optimum reaction value, the

AMDCKO method and experimental data show similar trends, however beyond the point of optimum reaction, they are significantly different.

3.2 Performance Prediction Using the AMDCKO Method

In order to know why AMDCKO performance prediction method may not correctly predict turbine aerodynamic performance in the higher reaction range and to find ways to improve it, a detailed analysis of the AMDCKO correlations must be made. This analysis will highlight the variation of individual loss components with reaction, as well as the changes in aerodynamic and geometric parameters with reaction. Therefore, several turbine stages are investigated using the AMDCKO method and the results are summarised in the following sections. It should be noted that except for reaction, all other input design parameters were kept unchanged. A list of the turbine stages that were tested are discussed in detail in Chapter 4 and are listed in Table 4.3.

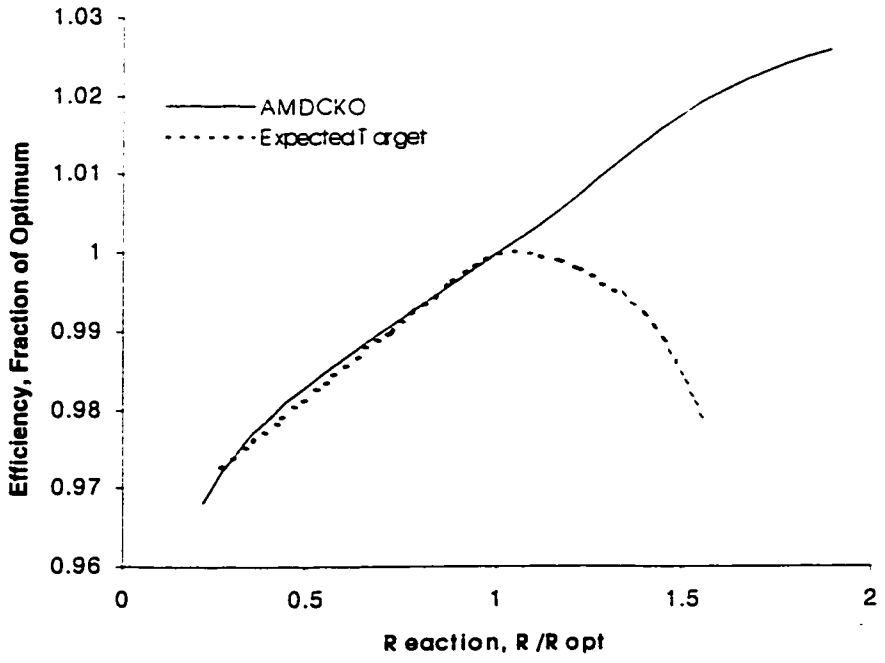

Fig. 3.1 Turbine stage efficiency Vs reaction, T45.

3.2.1 Effect of Reaction on the Loss Component

In the first instance, individual loss component variations with reaction are investigated on different turbine stages. Figures 3.2 and 3.3 show the results of two different stages, from which we can observe the following:

- Compared with vane losses, the blade losses are larger and more sensitive to reaction.
- For nozzle vanes, both profile losses and secondary losses are almost constant, while the trailing edge losses decrease slightly with reaction. However, for blades, both profile losses and secondary losses decrease significantly (compared with vanes), tip clearance losses decrease slightly, while trailing edge losses increase slightly with increasing reaction.
- The secondary flow losses are about half of the total losses while the other half is

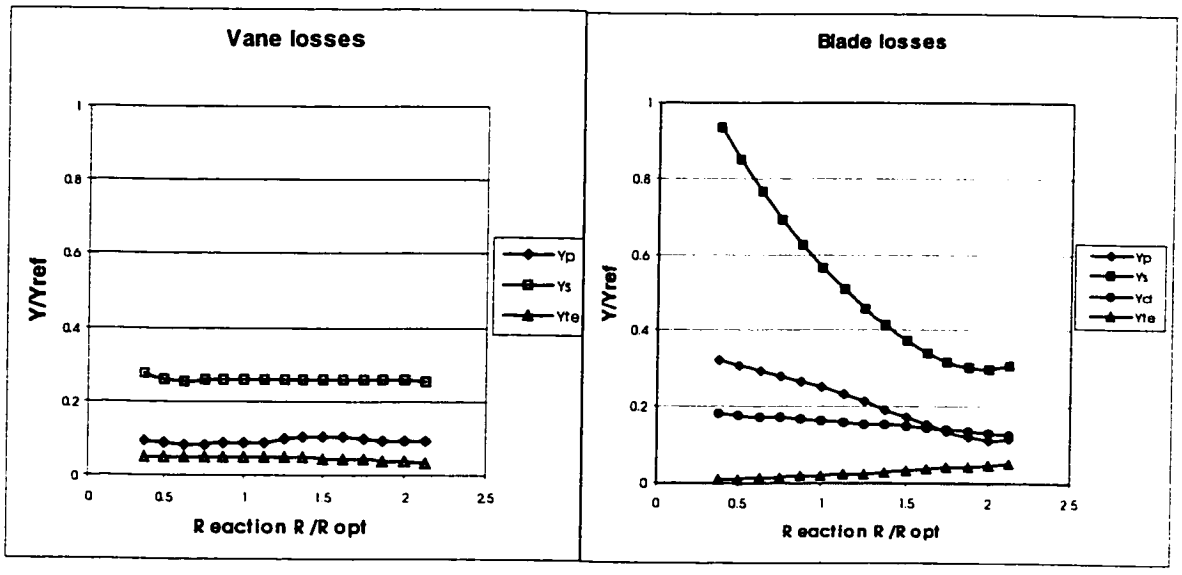

Fig. 3.2 Loss component variation with reaction, turbine stage T2.

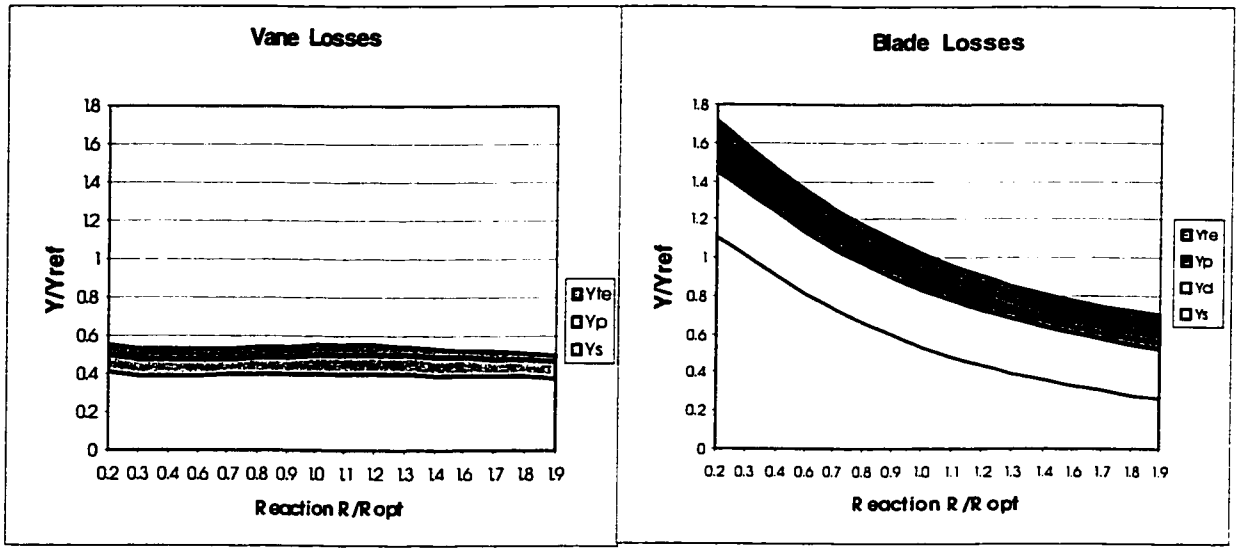

Fig. 3.3 Loss component variation with reaction, turbine stage T45.

shared between profile losses (including trailing edge losses) and tip clearance losses (the later two groups of losses are somewhat different in magnitude due to different tip clearances, trailing edge thickness and/or aspect ratio).

3.2.2 Effect of Reaction on the Aerodynamic and Geometric Parameters

To shed more light on the variation of losses with reaction, some aerodynamic and geometric parameters, which are implied in the loss calculations, are tabulated in Appendix II. Some of these parameters are also plotted against reaction and shown in Fig. 3.4. A schematic of the vane and blade airfoil 2-D profiles for three designs at different reaction conditions, generated using a P&WC in-house code, are shown in Fig. 3.5. It can be seen that the nozzle vane profiles almost don't change with reaction when compared with the blade profiles, which change significantly. The trends in flow angles, velocities and Mach numbers reflect the implications of the reaction variation.

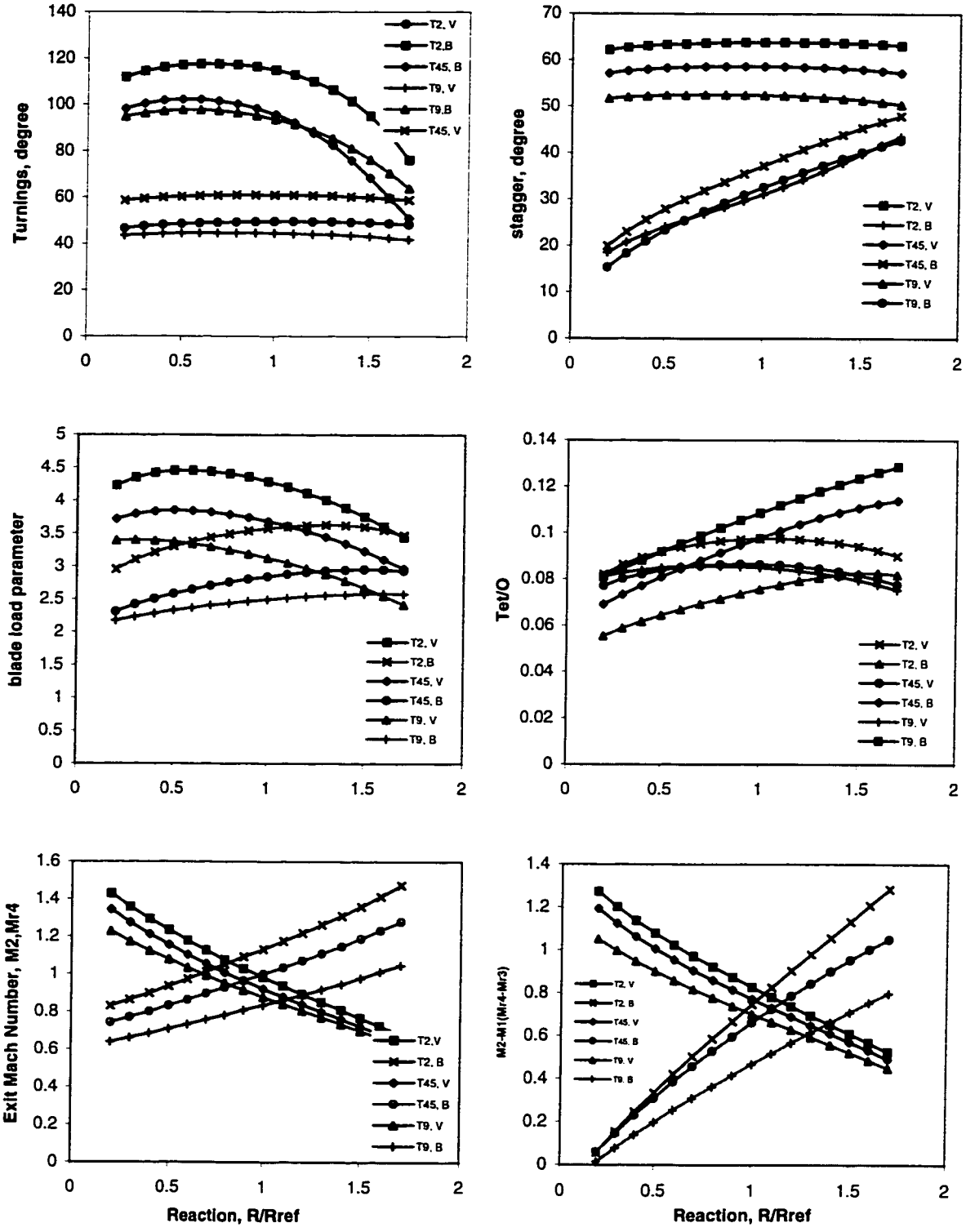

Fig. 3.4 Aerodynamic and geometric parameter variation with reaction

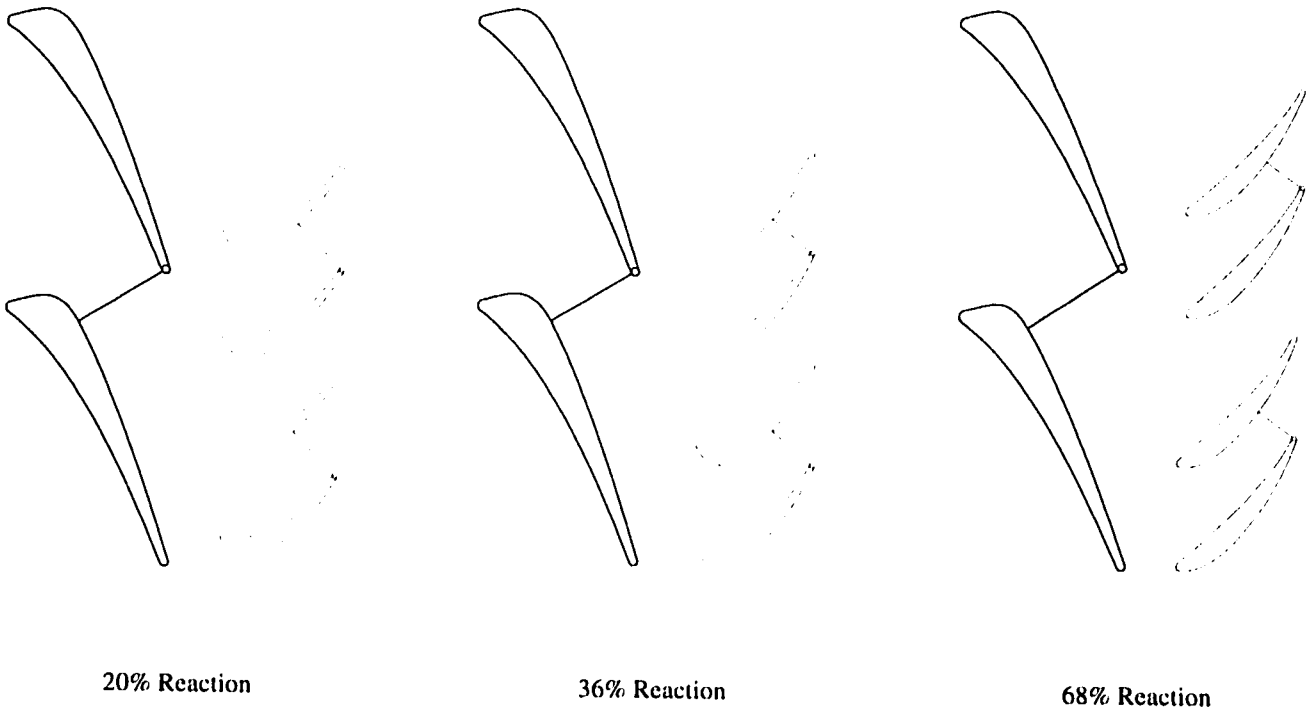

Fig. 3.5 Vane and blade profiles, T45.

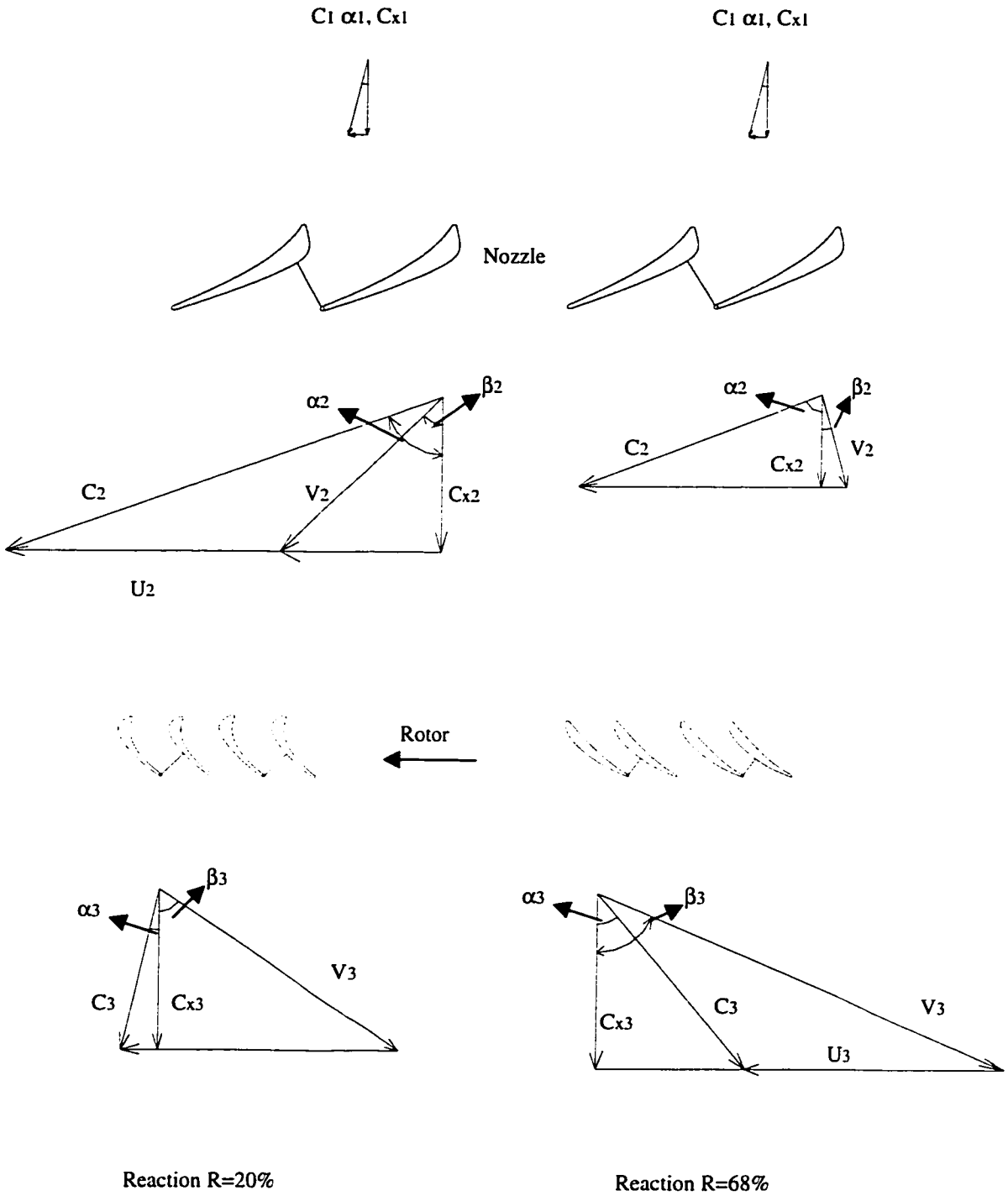

Fig. 3.6 Velocity Triangle Diagram, T45.

As the reaction increases, blade inlet flow angles decrease while exit flow angles increase only slightly, thus decreasing the flow turning, and increasing the blade stagger angles. From the velocity triangles shown in Fig. 3.6, it can also be seen that for vanes, as reaction increases, exit velocity as well as its axial component decrease. However for blades (relative condition), inlet velocity decreases and exit velocity increases to accommodate a larger pressure drop across the rotor, which is associated with a larger reaction. This increased flow expansion and acceleration in the blade passage implies a decreasing throat opening, which is reflected in the blade profile shown in Fig. 3.5. It is important to note that inlet and exit Mach numbers follow the same trends as the inlet and exit velocities (Fig. 3.4).

3.3 Assessment of the AMDCKO Loss System

The AMDCKO performance prediction is based on correlations of experimental data obtained for cascade or actual engine tests. Commenting on these methods, Denton [10] stated that although the predictions of the individual loss components were sometimes shown to be of limited accuracy, the overall methods were tuned by each manufacturer to match their engine data and were therefore extrapolated somewhat effectively to predict the losses for their new designs.

As mentioned earlier, AMDCKO method predicts stage performance rather well below and up to what is believed to be the optimum reaction. However, it fails to predict the optimum reaction and therefore the trend in losses beyond this optimum reaction, as shown in Figs. 3.1 to 3.3. To understand and evaluate this failure in correctly predicting the loss at high values of reaction, individual loss components are assessed in the following sections.

3.3.1 Trailing Edge Loss

Although the AMDCKO loss system predicts increased blade trailing edge losses with increased reaction due to the increased tet/o (ratio of trailing edge thickness to throat opening), it generally underestimates the trailing edge losses as it does not take Mach number effects into account. It is well known that as the exit Mach number is increased toward unity, the loss coefficient rises sharply (Haller, 1980 [16]; Martelli and Boretti, 1987 [24]; Xu and Denton, 1988 [42]; Mee *et al.*, 1992 [25]; and Jouini *et al.*, 2001 [19]). The boundary layer loss should, if anything, decrease with increasing Mach number (since a reduction in flow area produces a greater percentage increase in velocity in compressible flow than it does in incompressible flow, the velocity distribution on accelerating blades will tend to become more favourable as exit Mach number M_2 is increased [9]), so the increased loss must come from the complex shock pattern formed

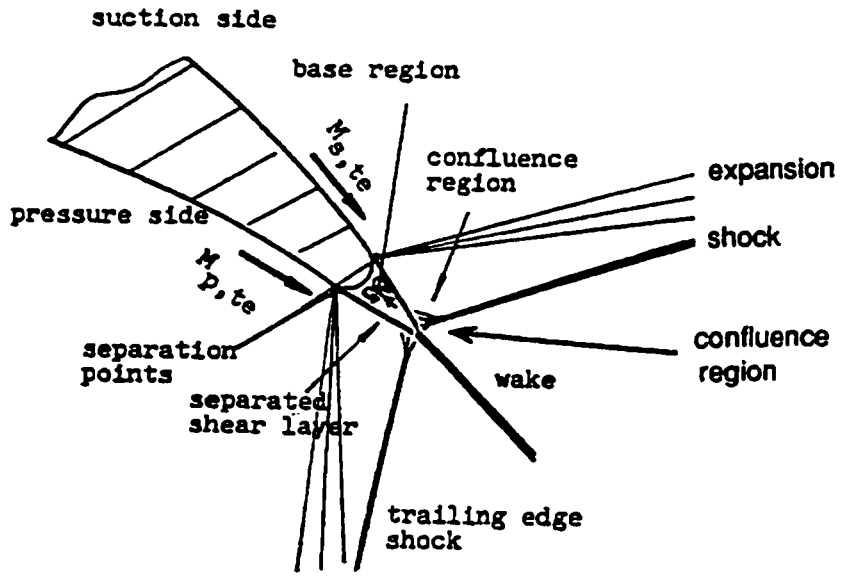

Fig. 3.7 Structure of supersonic trailing edge flow [12].

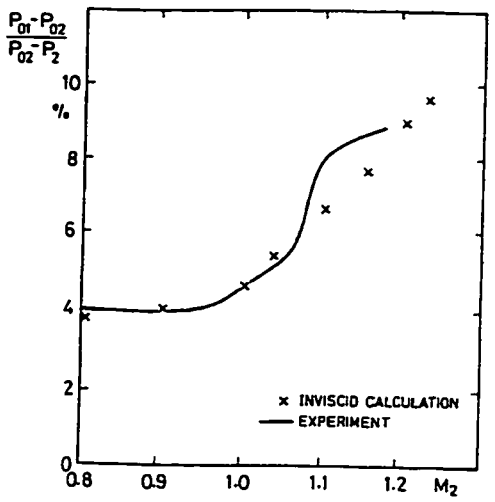

Fig. 3.8 Loss versus Mach number for a turbine cascade [16].

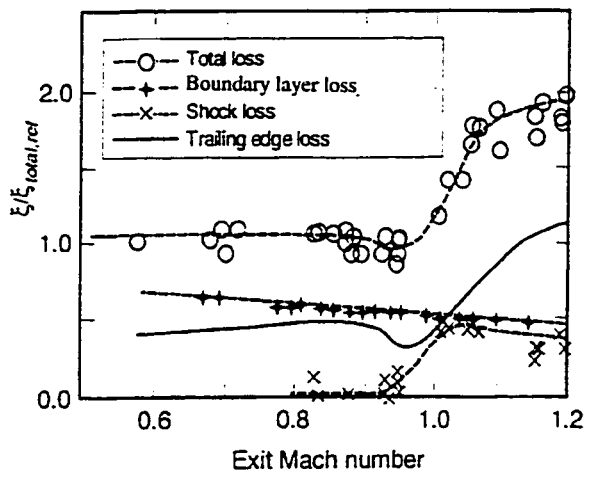

Fig. 3.9 Variation of the two-dimensional loss components with Mach number for a turbine cascade [25].

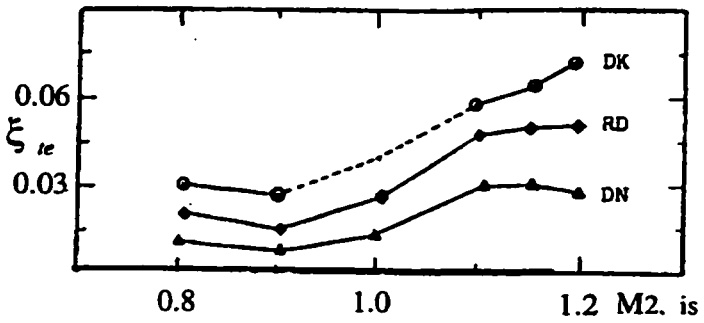

Fig. 3.10 Trailing edge loss Vs mach number [42].

around the trailing edge (it is believed that AMDCKO predicts profile loss well). Figure 3.7 shows the general features of the flow pattern at a supersonic trailing edge and Figs. 3.8 and 3.9 show Haller [16] and Mee *et al.* [25] data respectively. Xu and Denten [42] further gave the variations of trailing edge losses with exit Mach number (Fig. 3.10). All these figures show that the loss continues to rise with increasing Mach number for low supersonic outflow, M_2<1.2,

3.3.2 Tip-Clearance Loss

The AMDCKO loss system predicts that the tip-clearance losses decrease with increasing reaction. It is postulated, however, that Y_{TC} should increase with reaction: as the reaction increases, the blade loading increases and a greater pressure difference will result across the blade tip, causing higher tip flow and increased losses. This is shown in Fig. 3.11 from Roelke [30] for unshrouded blades. From this figure we can see that for a given value of tip clearance, the efficiency decreases with increasing reaction, demonstrating that tip clearance loss increases with increasing reaction.

3.3.3 Secondary Loss

For blades, the AMDCKO loss system predicts that secondary losses decrease with

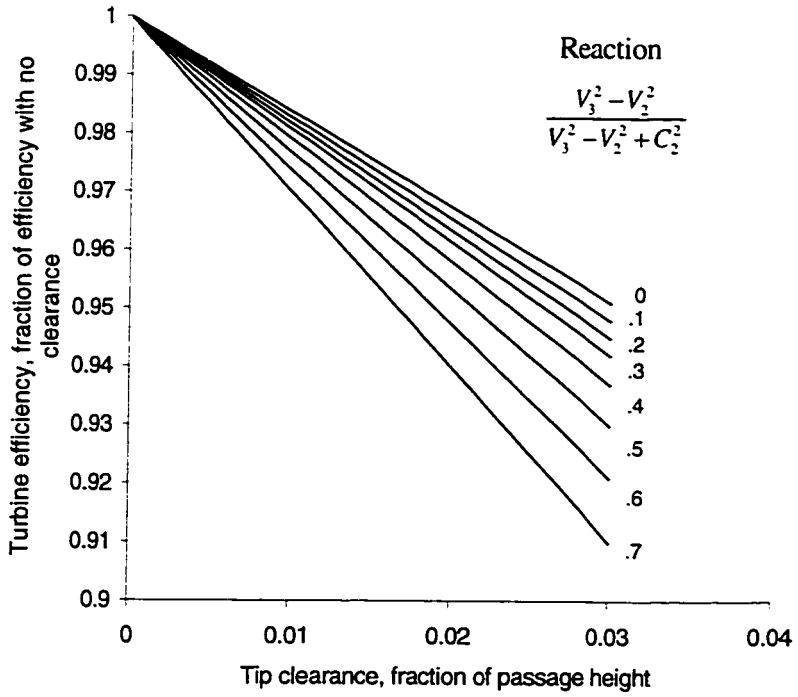

Fig 3.11 Effect of reaction and tip-clearance on efficiency [30].

reaction. It seems reasonable because the flow turning decreases as reaction increases. However, the AMDCKO correlations may underestimate the secondary losses when the flow turning decreases below a critical value that is stage-dependent. One of the reasons is that, as the flow turning decreases with increasing reaction, the flow expansion and acceleration increase and the flow will become supercritical. It is believed that the secondary loss should not be allowed to decrease below its value at this critical condition [37]. In addition, secondary loss does not arise directly from the secondary flow itself but is due to a combination of many factors such as the flow in blade boundary layers and especially the tip leakage flow. As the leakage flow is ejected from the tip gap into the blade passage, it rolls up into a vortex. This vortex interacts with the secondary flow passage vortex to form a region of complex flow and then causes more loss. In the case of unshrouded blades, this interaction is much stronger. Therefore, since tip leakage flow increases with increasing reaction, the interaction between secondary flow and tip leakage flow will increase and the secondary loss will increase accordingly.

It should also be noted that, compressibility effects on secondary loss was not studied since, in the open literature, most of the experimental studies on secondary flow patterns and loss mechanisms use low Mach number cascade flow.

4. Modification and Validation of AMDCKO Loss System

In the previous chapter it was shown that trailing edge loss, tip-clearance loss, or secondary loss correlations in the AMDCKO loss system do not follow the anticipated trend at high stage reactions which correspond to high rotor exit Mach numbers. Modern studies on profile loss, especially on trailing edge loss, show that trailing edge loss increases significantly with increasing Mach number due to the complex shock structure and shock-boundary layer interaction. The AMDCKO tip clearance loss correlation for unshrouded blades, when tested in terms of reaction at blade tip, is not in agreement with experimental data at high reactions. Also experimental data and analyses show that the AMDCKO secondary loss correlation underestimates the secondary loss in the high subsonic exit Mach number range. Therefore, the AMDCKO trailing edge loss, tip-clearance loss, and secondary loss correlations are modified and the modified AMDCKO loss system is validated.

The new AMDCKO loss system will be written as

$$Y_T = Y_P f_{(\mathrm{Re})} + f_{S.B} Y_S + f_{TE} Y_{TET}^{\cdot} + f_{TC} Y_{TC} \tag{4.1}$$

Where $f_{S.B}$, f_{TE}, and f_{TC} are correction factors for the blade secondary loss, trailing edge loss, and tip-clearance loss correlations. These correction factors will be derived in the following sections.

4.1 Modification to Trailing Edge Loss Correlation

In the open literature, there are several studies on trailing edge loss at transonic flow condition. The experimental data reported by five different researchers, showing the total

profile loss variation (which corresponds to Y_p+Y_{te} in AMDCKO model) with exit Mach number, are listed in Table 4.1 and are plotted in Fig. 4.1, where an average curve of all data is shown in dashed line. As noted above, profile loss should decrease with exit Mach number, therefore these curves actually show the trend of trailing edge loss variation with exit Mach number.

Table 4.1 Cascade Experimental Data

Investigator	Exit Mach Number				
	0.8	0.9	1.0	1.1	1.2
Jouini *et al.* [2001]	1	0.94	1.61	1.70	2.16
Mee *et al.* [1992]	1	0.98	1.08	1.76	1.98
Xu &Denton [1988]	1	0.8	1.25	1.95	2.0
VKI [1987]	1	1.07	1.48	1.68	1.61
Haller [1980]	1	1	1.14	1.99	2.24
Average	1	0.96	1.31	1.82	2.0

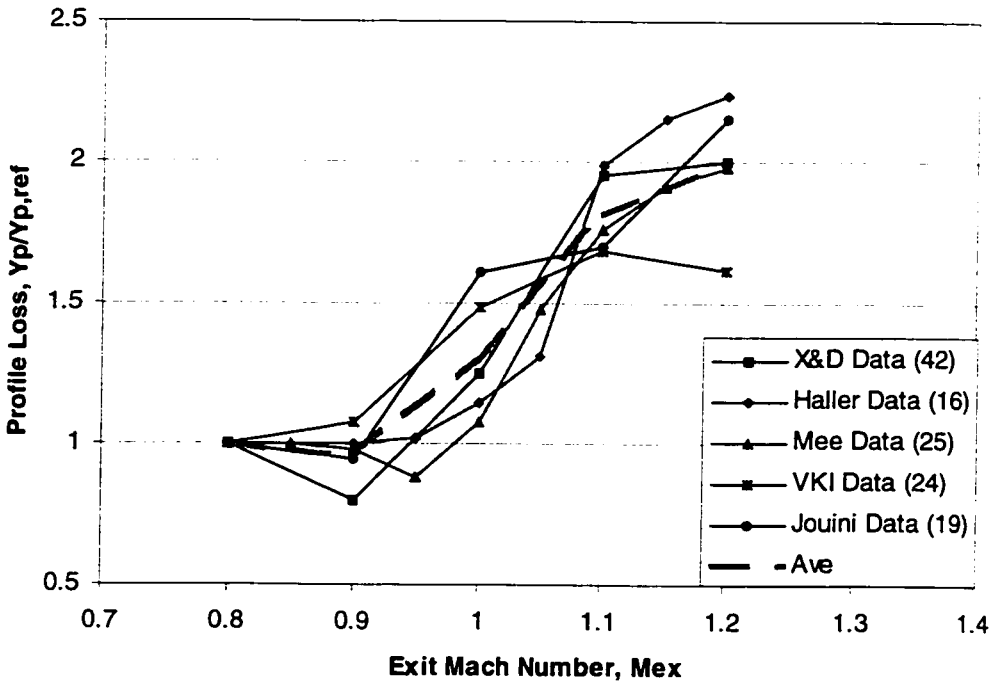

Fig. 4.1 Profile loss variation with exit Mach number from different investigators.

Table 4.2 lists the parameters describing the cascades for which the experimental data was taken. Those parameters namely, aspect ratio, pitch-chord ratio, inlet/outlet angles, staggers etc, indicate that the blades geometry are similar to those used in typical gas turbine applications. Therefore, it is reasonable to use these experimental data to modify the currently used loss correlations.

Table 4.2 Cascade Parameters for Profile Loss Experimental Data

	Jouini *et al.* (2001)	Mee *et al.* (1992)	Xu &Denton (1988)	Haller (1980)
Chord, mm	40.0	100.0	41.7	41.7
Axial Chord, mm	36.98	76.9	36.2	36.2
Span, mm	61.0	300	101.6	101.6
Spacing, mm	29.14	84.0	35.15	35.1
Trailing Edge Thickness, mm	1.25	2.0		
Aspect Ratio	1.525	3.0	2.44	2.4
Leading Metal Angle, °	50.5	42.8	56.7	56
Trailing Metal Angle, °	59.0	68	67.6	67.5
Leading Edge Wedge Angle, °	38.0			
Trailing Edge Wedge Angle, °	6.0		9	
Design Incidence, °	-4.5			
Stagger Angle, °	25.1	39.7	29.6	29.6
Throat Opening, mm	15.3	31.5	13.4	13.4
Unguided Turning, °	11.5			
Inlet Mach Number		0.31		
Inlet Total Temperature, K		285		
Inlet Turbulence Intensity, %		4.1		
Design *Mex*		0.92		
Design *Re,ex*		1,000,000		
Throat width/chord ratio	0.38	.315	0.3214	0.3214
Number of blades			6	6
Pitch/chord ratio	0.73	0.84	0.842	0.842

Note: VKI cascade parameters are not available.

In order to modify the trailing edge loss model in AMDCKO system, profile losses derived from AMDCKO are compared with the average of the experimental data, as shown in Fig. 4.2 where it can be observed that AMDCKO profile losses for vane and blade, do not reflect the sharp rise in trailing edge loss near transonic conditions.

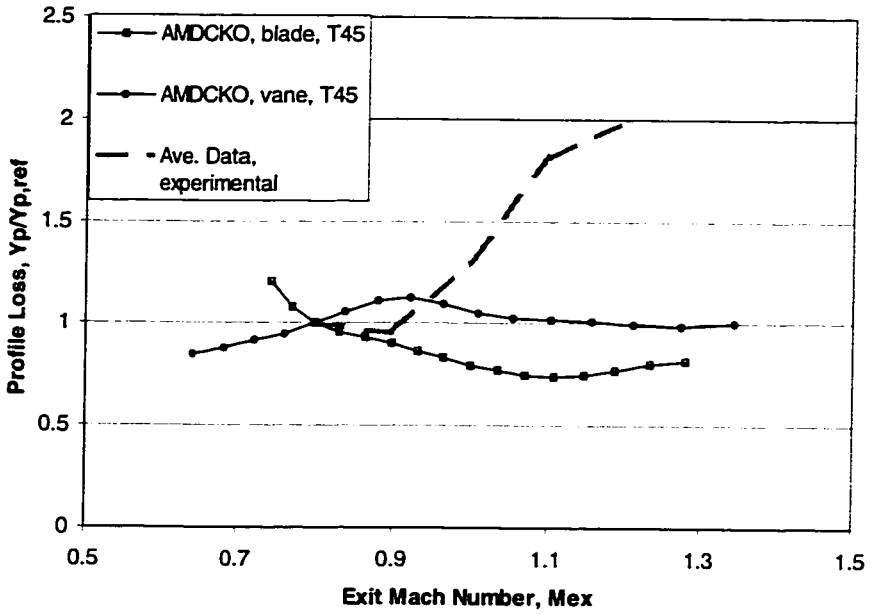

Fig. 4.2 Profile loss comparison between AMDCKO and experimental data.

Based on this comparison, a Mach number correction factor has been developed for both vane and blade trailing edge losses based on the fact that Y_{te} increases sharply with M_{ex}. This correction factor is effective through the current vane and blade exit Mach number range.

The correction factors for both vane and blade are given as a function of delta Mach number ΔM and optimum delta Mach number ΔM_{opt}. That is

$$\text{Vane:} \quad f_{te,V} = f(\Delta M, \Delta M_{opt}) \tag{4.2}$$

$$\text{Blade:} \quad f_{te,B} = f(\Delta M, \Delta M_{opt}) \tag{4.3}$$

where:

$$\Delta M = \text{Mex} - \text{Min} \tag{4.4}$$

$$\Delta M_{opt} = (M_{ex} - M_{in})_{opt} \tag{4.5}$$

Where M_{opt} and ΔM_{opt} are given in detail in Section 4.4. Note also that for blades, Mach numbers are relative values.

The results of the modifications for an engine stage are demonstrated in Fig 4.3 by comparing experimental data with the trailing edge losses before and after corrections.

* *It is believed that the AMDCKO profile loss Y_p (boundary layer loss) correlations for vanes and blades work well. Therefore, the trailing edge experimental data here are derived from subtracting Y_p from the averaged experimental data given in Table 4.1.*

4.2 Modification of Tip-Clearance Loss Correlation

Experimental results given by Roelke [30] show a relation between efficiency penalty (or Y_{cl}) and "velocity-based reaction at blade tip" for unshrouded blades (see Fig. 3.11). A comparison between this data and the AMDCKO results for an engine stage is given in Fig. 4.4 where it can be seen that there is a discrepancy between the AMDCKO

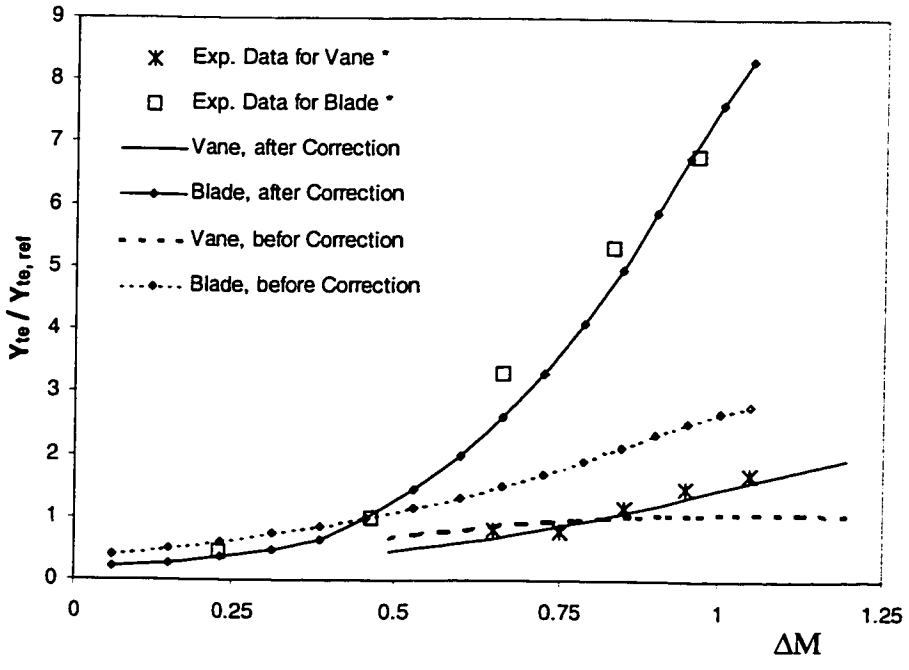

Fig. 4.3 Correction to trailing edge loss , T45.

prediction and experimental data. When velocity-based reaction at blade tip *Rvt* is less than a certain value, the AMDCKO loss system overestimates the tip-clearance loss, and when *Rvt* is greater than that value, the AMDCKO underestimates significantly the tip-clearance loss.

The correction factor is given as a function of "velocity-based reaction at blade tip" Rvt as follows:

$$f_{TC} = f(R_{vt}) \tag{4.6}$$

Where

$$R_{vt} = \frac{V_3^2 - V_2^2}{V_3^2 - V_2^2 + C_2^2} \tag{4.7}$$

The result of this correction is also compared with the experimental data and shown in Fig. 4.4.

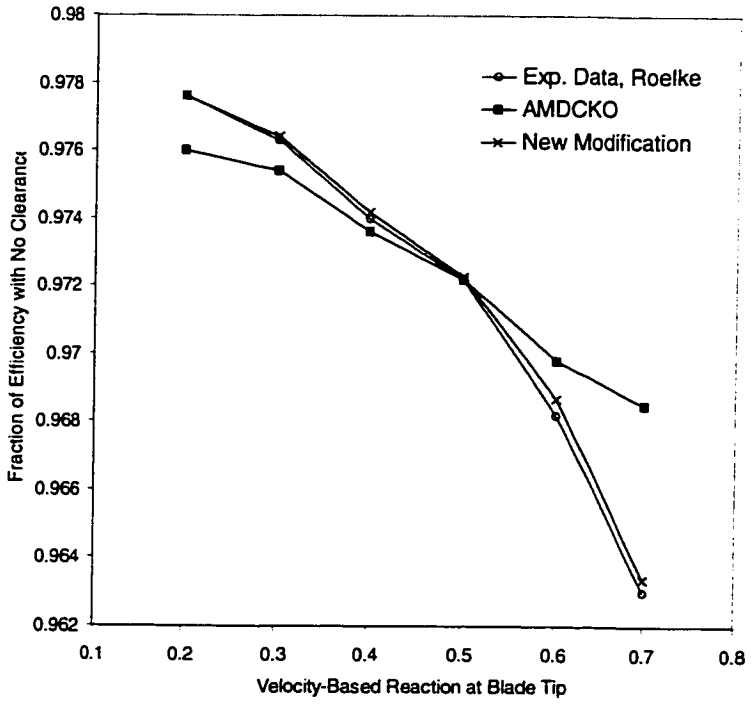

Fig. 4.4 Comparison and correction of tip-clearance loss correlation with Roelke data, T45, k/h=0.011, unshrouded

4.3 Modification to Secondary Loss Correlation

Studies carried out in P&WC show that, for each turbine stage, there is an optimum reaction at which maximum efficiency is achieved. Above or below this optimum reaction, the efficiency decreases. The rationale for the secondary loss modification is based on the following: (i) The AMDCKO model performs well at low reactions, so any major loss component modification should focus on the higher reaction range. (ii) The most significant aerodynamic characteristic of this range is that blades have a higher exit Mach number. Therefore, a Mach number correction factor was introduced based on the P&WC data to modify the blade secondary loss in the post-optimum range of reaction.

The Mach number correction factor for blade secondary loss is given as a function of delta Mach number ΔM, optimum delta Mach number ΔM_{opt}, and optimum exit Mach number $M_{ex,opt}$. That is

$$f_{S.B} = f\left(\Delta M, \Delta M_{opt}, M_{ex,opt}\right) \tag{4.8}$$

where:

$$\Delta M = M_{ex} - M_{in} \tag{4.9}$$

$$\Delta M_{opt} = \left(M_{ex} - M_{in}\right)_{opt} \tag{4.10}$$

$M_{ex,opt}$ = Optimum exit Mach number

(In this case, the Mach numbers refer to blade relative condition and the optimum Mach numbers are introduced in Section 4.4).

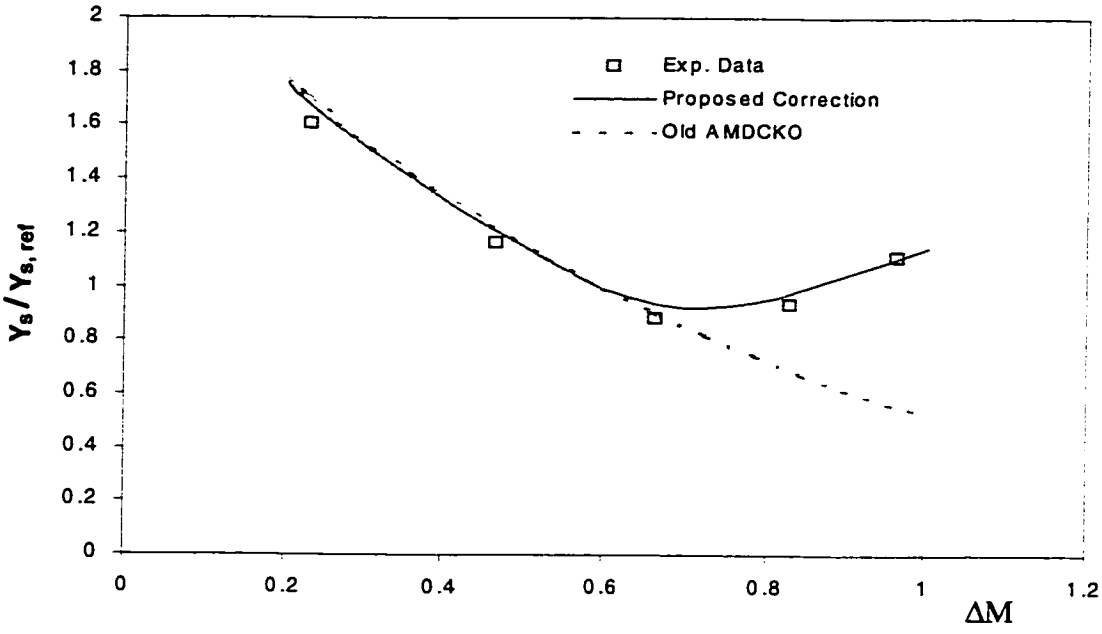

Fig. 4.5 Correction to secondary loss, T45.

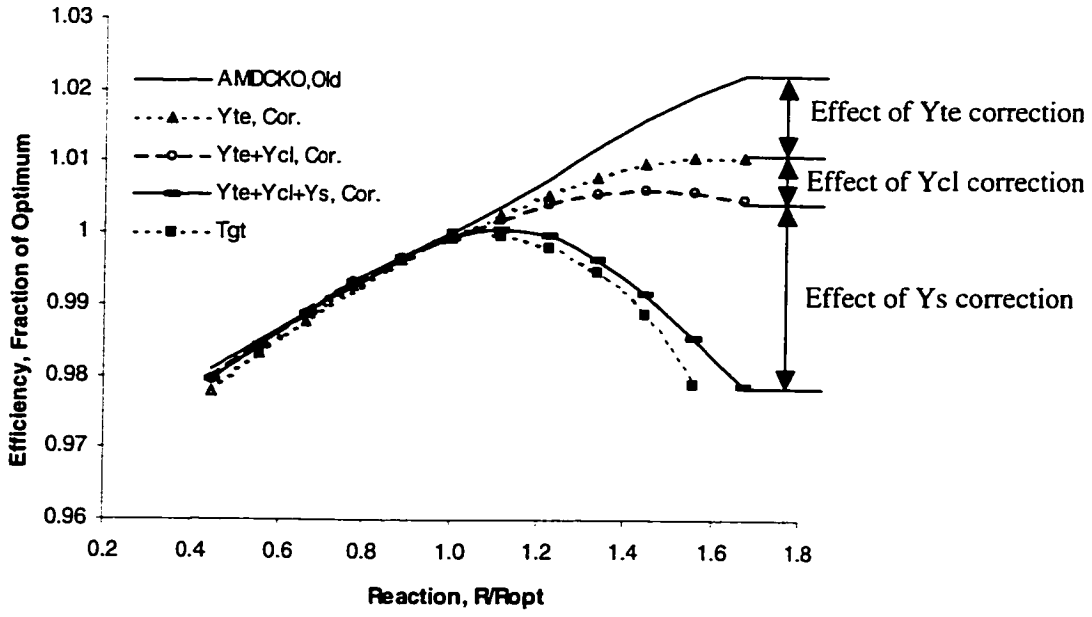

Fig. 4.6 Effects of Yte, Ycl, Ys corrections, T45.

After this modification, the change of secondary loss variation with ΔM for a turbine stage is shown in Fig. 4.5.

Figure 4.6 shows the effects of the modifications to trailing edge loss, tip-clearance loss, and secondary loss correlations by individually plotting the efficiency versus reaction. Figures 4.7 and 4.8 show the individual loss component variation with reaction before and after these modifications. It can be seen that beyond the optimum reaction, the efficiency decreases with increasing reaction due to the increased trailing edge loss, tip-clearance loss and secondary loss. Compared with the old loss components, all the three modified components increase with increasing reaction for values of reaction past the optimum.

4.4 Optimum Exit Mach Number $M_{ex,opt}$ and Optimum Delta Mach number ΔM_{opt}

At the stage optimum reaction, the blade row exit Mach number M_{ex} and delta Mach number ΔM $(M_{ex}$-$M_{in})$ are referred to as optimum exit Mach number $M_{ex,opt}$ and optimum delta Mach number ΔM_{opt}. After having studied 46 different turbine stages from 17 different engines, it was found that the optimum exit Mach number $M_{ex,opt}$ and the optimum delta Mach number ΔM_{opt} are function of stage pressure ratio PR, (see Figs. 4.9 and 4.10). They tend to increase as PR increases, these experimental data were fitted with shown curves, which were used in evaluating the correction factors presented earlier.

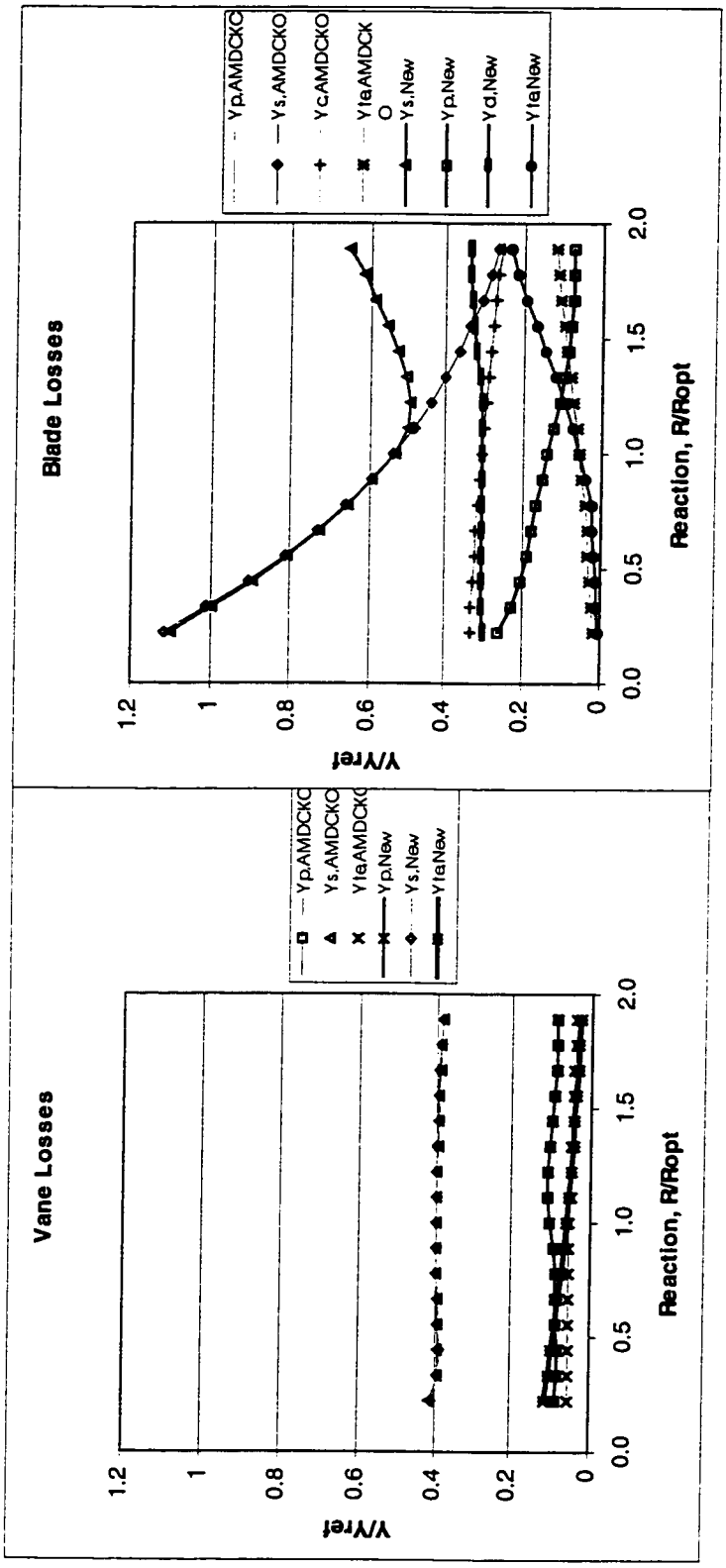

Fig. 4.7 Comparison of loss component variation with reaction before and after modification, T45

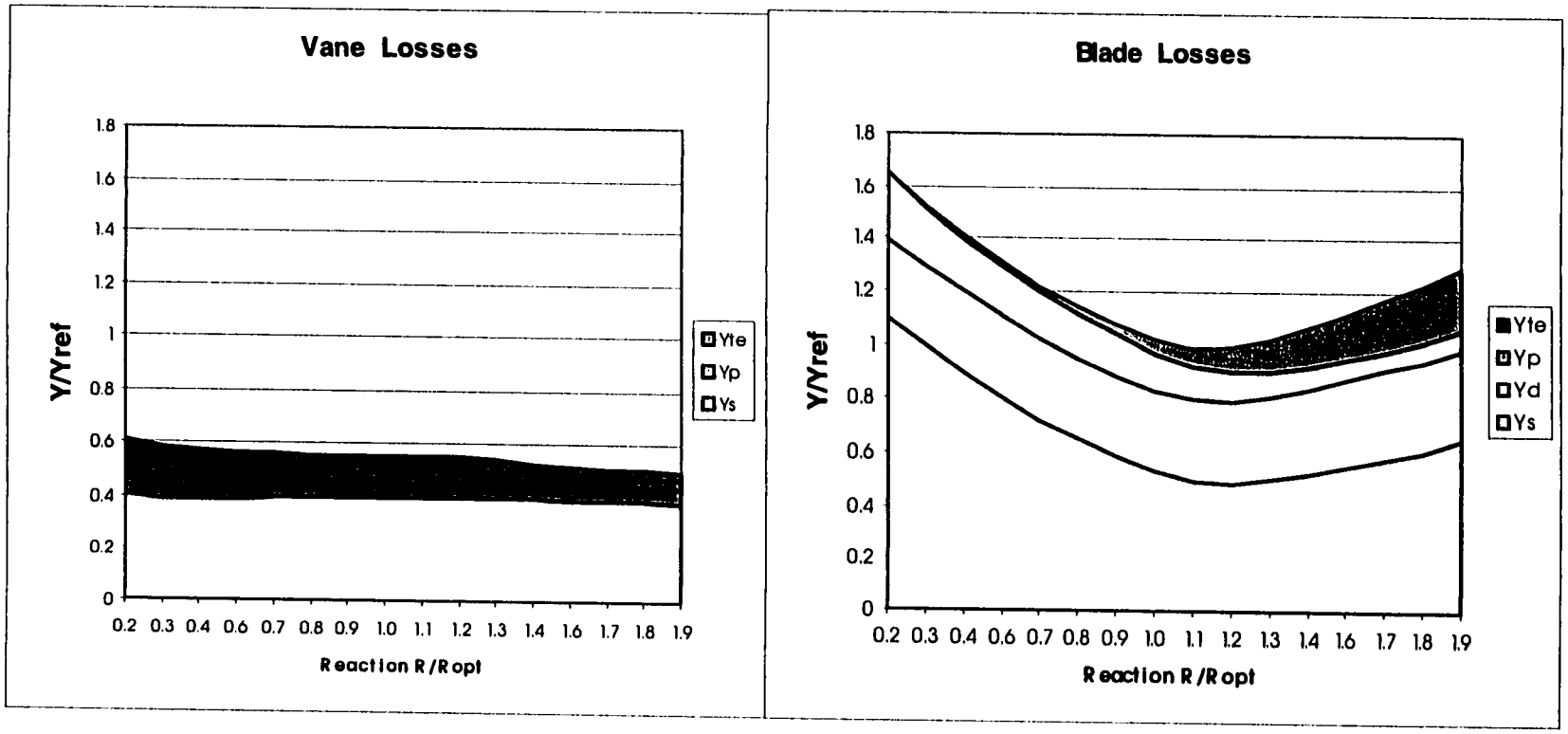

Fig. 4.8 Loss component variation with reaction after modification, T45.

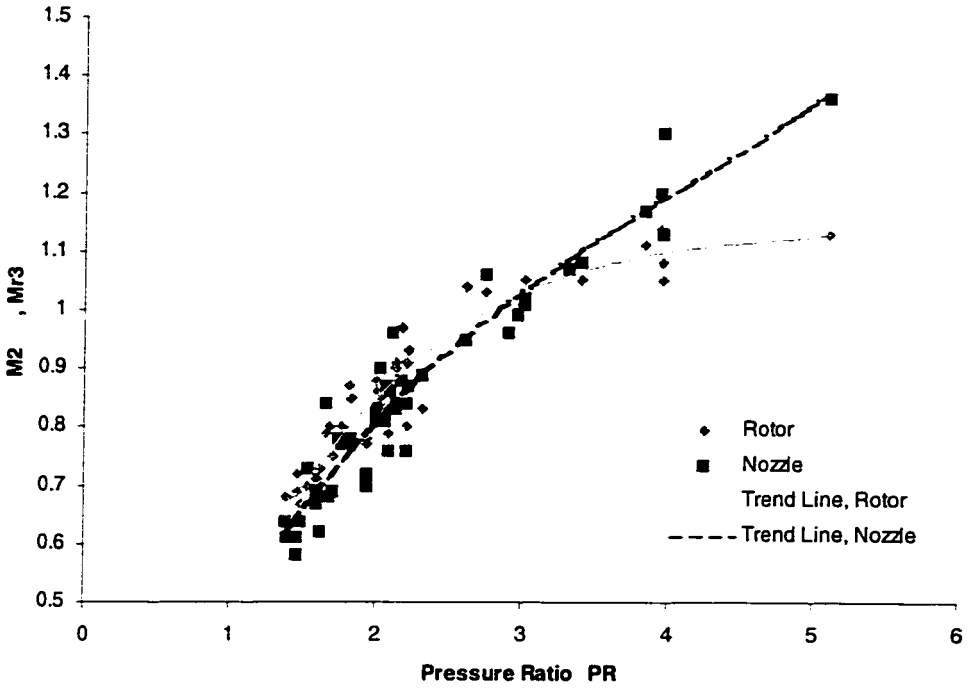

Fig. 4.9 Optimum exit Mach number vs pressure ratio

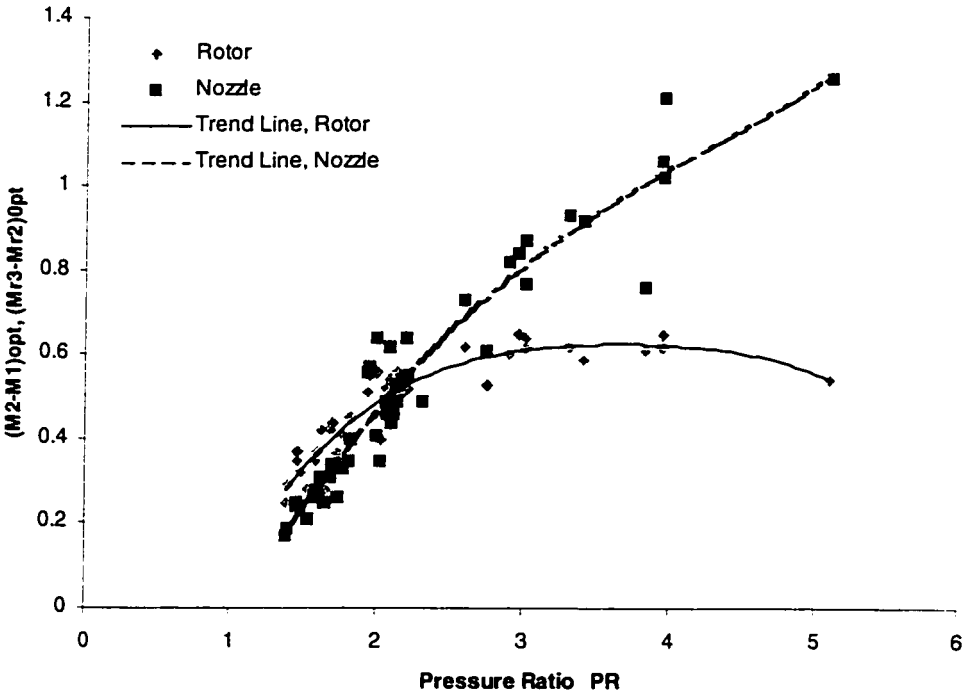

Fig. 4.10 Optimum delta Mach number vs pressure ratio

4.5 Validation

In order to validate the proposed mean line loss system, the modifications have been implemented in the P&WC aerodynamic mean line design system. The program was then run for 46 different turbine stages corresponding to 17 different engines. These engines cover a wide range of applications going from single-stage to five-stage turbines with both cooled and uncooled turbine stages, and from subsonic to supersonic flows. The curves showing the variation of stage efficiency with reaction for the old and the new AMDCKO models for some of the representative stages are shown in Appendix III, Fig. III.1. These predicted results show an improvement compared with the old AMDCKO, which shows almost no optimum reaction at which the maximum efficiency has been shown to occur in engine and rig test cases. Table 4.3 provides the detailed results of optimum reaction and efficiency after modification and their target values for the purpose of comparison. Figure 4.11 compares the predicted optimum efficiency with the expected target efficiency (from P&WC unpublished experimental data), where we can see that the results fall within a $\pm 1\%$ error band, for almost all the stages.

The predicted optimum reactions are also compared with experimental data and are shown in Fig. 4.12. It was found that the modified loss system generally predicts a slightly higher optimum reaction trend compared with experimental data. However, most of the reactions predicted by the modified AMDCKO loss system fall within the experimental data band.

4.6 Concluding Remarks

The AMDCKO trailing edge loss correlation was modified based on the physical implication of high Mach number flow on the different loss components and based on

Table 4.3 Results of validation against 46 turbines of 17 engines

Turbine Stages	Cooled	PR	η/ηRef Expected Target	η/ηRef AMDCKO, New	Error, %
T1	V/B	5.1	0.9409	0.9431	-0.01
T2	V	3.4	0.9758	0.9742	0.39
T3	None	1.7	1.0228	1.0201	0.48
T4	None	1.8	0.9999	1.0055	-0.34
T5	V/B	1.9	0.9565	0.9612	0.92
T6	V	2.2	1.0087	1.0093	0.16
T7	None	1.6	1.0283	1.0314	-0.09
T8	None	2.2	1.0046	1.0026	0.41
T9	V/B	2.0	1.0010	1.0067	-0.35
T10	V/B	2.1	1.0030	1.0024	0.27
T11	None	1.8	1.0240	1.0292	-0.29
T12	None	2.0	1.0124	1.0077	0.69
T13	V	3.0	0.9984	1.0015	-0.09
T14	None	2.7	1.0171	1.0098	0.94
T15	V/B	1.9	0.9874	0.9941	-0.45
T16	V/B	2.1	1.0091	1.0083	0.29
T17	V/B	2.1	0.9754	0.9791	-0.16
T18	V/B	2.1	1.0273	1.0300	-0.04
T19	V/B	2.2	0.9663	0.9711	-0.27
T20	V/B	2.2	1.0113	1.0142	-0.07
T21	None	1.4	1.0059	1.0051	0.30
T22	None	1.5	1.0161	1.0238	-0.54
T23	None	1.5	1.0224	1.0247	-0.01
T24	V	3.0	0.9941	0.9963	-0.01
T25	None	1.5	1.0151	1.0102	0.70
T26	None	1.7	1.0207	1.0249	-0.20
T27	V	3.9	0.9580	0.9595	0.06
T28	None	1.6	1.0205	0.9933	2.90
T29	None	1.8	1.0021	0.9981	0.62
T30	V	3.3	0.9653	0.9673	0.01
T31	None	1.4	0.9800	0.9711	1.14
T32	None	1.6	0.9749	0.9755	0.15
T33	None	1.7	0.9704	0.9720	0.06
T34	V/B	4.0	0.9688	0.9678	0.33
T35	V	3.8	0.9699	0.9710	0.10
T36	None	1.5	1.0265	1.0300	-0.12
T37	None	1.6	1.0249	1.0321	-0.49
T38	V/B	4.0	0.9910	0.9921	0.10
T39	V/B	2.1	1.0199	1.0221	0
T40	None	2.1	1.0414	1.0361	0.73
T41	V	3.0	0.9759	0.9787	-0.07
T42	None	2.0	1.0439	1.0328	1.30
T43	V	2.6	0.9902	0.9928	-0.05
T44	None	2.1	1.0379	1.0322	0.47
T45	V	2.9	0.9906	0.9919	0.09
T46	None	2.3	1.0008	0.9985	0.45

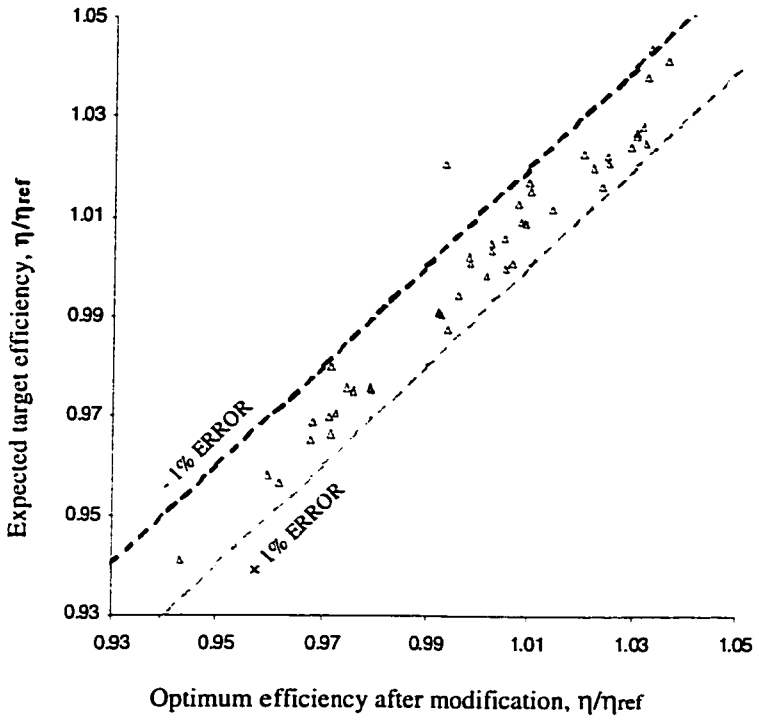

Fig. 4.11 Comparison of predicted optimum efficiencies of 46 turbine stages.

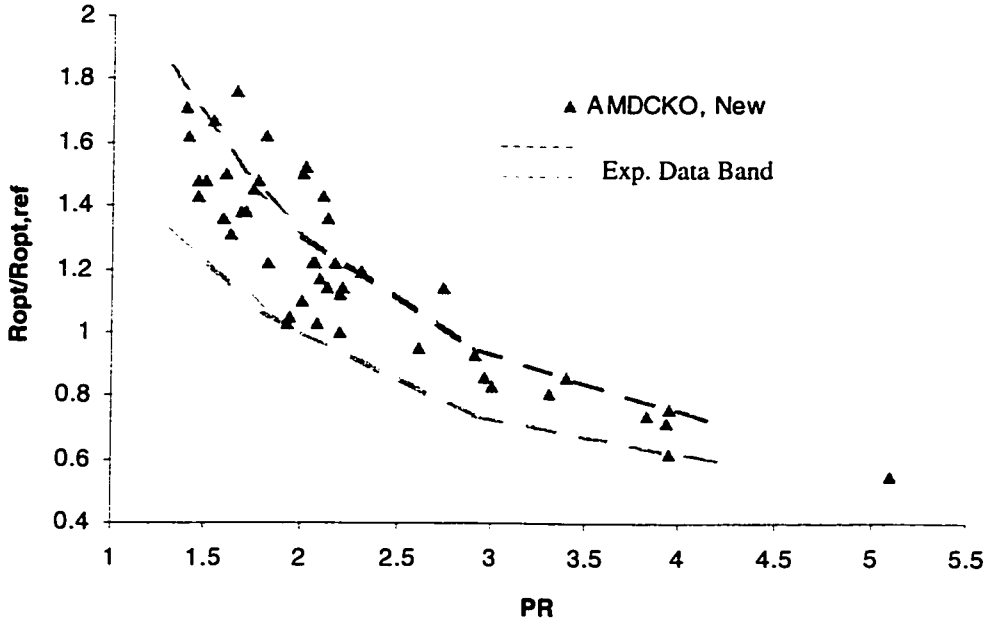

Fig. 4.12 Optimum reaction Vs pressure ratio.

experimental data found in the open literature as discussed in Section 4.1. It was shown (Fig. 4.1) that total profile loss (Y_p+Y_{te} in AMDCKO) increases significantly with exit Mach number in the transonic range (0.8-1.2). However, the AMDCKO profile loss (boundary layer loss) Y_p plus trailing edge loss Y_{te} for both vanes and blades remain unchanged, or even decrease slightly, with exit Mach number in this range (Fig. 4.2). As mentioned earlier, this is postulated to be due to the shock loss at the trailing edge that was not taken into account in the AMDCKO loss system. Therefore, the trailing edge loss was underestimated (Fig. 4.3). The proposed modification remedied this situation. The AMDCKO tip-clearance loss correlation for unshrouded blades was inconsistent when tested against NASA's study on the reaction effect on turbine efficiency (Fig. 4.4). Therefore, a correction factor involving the "velocity-based reaction at blade tip" was developed and was successfully applied to the old model for unshrouded blades. Lastly, the AMDCKO secondary loss model was modified to reflect recent knowledge and experimental results for transonic turbines. This modification improved the overall mean line performance prediction, when compared with experimental data. The effects of all these three modifications can be depicted in Figs. 4.6-4.8, where efficiency as well as loss coefficient are plotted versus reaction.

It was demonstrated that the modified AMDCKO loss system not only predicted the expected optimum efficiency (Fig. 4.11), but also predicted the optimum reaction value reasonably well (Fig. 4.12).

5. Conclusion, Suggestions, and Future Work

5.1 Conclusion

An aerodynamic loss system is essential to turbine mean line design which in turn plays an important role in the entire engine design cycle. Therefore, the loss system must be reviewed and updated from time to time to reflect the latest knowledge and design practices. In general, the AMDCKO loss system performs well up to the optimum reaction range, but it overpredicts aerodynamic efficiency when the stage reaction exceeds its optimum value. This range of reaction usually corresponds to higher rotor exit Mach numbers (transonic flow regime).

It is determined that the existing AMDCKO loss system needs improvement in three aspects.

1. It underestimates the trailing edge loss because it doesn't take into account the complex shock pattern formed around the trailing edge in transonic flow. Recent studies in the open literature show that this is a major source of loss and it rises sharply as the exit Mach number is increased toward one (usually continues to 1.2).

2. It fails to predict an increased tip-clearance loss as the reaction is increased, corresponding to increased blade loading and exit Mach number.

3. It underestimates the secondary loss when the reaction exceeds a certain value.

The discrepancy between the AMDCKO results and both the experimental results from P&WC and in the open literature were explained based on the implication of high Mach number flow in the turbine stage. The experimental results were used to modify the

AMDCKO system to reflect compressibility effect in the transonic flow regime. Modifications are made to the AMDCKO trailing edge loss, tip-clearance loss, and secondary loss correlations.

The modified AMDCKO loss system has improved the performance prediction capability of turbine mean line design in that it predicts an optimum reaction at which the maximum efficiency has been shown to occur in engine and rig test cases to within ±1%, and therefore it is now applicable to a larger design range. This also allows the loss model to be used as a useful tool within a multidiscipline optimisation design environment.

5.2 Suggestions and Future Work

Although the modified AMDCKO loss system has improved the performance prediction capability of turbine mean line design program, the proposed modification hasn't modified the structure of the AMDCKO loss system that doesn't reasonably reflect the latest understanding about loss components and their magnitudes. Moreover, the effect of high Mach number on secondary loss is still not clear. Therefore, further efforts need to be made and the AMDCKO loss system may be further improved in the following major aspects:

- ***Secondary loss variation with Mach number.*** Further understanding, and solid and complete experimental data relating secondary loss variation with Mach number is required for further improvement of the AMDCKO loss system.
- ***CFD assessment of secondary loss.*** Since neither a qualitative nor a quantitative study of the compressibility effect on secondary loss is available, further work would

include using CFD (Computational Fluid Dynamics) to validate the relationship between secondary losses and exit Mach number.

References

1. Ainley, D. G., and Mathieson, G. C. R., 1951, "An Examination of the Flow and Pressure Losses in Blade Rows of Axial-Flow Turbines", British ARC, R&M 2891

2. Baljé, O.E., and Binsley, R. L., 1968, "Axial Turbine Performance Evaluation. Part A --- Loss - Geometry Relationships," ASME, Journal of Engineering for Power, pp. 341-348

3. Baljé, O.E., and Binsley, R. L., 1968, "Axial Turbine Performance Evaluation. Part B --- Optimization With and Without Constraints," ASME, Journal of Engineering for Power, pp. 349-360

4. Bindon, J. P., 1989, "The Measurement and Formation of Tip Clearance Loss", ASME, Journal of Turbomachinery, Vol. 111, pp. 257-263

5. Came, P. M., 1973, "Secondary Loss Measurements in a Cascade of Turbine Blades", IMechE Conference Publication on "Heat and Fluid Flow in Steam and Gas Turbine Plant", C33/73

6. Chen, L. D., and Dixon, S. L., 1986, "Growth of Secondary Flow Losses Downstream of a Turbine Blade Cascade", ASME Journal of Engineering for Gas Turbines and Power, Vol.108, pp 270-276

7. Cohen, H., Rogers, G. F. C., and Saravanamuttoo, H. I. H., 1996, *Gas Turbine Theory*, 4th Edition, Addison Wesley Longman Limited, England

8. Craig, H. R. M., and Cox, H. J. A., 1970, "Performance Estimation of Axial Flow Turbines," Proc. Instn. Mech. Engrs. 1970-71, Vol. 185 32/71

9. Denton, J. D., 1973, "A Survey and Comparison of Methods of Predicting the Profile Loss of Turbine Blades", IMechE Conference Publication on "Heat and Fluid Flow in Steam and Gas Turbine Plant", C76/73

10. Denton, J. D., 1993, "Loss Mechanisms in Turbomachines," ASME Journal of Turbomachinery, Vol.115, pp 621-656

11. Denton, J. D., and Cumpsty, N. A., 1987, "Loss Mechanisms in Turbomachines. Turbomachinery – Efficiency Prediction and Improvement", Inst. Mech. Engrs, pp 1-14

12. Denton, J.D., and Xu, L., 1990, "the Trailing Edge Loss of Transonic Turbine Blades", ASME Journal of Engineering for Power, Vol.112, pp 277-285

13. Dixon, S. L., *Fluid Mechanics, Thermodynamics of Turbomachinery*, 3rd edition, Pergamon Press, Oxford

14. Dunham, J., 1970, "A Review of Cascade Data on Secondary Losses in Turbines", IMechE J. Mech. Sci., Vol. 12, No.1.

15. Dunham, J., and Came, P.M., 1970, "Improvements to the Ainley-Mathieson Method of Turbine Performance Prediction", ASME Journal of Engineering for Power, Vol.92, pp 252-256

16. Haller, B. R., 1980, *The Effects of Film Cooling on the Aerodynamic Performance of Transonic Turbine Blades*, Phd thesis, Cambridge University, United Kingdom

17. Horlock, J. H., 1973, *Axial Flow Turbines – Fluid Mechanics and Thermodynamics*, Robert E. Krieger Publishing Company, New York

18. Japikse, D., and Baines, N. C., 1994, *Introduction to Turbomachinery*, Concepts ETI, Inc. and Oxford University Press, pp 6-1 to 6-39

19. Jouini, D. B. M., Sjolander, S. A., and Moustapha, S. H., 2001, "Aerodynamic Performance of a Transonic Turbine Cascade at Off-Design Condition," ASME, Journal of Turbomachinery, Vol. 123, pp. 510-517

20. Kacker, S.C., and Okapuu, U., 1982, "A Mean Line Prediction Method for Axial Flow Turbine Efficiency", ASME Journal of Engineering for Power, Vol.104, pp 111-119

21. Lakshminarayana, B., 1970, "Methods of Predicting the Tip Clearance Effects in Axial Flow Turbomachinery", ASME Journal of Basic Engineering, Sep. 1970

22. Lakshminarayana, B., 1996, *Fluid Dynamics and Heat Transfer of Turbomachinery*, Wiley, New York

23. Langston, L. S., 1980, "Crossflows in a Turbine Cascade Passage," ASME Journal of Engineering for Power, Vol. 102, pp. 866-874

24. Martelli, F., and Boretti, A., 1987, "Development of an Experimental Correlation for Transonic Turbine Flow", ASME, Journal of Turbomachinery, Vol. 109, pp. 246-250

25. Mee, D. J., Baines, N. C., Oldfield, M. L. G., and Dickens, T E., 1992, "an Examination of the Contributions to Loss on a Transonic Turbine Blade in Cascade", ASME JOURNAL OF TURBOMACHINERY, Vol. 114, pp. 155-162

26. Moustapha, S. H., 1998, *Gas Turbine Design*, Concordia University, Handbook for course Mech 465/616

27. Moustapha, S. H., Kacker, S. C., and Tremblay, B., 1990, "An Improved Incidence Losses Prediction Method for Turbine Airfoils", ASME, Journal of Turbomachinery, Vol. 112, pp. 267-276

28. Okan, M. B., and Gregory-Smith, D. G., 1992, "A Simple Method for Estimating Secondary Losses in Turbines at the Preliminary Design Stage", ASME Paper No. 92-GT-294

29. Qiang, K. F., and Chen, N. X., 1982, "New Correlations of the Two Dimensional Turbine Cascade Aerodynamic Performance," ASME Journal of Engineering for Power, Vol. 104, pp.458-466

30. Roelke, R. J., 1973, "Miscellaneous Losses" in *Turbine Design and Application*, Vol 2, Ed. by Glassman, A. J., NASA SP-290.

31. Sharma, O. P., and Butler, T. L., 1987, "Predictions of Endwall Losses and Secondary Flows in Axial Flow Turbine Cascades", ASME JOURNAL OF TURBOMACHINERY, Vol.109, pp 229-236

32. Sieverding, C. H., 1985, "Axial Turbine Performance Prediction Methods," NATO ASI Series, No. 97B, Vol. 2

33. Sieverding, C. H., 1985, "Recent Progress in the Understanding of Basic Aspects of Secondary Flow in Turbine Blade Passages," ASME Journal of Engineering for Gas Turbines and Power, Vol. 107, pp.248-257

34. Sjolander, S. A., Yaras, M. I., 1989, "Losses in the Tip-Leakage Flow of a Planar Cascade of Turbine Blade," AGARD Paper CP-469

35. Smith, S. F., 1965, "A Simple Correlation of Turbine Efficiency", J Royal Aeron. Soc., Vol. 69, 1965, p 467

36. Stewart, W. L., 1961, "A Study of Axial Flow Turbine Efficiency Characteristics in Terms of Velocity Diagram Parameters," ASME Paper No. 61-WA-37

37. Turyk, P. J., 1989, "Turbine Meanline Design Program --- Recent Work on Optimum Reaction Prediction," P&WC Internal MEMO

38. Vlasic, E. P., 1997, "Optimum Reaction and Summary of the Reaction Effects in Turbines," P&WC Internal MEMO

39. Vlasic, E. P., Girgis, S., Moustapha, S. H., 1996, "The Design and Performance of a High Work Research Turbine," ASME JOURNAL OF TURBOMACHINERY, Vol. 118, pp. 792-799

40. Wei, N., 2000, *Significance of Loss Models in Aerothermodynamic Simulation for Axial Turbines*, Doctoral Thesis, Royal Institute of Technology, Sweden

41. Wilson, D. G., 1984, *The Design of High-Efficiency Turbomachinery and Gas Turbines*, The MIT Press, Cambridge, Massachusetts/London, England

42. Xu, L., and Denton, J. D., 1988, "The Base Pressure and Loss of a Family of Four Turbine Blades," ASME JOURNAL OF TURBOMACHINERY, Vol. 110, pp. 9-11

43. Yaras, M. I., and Sjolander, S. A., 1992, "Prediction of Tip-Leakage Losses in Axial Turbines", ASME Journal of Turbomachinery, Vol.114, pp 204-210

Appendices

Appendix I Terminology and Definitions

I.1 Blade Section Terminology

Blade section terminology is far from identical from one investigator to another. A more detailed description of the blade section notation for axial flow turbines is introduced by Wilson [41] and is shown in Fig. I.1. The purpose of Fig. I.1 is to illustrate the notation which is commonly used for cascade geometrical parameters and which will be followed in this work.

Fig. I.1 is drawn with α representing the flow angle and β representing the blade 'metal' angle measured between the axial direction and the tangent to the camber line at leading and trailing edges. The camber line is obtained by bisecting the thickness of the airfoil.

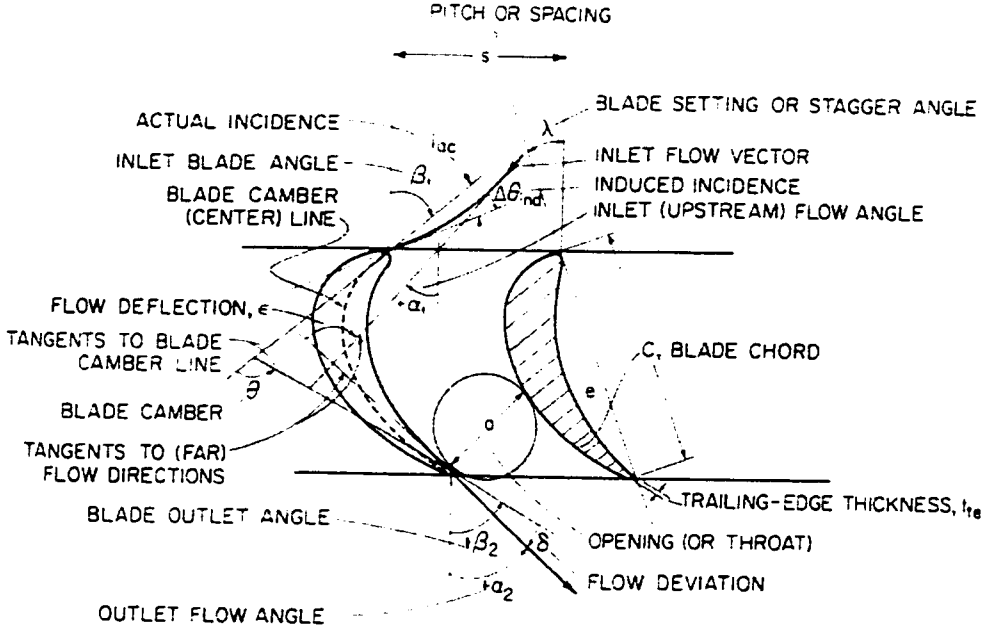

Fig. I.1 Blade section terminology [41].

The chord is defined as the straight line joining the leading and trailing edges. The airfoil chord makes a certain angle with respect to the axial direction. This angle is designated the blade stagger angle, λ. If the tangents to the camber line at the leading and trailing edges are extrapolated the angle included between these lines is termed the camber angle, θ. The distance between blade leading and trailing edges is the chord length, c, and that between the edges of two adjacent blades is the pitch or spacing, s. In this paper we use the pitch-chord ratio, s/c, following the British cascade practice, whereas American practice uses the solidity, c/s.

The incidence angle, i, is defined as the difference between the flow and blade angles at inlet, i. e.

$$i = \alpha_1 - \beta_1 \tag{I.1}$$

In general there will be an underturning of the fluid by the blade row; accordingly a deviation angle, δ, is defined for discharge angles, i. e.

$$\delta = \beta_2 - \alpha_2 \tag{I.2}$$

A fluid deflection angle, also often called turning angle, ε, is defined as

$$\varepsilon = \alpha_1 + \alpha_2 \tag{I.3}$$

It is noted that flow angles α_1 and α_2 shown in Fig. 1.14 are designated positive flow angles.

I.2 Velocity Triangle

Fig. I.2 shows the velocity triangles for one axial flow turbine stage and the nomenclature employed. The preliminary analysis of a turbine stage always begins with the velocity triangles (velocity vectors). The gas approaches the row of nozzle blades (more often called "vanes" in case of nozzle or stator) with total temperature and pressure T_1 and P_1 and velocity C_1 inclined to the axis at angle α_1, then is expanded to P_2, T_2 and leaves with an increased velocity C_2 at an angle α_2. The rotor blade inlet angle will be chosen to suit the direction β_2 of the gas velocity V_2 relative to the blade at inlet. β_2 and V_2 are found by vectorial subtraction of the blade speed U from the absolute velocity C_2. After being deflected and usually further expanded, in the rotor blade passages, the gas leaves at P_3, T_3 with relative velocity V_3 at angle β_3. Vectorial addition of U yields the magnitude and direction of the gas velocity at exit from the stage, C_3 and α_3. α_3 is known as the stage exit swirl angle.

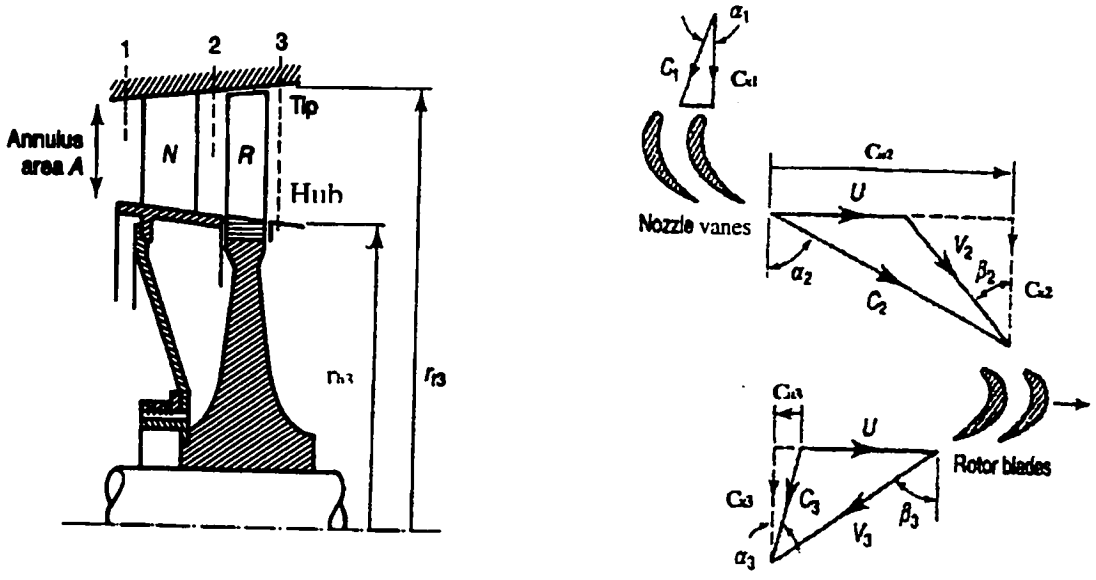

Fig. I.2 Axial flow turbine stage and velocity triangles

I.3 Turbine Isentropic Efficiency

In conventional turbines, the flow through a stage can be regarded as adiabatic since heat losses are usually small in relation to work outputs. The performance of the flow can be represented in an enthalpy-entropy or a temperature-entropy diagram in Fig. I.3. An ideal process (no losses) through the turbine stage is from point 1 to 3' and a real process (with losses) is from point 1 to 3. The difference between the ideal and real points 3' and 3 at the exit of the turbine stage is mainly caused by the losses in the flow described in the previous section. In turbines, the term efficiency is used to evaluate quantitatively how effectively the flow is expanded through the turbine or, in another words, what percent of the total work available can be achieved after losses are considered.

Traditionally the efficiency calculated for turbines can be total-to-total, total-to-static or static-to-static efficiency:

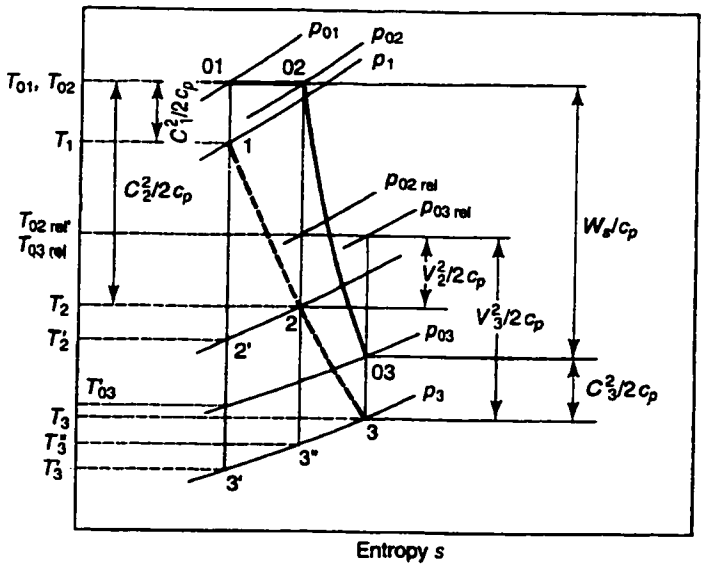

Fig. I.3 T – s diagram for a reaction stage [7].

Total-to-total efficiency: $$\eta_{tt} = \frac{T_{01} - T_{03}}{T_{01} - T_{03}'} \quad \text{(I.4)}$$

Total-to-static efficiency: $$\eta_{ts} = \frac{T_{01} - T_{03}}{T_{01} - T_{3}'} \quad \text{(I.5)}$$

Static-to-static efficiency: $$\eta_{ss} = \frac{T_{1} - T_{3}}{T_{1} - T_{3}'} \quad \text{(I.6)}$$

The total-to-total efficiency should generally be used in multi-stage turbines where the exhaust velocity from a stage is not lost. The total-to-static efficiency is used when the exit velocity is not recovered, such as the single stage turbine and the last stage in a multi-stage turbine. For a turbine stage where the inlet and outlet velocities are approximately the same, the total-to-total efficiency can be regarded as the same as the static-to-static efficiency.

I.4 Loss Coefficient

There are many different definitions of loss coefficient in regular use for turbine blades. But the most common ones are the stagnation pressure loss coefficient and the energy or enthalpy loss coefficient.

Stagnation pressure loss coefficient (used by AMDCKO and in this work):

Nozzle: $$Y_N = \frac{p_{01} - p_{02}}{p_{02} - p_2} \quad \text{(I.7)}$$

Rotor: $$Y_R = \frac{p_{02rel} - p_{03rel}}{p_{03rel} - p_3} \quad \text{(I.8)}$$

Energy (enthalpy) loss coefficient:

Nozzle: $$\zeta_N = \frac{h_2 - h_{2s}}{h_{02} - h_2} = \frac{h_2 - h_{2s}}{\frac{1}{2}C_2^2} \tag{I.9}$$

Rotor: $$\zeta_R = \frac{h_3 - h_{3s}}{h_{03rel} - h_3} = \frac{h_3 - h_{3s}}{\frac{1}{2}V_3^2} \tag{I.10}$$

Sometimes another kind of energy loss coefficient, in terms of isentropic velocity, is used. It is defined as:

$$\xi = \frac{h_2 - h_{2s}}{h_{02} - h_{2s}} = 1 - \frac{C_2^2}{C_{2s}^2} = 1 - \phi^2 \tag{I.11}$$

where ϕ is the velocity coefficient, i.e., the ratio of the blade outlet velocity to the velocity which could be attained in an isentropic expansion from inlet conditions to the actual outlet pressure.

The relationship between the two kinds of energy loss coefficients ζ and ξ is

$$\xi = \frac{\zeta}{1+\zeta} \tag{I.12}$$

and the relationship between the stagnation pressure and energy loss coefficients Y and ξ is

$$Y = \frac{\left[1 - \frac{\gamma - 1}{2} M_2^2 \left(\frac{1}{1-\xi} - 1\right)\right]^{\frac{\gamma}{\gamma-1}} - 1}{1 - \left(1 + \frac{\gamma - 1}{2} M_2^2\right)^{\frac{\gamma}{\gamma-1}}} \tag{I.13}$$

A more recent loss coefficient was defined by Denton [10] in terms of entropy. It is called entropy loss coefficient,

$$\zeta_s = \frac{T_2 \Delta s}{h_{02} - h_2} \tag{1.14}$$

Denton [10] also proved that the numerical value difference between the energy and entropy loss coefficients (ζ and ζ_s) is of the order of 10^{-3} and so is always negligible.

I.5 Reaction

A turbine stage is composed of a rotating and a stationary component and expansion may occur in both. An important design parameter is the way in which the expansion is shared between the two, and this is determined by the degree of reaction of the stage. Reaction can be defined as the ratio of the static enthalpy change in the rotor to the total enthalpy change across the stage:

$$\Lambda = \frac{\Delta h_{rotor}}{\Delta h_{0,stage}} \tag{I.15}$$

Thus a high degree of reaction implies that most of the enthalpy change, and hence the expansion occurs in the rotor. Conversely, a low degree of reaction implies that little enthalpy change occurs in the rotor and the majority takes place in the stator. This has strong implications for gas turbine design.

There are also a lot of occasions where reaction is defined in terms of static pressure drop, namely the ratio of that across the blade to that of the stage:

$$R = \frac{p_2 - p_3}{p_1 - p_3} \tag{I.16}$$

In this work, when reaction is mentioned, it refers to this static pressure-based reaction R, where otherwise stated.

Appendix II

Turbine Stage Aerodynamic and Geometric Data

Appendix II: Turbine Stage Aerodynamic and Geometric Data

Table II.1 Aerodynamic and Geometric Data, T2

R/Ropt	Eta/Eta,ref	PR	Yp/Yref Vane	Ys/Yref Vane	Yte/Yref Vane	Yp/Yref Blade	Ys/Yref Blade	Ycl/Yref Blade	Yte/Yref Blade
0.4	0.97582	3.499	0.09357	0.27658	0.04965	0.32463	0.93635	0.18046	0.00923
0.5	0.98228	3.4655	0.08721	0.2613	0.05124	0.30904	0.85041	0.17823	0.01082
0.6	0.98697	3.4419	0.08498	0.25684	0.05188	0.29631	0.76862	0.17473	0.01273
0.8	0.99108	3.4215	0.0853	0.2578	0.05188	0.28262	0.69351	0.17123	0.01464
0.9	0.99542	3.4007	0.08593	0.25939	0.05156	0.2683	0.6254	0.16741	0.01687
1	1	3.3787	0.08721	0.26066	0.05092	0.25271	0.56429	0.16359	0.01941
1.1	1.00481	3.3559	0.09039	0.2613	0.05029	0.23456	0.50923	0.15977	0.02196
1.3	1.00998	3.3323	0.09675	0.26194	0.04901	0.21419	0.45926	0.15595	0.02482
1.4	1.01526	3.3089	0.10439	0.26194	0.04742	0.19383	0.4147	0.15213	0.02801
1.5	1.02089	3.2834	0.10757	0.26194	0.04583	0.17346	0.3746	0.14799	0.03183
1.6	1.02699	3.2573	0.10407	0.26162	0.04424	0.15404	0.34182	0.14418	0.03565
1.8	1.03239	3.2346	0.09835	0.26098	0.04233	0.1359	0.31795	0.14036	0.0401
1.9	1.03615	3.219	0.09421	0.26003	0.0401	0.12094	0.30395	0.13622	0.04424
2	1.03767	3.2131	0.09262	0.25843	0.03756	0.11203	0.29981	0.13176	0.04838
2.1	1.03568	3.2221	0.09293	0.25652	0.03501	0.11553	0.30777	0.12667	0.05124

R/Ropt	alfa1	alfa2	beta2	beta3	Tng,n	Tng,r	C1	C2	V2	V3	M1	M2	Mr2	Mr3	M2-M1	Mr3-Mr2
0.3	-25.3	71.94	57.55	54.36	46.64	111.91	362.67	2880.19	1556.68	1660.74	0.1573	1.4311	0.7741	0.8315	1.2738	0.0574
0.4	-25.3	72.86	57.88	56.63	47.56	114.51	362.67	2766.84	1442.8	1726.36	0.1573	1.3582	0.7095	0.864	1.2009	0.1545
0.5	-25.3	73.49	57.76	58.39	48.19	116.15	362.67	2663.88	1341.01	1796.49	0.1573	1.2942	0.6531	0.8992	1.1369	0.2461
0.6	-25.3	73.94	57.3	59.84	48.64	117.14	362.67	2566.37	1246.19	1869.15	0.1573	1.2353	0.6016	0.9362	1.0781	0.3346
0.8	-25.3	74.27	56.54	61.07	48.97	117.61	362.67	2472.33	1156.07	1943.19	0.1573	1.18	0.5537	0.9744	1.0228	0.4207
0.9	-25.3	74.52	55.5	62.15	49.22	117.65	362.67	2381.4	1070.1	2017.41	0.1572	1.1278	0.5088	1.013	0.9706	0.5042
1	-25.3	74.7	54.16	63.1	49.4	117.25	362.67	2292.72	987.54	2091.96	0.1572	1.0781	0.4663	1.0522	0.9208	0.5859
1.1	-25.3	74.82	52.44	63.93	49.52	116.37	362.67	2205.48	907.84	2167.28	0.1572	1.0301	0.426	1.0923	0.8729	0.6663
1.3	-25.3	74.87	50.26	64.67	49.57	114.93	362.67	2118.88	830.61	2243.9	0.1572	0.9834	0.3874	1.1335	0.8262	0.7462
1.4	-25.3	74.86	47.54	65.31	49.56	112.84	362.67	2032.88	756.34	2321.66	0.1572	0.9378	0.3507	1.176	0.7806	0.8253
1.5	-25.3	74.8	44.15	65.86	49.5	110.02	362.67	1947.93	685.57	2399.9	0.1572	0.8936	0.3162	1.2194	0.7364	0.9032
1.6	-25.3	74.7	39.98	66.34	49.4	106.32	362.67	1864.04	619.15	2478.78	0.1572	0.8506	0.2841	1.2638	0.6935	0.9796
1.8	-25.3	74.54	34.74	66.69	49.24	101.44	362.67	1780.3	557.78	2559.62	0.1572	0.8084	0.2548	1.3101	0.6512	1.0553
1.9	-25.3	74.31	28.09	66.9	49.01	94.99	362.67	1695.81	502.76	2644.3	0.1572	0.7664	0.2286	1.3596	0.6092	1.131
2	-25.3	73.99	19.68	66.93	48.69	86.61	362.66	1609.85	456.51	2734.52	0.1571	0.7242	0.2066	1.4137	0.567	1.207
2.1	-25.3	73.58	9.34	66.69	48.28	76.03	362.66	1522.1	422.7	2832.52	0.1571	0.6817	0.1905	1.4741	0.5245	1.2836

Table II.1 Aerodynamic and Geometric Data, T2 (continued)

R/Ropt	Cxm,n	Cxm,r	Rv(2)	Rb(2)	Du,n	Du,r	phi	psi	Z3d,n	Z3d,r	stag,n	stag,r	Rv(1)	Rb(1)
0.3	610.45	901.52	0.9841	0.1214	4.2317	2.9542	0.6678	1.9835	1.1615	1.5806	62.22	18.57	0.8741	0.0627
0.4	571.61	858.32	0.9828	0.3015	4.3543	3.1035	0.6358	1.9836	1.1071	1.435	62.74	20.75	0.8689	0.1643
0.5	542.44	828.43	0.9815	0.4428	4.4228	3.216	0.6137	1.9835	1.0688	1.3141	63.09	22.52	0.8639	0.2535
0.6	518.89	806.21	0.98	0.5555	4.4542	3.3053	0.5972	1.9833	1.0403	1.2109	63.34	24.08	0.8587	0.3333
0.8	498.99	788.69	0.9785	0.6461	4.4586	3.3793	0.5842	1.9835	1.0185	1.1213	63.53	25.52	0.8533	0.4051
0.9	481.68	774.29	0.9768	0.7186	4.4429	3.4427	0.5736	1.9835	1.0013	1.0431	63.66	26.9	0.8477	0.4696
1	466.38	762.42	0.975	0.7772	4.4095	3.4969	0.5648	1.9835	0.9881	0.9743	63.76	28.26	0.8418	0.5279
1.1	452.76	752.86	0.973	0.8245	4.3588	3.5418	0.5577	1.9835	0.9785	0.9133	63.82	29.64	0.8356	0.5811
1.3	440.52	745.47	0.9707	0.863	4.2913	3.5775	0.5522	1.9835	0.9724	0.8588	63.85	31.08	0.8288	0.6298
1.4	429.42	740.24	0.9682	0.8939	4.2087	3.6033	0.5484	1.9835	0.9694	0.8105	63.85	32.59	0.8216	0.6742
1.5	419.27	736.59	0.9653	0.9184	4.1138	3.6216	0.5456	1.9834	0.969	0.7675	63.81	34.22	0.8138	0.7143
1.6	409.85	734.64	0.9621	0.9376	4.0088	3.632	0.5442	1.9835	0.9707	0.7294	63.76	35.97	0.8054	0.7502
1.8	401.19	735.51	0.9585	0.9525	3.8907	3.6283	0.5448	1.9835	0.9753	0.6963	63.67	37.83	0.7963	0.7821
1.9	393.23	740.45	0.9543	0.9639	3.7577	3.6047	0.5485	1.9835	0.9834	0.6683	63.55	39.78	0.7861	0.8099
2	385.88	750.77	0.9492	0.9721	3.6085	3.5557	0.5562	1.9835	0.9952	0.6456	63.37	41.74	0.7747	0.8331
2.1	379.05	769.05	0.9432	0.9777	3.4429	3.4716	0.5697	1.9834	1.0112	0.6294	63.14	43.52	0.7617	0.8508

R/Ropt	pitch,n	pitch,r	chord,n	chord,r	S/C,n	S/C,r	AR,n	AR,r	Tmax/C	,, ,, ,r	Tet/O,n	Tet/O,r	O,n	O,r
0.3	1.9259	0.6179	1.9308	0.7965	0.9975	0.7758	0.5487	1.4194	0.1529	0.2252	0.0821	0.0555	0.5971	0.3601
0.4	1.9259	0.6179	1.9649	0.8073	0.9801	0.7654	0.5392	1.4003	0.154	0.2328	0.0863	0.0589	0.5675	0.3398
0.5	1.9259	0.6179	1.9887	0.8173	0.9684	0.756	0.5328	1.3832	0.1547	0.2378	0.0895	0.0618	0.5473	0.3238
0.6	1.9259	0.6179	2.006	0.8269	0.9601	0.7472	0.5282	1.3671	0.1552	0.2408	0.092	0.0644	0.5327	0.3105
0.8	1.9259	0.6179	2.0188	0.8366	0.954	0.7386	0.5248	1.3512	0.1556	0.2423	0.0939	0.0669	0.522	0.2989
0.9	1.9259	0.6179	2.0286	0.8466	0.9494	0.7299	0.5223	1.3353	0.1559	0.2424	0.0953	0.0693	0.5139	0.2887
1	1.9259	0.6179	2.0356	0.8572	0.9461	0.7209	0.5205	1.3189	0.1561	0.2412	0.0964	0.0715	0.5081	0.2796
1.1	1.9259	0.6179	2.0401	0.8687	0.944	0.7113	0.5193	1.3014	0.1563	0.2384	0.0971	0.0737	0.5044	0.2715
1.3	1.9259	0.6179	2.0421	0.8815	0.9431	0.701	0.5188	1.2824	0.1563	0.234	0.0975	0.0757	0.5028	0.2643
1.4	1.9259	0.6179	2.0418	0.8961	0.9432	0.6895	0.5189	1.2616	0.1563	0.2279	0.0974	0.0775	0.503	0.2581
1.5	1.9259	0.6179	2.0395	0.9131	0.9443	0.6767	0.5195	1.2381	0.1562	0.2199	0.0971	0.0792	0.5049	0.2527
1.6	1.9259	0.6179	2.0356	0.9329	0.9461	0.6624	0.5205	1.2119	0.1561	0.2102	0.0964	0.0806	0.5081	0.248
1.8	1.9259	0.6179	2.0293	0.9559	0.9491	0.6464	0.5221	1.1826	0.1559	0.1983	0.0955	0.0818	0.5133	0.2445
1.9	1.9259	0.6179	2.0202	0.9825	0.9533	0.6289	0.5244	1.1506	0.1557	0.1844	0.0941	0.0825	0.5208	0.2424
2	1.9259	0.6179	2.008	1.0118	0.9591	0.6107	0.5276	1.1173	0.1553	0.1689	0.0923	0.0826	0.531	0.2422
2.1	1.9259	0.6179	1.9921	1.0411	0.9668	0.5935	0.5318	1.0858	0.1548	0.1532	0.09	0.0818	0.5444	0.2445

Table II.2 Aerodynamic and Geometric Data, T45

R/Ropt	Eta/Eta,ref	PR	Yp/Yref Vane	Ys/Yref Vane	Yte/Yref Vane	Yp/Yref Blade	Ys/Yref Blade	Ycl/Yref Blade	Yte/Yref Blade
0.3	0.97591	2.9173	0.08668	0.41418	0.05551	0.25833	1.11272	0.33049	0.01665
0.4	0.98098	2.8988	0.08369	0.39368	0.05679	0.22502	1.00811	0.32921	0.02092
0.6	0.9849	2.8851	0.08412	0.39026	0.05722	0.20239	0.90521	0.32536	0.02519
0.7	0.9887	2.8718	0.08582	0.39283	0.05722	0.1883	0.81255	0.32024	0.03032
0.8	0.99251	2.8584	0.08711	0.39496	0.05636	0.1772	0.73015	0.31554	0.03544
0.9	0.99631	2.8457	0.08967	0.39624	0.05594	0.16482	0.6567	0.31042	0.04099
1.0	1	2.8331	0.09436	0.3971	0.05465	0.1503	0.59223	0.30529	0.0474
1.1	1.00369	2.821	0.10162	0.3971	0.05337	0.13493	0.53459	0.29974	0.05423
1.2	1.00772	2.8077	0.10717	0.3971	0.05167	0.11998	0.48377	0.29419	0.06191
1.3	1.0121	2.7939	0.1076	0.39624	0.04996	0.10547	0.43894	0.28907	0.0696
1.4	1.01602	2.7814	0.10248	0.39539	0.04825	0.09223	0.3988	0.28395	0.07857
1.6	1.01936	2.7709	0.09607	0.39411	0.04611	0.08155	0.36336	0.27882	0.08711
1.7	1.02213	2.7624	0.09137	0.39197	0.04355	0.07472	0.33219	0.27284	0.09564
1.8	1.0242	2.7561	0.08839	0.38941	0.04142	0.07259	0.30401	0.26729	0.10376
1.9	1.02593	2.7506	0.08668	0.38599	0.03843	0.07344	0.28053	0.26089	0.11016

R/Ropt	alfa1	alfa2	beta2	beta3	Tng,n	Tng.r	C1	C2	V2	V3	M1	M2	Mr2	Mr3	M2-M1	Mr3-Mr2
0.2	-10	68.66	48.76	49.48	58.66	98.25	354.19	2792.85	1419.46	1531.62	0.1508	1.3447	0.6831	0.7423	1.1939	0.0591
0.3	-10	69.47	48.3	52.18	59.47	100.48	354.19	2677.77	1306.91	1591.39	0.1508	1.2748	0.6225	0.7701	1.124	0.1476
0.4	-10	70.02	47.36	54.4	60.02	101.76	354.19	2572.09	1206.4	1655.74	0.1508	1.2126	0.5694	0.8004	1.0618	0.231
0.6	-10	70.41	46.04	56.27	60.41	102.31	354.19	2473.87	1114.94	1722.17	0.1508	1.1564	0.5221	0.8321	1.0056	0.3101
0.7	-10	70.69	44.36	57.89	60.69	102.25	354.19	2380.72	1030.33	1789.13	0.1508	1.1043	0.479	0.8644	0.9535	0.3854
0.8	-10	70.88	42.28	59.32	60.88	101.59	354.19	2291.16	951.39	1856.72	0.1508	1.0554	0.4394	0.8972	0.9046	0.4578
0.9	-10	70.99	39.73	60.57	60.99	100.3	354.19	2204.36	877.67	1925.29	0.1508	1.0089	0.4028	0.9307	0.8581	0.5279
1	-10	71.03	36.65	61.68	61.03	98.33	354.19	2119.56	808.99	1994.51	0.1508	0.9643	0.3692	0.9649	0.8135	0.5957
1.1	-10	71	32.96	62.66	61	95.62	354.19	2036.42	745.53	2064.8	0.1508	0.9213	0.3384	0.9999	0.7705	0.6615
1.2	-10	70.91	28.59	63.53	60.91	92.12	354.19	1954.82	687.84	2135.27	0.1508	0.8798	0.3107	1.0354	0.729	0.7247
1.3	-10	70.77	23.44	64.31	60.77	87.75	354.19	1874.41	636.61	2206.3	0.1508	0.8395	0.2862	1.0715	0.6887	0.7853
1.4	-10	70.56	17.39	64.99	60.56	82.38	354.19	1794.28	592.83	2278.84	0.1508	0.7999	0.2654	1.1088	0.6491	0.8434
1.6	-10	70.27	10.33	65.58	60.27	75.91	354.19	1713.93	557.84	2353.87	0.1508	0.7607	0.2486	1.1478	0.6099	0.8992
1.7	-10	69.88	2.29	66.06	59.88	68.35	354.19	1632.47	533.46	2432.01	0.1508	0.7215	0.2368	1.189	0.5707	0.9522
1.8	-10	69.39	-6.55	66.46	59.39	59.91	354.19	1549.5	521.68	2513.85	0.1508	0.682	0.2307	1.2329	0.5313	1.0022
1.9	-10	68.77	-15.86	66.77	58.77	50.91	354.19	1464.21	524.26	2600.1	0.1508	0.642	0.2309	1.2799	0.4912	1.0489

Table II.2 Aerodynamic and Geometric Data, T45 (continued)

R/Ropt	Cxm,n	Cxm,r	Rv**2	Rb**2	Du,n	Du,r	phi	psi	Z3d,n	Z3d,r	stag,n	stag,r	Rv**1	Rb**1
0.2	682.62	965.35	0.9839	0.1411	3.7207	2.3119	0.6563	1.5405	1.0415	1.8189	57.16	19.99	0.8732	0.0732
0.3	643.86	922.59	0.9825	0.3256	3.7994	2.4203	0.6272	1.5405	1.008	1.6522	57.68	23.04	0.8677	0.1788
0.4	613.74	890.53	0.981	0.4691	3.8385	2.5083	0.6054	1.5403	0.9846	1.5074	58.03	25.63	0.8623	0.2714
0.6	589.08	865.09	0.9795	0.5809	3.8521	2.5834	0.5881	1.5405	0.9676	1.3824	58.27	27.89	0.8568	0.3526
0.7	567.98	843.79	0.9779	0.6684	3.8475	2.6498	0.5736	1.5404	0.955	1.2738	58.45	29.95	0.8512	0.4241
0.8	549.6	825.68	0.9761	0.7374	3.827	2.7091	0.5613	1.5404	0.946	1.1784	58.56	31.87	0.8454	0.4876
0.9	533.4	810.47	0.9742	0.7922	3.792	2.7612	0.551	1.5404	0.9403	1.0943	58.63	33.71	0.8393	0.5441
1	518.99	797.65	0.9721	0.8355	3.7436	2.8066	0.5423	1.5404	0.9377	1.0199	58.65	35.51	0.8329	0.5944
1.1	505.96	786.96	0.9697	0.8696	3.6839	2.846	0.535	1.5405	0.9377	0.9539	58.63	37.26	0.8261	0.6389
1.2	494.07	777.81	0.9672	0.8962	3.6145	2.8806	0.5288	1.5405	0.9399	0.895	58.58	39	0.8188	0.6779
1.3	483.12	770.19	0.9643	0.9167	3.536	2.9103	0.5236	1.5405	0.9444	0.8424	58.49	40.7	0.811	0.7115
1.4	473.04	764.52	0.961	0.9323	3.4468	2.933	0.5197	1.5405	0.9515	0.7954	58.36	42.34	0.8026	0.7399
1.6	463.77	761.04	0.9573	0.9438	3.346	2.9476	0.5174	1.5405	0.9616	0.7532	58.18	43.9	0.7933	0.763
1.7	455.16	759.85	0.9529	0.9519	3.2326	2.9535	0.5166	1.5404	0.9751	0.7153	57.94	45.36	0.783	0.7807
1.8	447.12	761.18	0.9478	0.9569	3.1062	2.9495	0.5175	1.5404	0.9923	0.6813	57.63	46.7	0.7714	0.7925
1.9	439.52	764.97	0.9415	0.9593	2.9653	2.9361	0.52	1.5403	1.0137	0.6505	57.23	47.91	0.7581	0.7984

R/Ropt	pitch,n	pitch,r	chord,n	chord,r	S/C,n	S/C,r	AR,n	AR,r	Tmax/C	''',	Tet/O,n	Tet/O,r	O,n	O,r
0.2	1.6538	0.601	1.7159	0.7077	0.9638	0.8493	0.4263	1.0521	0.1618	0.2045	0.0773	0.0692	0.6019	0.3904
0.3	1.6538	0.601	1.7405	0.7227	0.9502	0.8316	0.4203	1.0302	0.1627	0.2085	0.0802	0.0733	0.5799	0.3685
0.4	1.6538	0.601	1.7574	0.7376	0.9411	0.8148	0.4162	1.0094	0.1633	0.2109	0.0823	0.0772	0.565	0.3498
0.6	1.6538	0.601	1.7694	0.7524	0.9347	0.7988	0.4134	0.9895	0.1638	0.2119	0.0839	0.0809	0.5544	0.3337
0.7	1.6538	0.601	1.7782	0.7675	0.9301	0.7831	0.4114	0.9701	0.1641	0.2118	0.085	0.0845	0.5468	0.3194
0.8	1.6538	0.601	1.7841	0.7831	0.927	0.7675	0.41	0.9507	0.1643	0.2106	0.0858	0.088	0.5416	0.3067
0.9	1.6538	0.601	1.7876	0.7995	0.9252	0.7517	0.4092	0.9313	0.1644	0.2082	0.0863	0.0914	0.5387	0.2953
1	1.6538	0.601	1.7887	0.8169	0.9246	0.7357	0.409	0.9114	0.1645	0.2046	0.0865	0.0947	0.5377	0.2851
1.1	1.6538	0.601	1.7877	0.8356	0.9251	0.7192	0.4092	0.891	0.1644	0.1999	0.0863	0.0978	0.5385	0.276
1.2	1.6538	0.601	1.785	0.8557	0.9265	0.7024	0.4098	0.8701	0.1643	0.1941	0.086	0.1008	0.5409	0.2678
1.3	1.6538	0.601	1.7805	0.8771	0.9288	0.6852	0.4108	0.8488	0.1642	0.1872	0.0854	0.1037	0.5448	0.2605
1.4	1.6538	0.601	1.7739	0.8996	0.9323	0.668	0.4124	0.8276	0.1639	0.1793	0.0845	0.1063	0.5505	0.254
1.6	1.6538	0.601	1.7648	0.9229	0.9371	0.6512	0.4145	0.8067	0.1636	0.1706	0.0833	0.1087	0.5584	0.2485
1.7	1.6538	0.601	1.753	0.9465	0.9434	0.635	0.4173	0.7866	0.1632	0.1615	0.0817	0.1107	0.5689	0.2438
1.8	1.6538	0.601	1.7379	0.9696	0.9516	0.6198	0.4209	0.7678	0.1626	0.1523	0.0799	0.1125	0.5822	0.24
1.9	1.6538	0.601	1.7192	0.992	0.962	0.6058	0.4255	0.7505	0.1619	0.1435	0.0776	0.1139	0.5989	0.2371

Table II.3 Aerodynamic and Geometric Data, T9

R/Ropt	Eta/Eta,ref	PR	Yp/Yref Vane	Ys/Yref Vane	Yte/Yref Vane	Yp/Yref Blade	Ys/Yref Blade	Ycl/Yref Blade	Yte/Yref Blade
0.3	0.95891	2.0714	0.09774	0.38722	0.07769	0.30326	1.44424	0.18108	0.03446
0.3	0.96447	2.062	0.10025	0.39098	0.07769	0.2688	1.29762	0.17794	0.04198
0.4	0.96947	2.0535	0.10213	0.39348	0.07644	0.24561	1.16729	0.17419	0.0495
0.5	0.97423	2.0457	0.10589	0.39536	0.07519	0.22494	1.05263	0.17105	0.05764
0.6	0.97866	2.0385	0.11216	0.39599	0.07393	0.20677	0.9505	0.16792	0.06642
0.7	0.98263	2.0321	0.1203	0.39599	0.07206	0.19236	0.8609	0.16416	0.07581
0.8	0.98695	2.0253	0.12469	0.39536	0.06955	0.17794	0.78133	0.16103	0.08584
0.9	0.99137	2.0185	0.12406	0.39411	0.06767	0.16291	0.71115	0.15789	0.09649
0.9	0.99591	2.0116	0.11842	0.39223	0.06516	0.14975	0.64912	0.15476	0.10777
1	1.00034	2.0048	0.1109	0.38972	0.06266	0.13596	0.59273	0.15163	0.11967
1.1	1.00454	1.9985	0.10464	0.38596	0.05952	0.12155	0.54198	0.1485	0.13283
1.2	1.00851	1.9927	0.10025	0.38158	0.05639	0.10777	0.49561	0.14474	0.14662
1.3	1.01192	1.9877	0.09712	0.37531	0.05326	0.09649	0.45363	0.1416	0.15977
1.4	1.01476	1.9835	0.09461	0.36842	0.05013	0.0896	0.41604	0.13784	0.17356
1.4	1.01703	1.9803	0.09148	0.35965	0.04637	0.08897	0.38158	0.13471	0.18546

R/Ropt	alfa1	alfa2	beta2	beta3	Tng,n	Tng.r	C1	C2	V2	V3	M1	M2	Mr2	Mr3	M2-M1	Mr3-Mr2
0.2	-25	68.61	49.08	45.8	43.61	94.88	451	2835.24	1421.95	1453.18	0.1773	1.229	0.6251	0.6397	1.0518	0.0145
0.3	-25	69.02	48.15	48.17	44.02	96.32	451	2731.1	1335.75	1504.74	0.1773	1.1745	0.5836	0.6619	0.9973	0.0783
0.3	-25	69.32	47.01	50.26	44.32	97.27	451	2633.54	1255.72	1557.7	0.1773	1.1246	0.5456	0.6849	0.9474	0.1393
0.4	-25	69.53	45.66	52.08	44.53	97.75	451	2541.31	1181.23	1611.59	0.1773	1.0784	0.5106	0.7084	0.9011	0.1978
0.5	-25	69.66	44.09	53.71	44.66	97.8	451	2452.74	1111.1	1666.49	0.1773	1.0348	0.4781	0.7326	0.8575	0.2545
0.6	-25	69.72	42.26	55.16	44.72	97.42	451	2366.98	1044.84	1722.47	0.1773	0.9932	0.4476	0.7573	0.8159	0.3097
0.7	-25	69.72	40.14	56.46	44.72	96.6	451	2283.55	982.25	1779.39	0.1773	0.9534	0.4191	0.7826	0.7762	0.3635
0.8	-25	69.66	37.71	57.64	44.66	95.35	451	2201.49	922.79	1837.01	0.1773	0.9149	0.3922	0.8083	0.7376	0.4161
0.9	-25	69.56	34.94	58.72	44.56	93.66	451	2121.09	867	1895.33	0.1773	0.8776	0.3672	0.8345	0.7003	0.4673
0.9	-25	69.4	31.77	59.69	44.4	91.47	451	2041.83	814.72	1954.39	0.1773	0.8413	0.3439	0.8612	0.664	0.5174
1	-25	69.18	28.12	60.59	44.18	88.71	451	1962.85	766.16	2014.81	0.1773	0.8056	0.3223	0.8887	0.6283	0.5664
1.1	-25	68.9	23.89	61.41	43.9	85.3	451	1883.35	721.67	2077.36	0.1773	0.77	0.3027	0.9173	0.5928	0.6147
1.2	-25	68.53	19	62.15	43.53	81.16	451	1802.96	682.08	2142.26	0.1773	0.7345	0.2852	0.9473	0.5572	0.6621
1.3	-25	68.07	13.39	62.83	43.07	76.22	451	1721.19	648.4	2210.03	0.1772	0.6987	0.2703	0.9789	0.5215	0.7085
1.4	-25	67.5	7.01	63.43	42.5	70.45	451	1637.58	622.02	2281.17	0.1772	0.6625	0.2586	1.0123	0.4853	0.7537
1.4	-25	66.79	-0.12	63.97	41.79	63.85	451	1551.35	604.55	2356.49	0.1772	0.6255	0.2506	1.048	0.4483	0.7974

Table II.3 Aerodynamic and Geometric Data, T9 (continued)

R/Ropt	Cxm,n	Cxm,r	Rv-2	Rb-2	Du,n	Du,r	phi	psi	Z3d,n	Z3d,r	stag,n	stag,r	Rv-1	Rb-1
0.2	721.45	972.23	0.9747	0.0425	3.395	2.1767	0.7689	1.6737	0.7157	1.8465	51.74	15.39	0.8409	0.0215
0.3	693.29	947.36	0.9727	0.212	3.4032	2.2338	0.7492	1.6738	0.7025	1.7058	52.03	18.37	0.8349	0.1123
0.3	669.41	926.07	0.9707	0.3501	3.3959	2.2852	0.7324	1.6738	0.6923	1.5798	52.25	21	0.8287	0.1939
0.4	648.82	907.92	0.9685	0.4628	3.3756	2.3309	0.718	1.6738	0.6845	1.4677	52.39	23.33	0.8225	0.267
0.5	630.72	892.22	0.9662	0.5555	3.3441	2.372	0.7056	1.6737	0.6788	1.3671	52.49	25.44	0.8161	0.3333
0.6	614.63	878.68	0.9637	0.632	3.3022	2.4085	0.6949	1.6737	0.6749	1.2766	52.53	27.39	0.8095	0.3934
0.7	600.19	867.05	0.961	0.6953	3.2512	2.4408	0.6857	1.6737	0.6725	1.1953	52.53	29.2	0.8025	0.448
0.8	586.97	856.65	0.958	0.7477	3.192	2.4702	0.6775	1.6735	0.6715	1.1214	52.49	30.94	0.7951	0.4977
0.9	574.8	847.48	0.9548	0.7907	3.1262	2.4972	0.6702	1.6736	0.6717	1.0546	52.42	32.59	0.7874	0.5426
0.9	563.57	839.42	0.9512	0.8262	3.0532	2.5212	0.6639	1.6737	0.673	0.9938	52.3	34.18	0.7791	0.5831
1	553.15	832.56	0.9472	0.8554	2.9723	2.5419	0.6584	1.6737	0.6756	0.9381	52.15	35.73	0.7702	0.6197
1.1	543.44	827	0.9427	0.8793	2.8824	2.559	0.654	1.6737	0.6796	0.8867	51.94	37.24	0.7605	0.6526
1.2	534.36	822.77	0.9374	0.8986	2.7832	2.5722	0.6507	1.6737	0.6851	0.8392	51.68	38.71	0.7499	0.6816
1.3	525.83	819.97	0.9313	0.9139	2.6739	2.5809	0.6485	1.6737	0.6922	0.7953	51.35	40.11	0.738	0.7066
1.4	517.77	818.77	0.9242	0.9256	2.5538	2.5847	0.6475	1.6737	0.701	0.7546	50.93	41.44	0.7246	0.7273
1.4	510.1	819.3	0.9155	0.9342	2.4214	2.583	0.648	1.6737	0.7116	0.7167	50.41	42.69	0.7093	0.7435

R/Ropt	pitch,n	pitch,r	chord,n	chord,r	S/C,n	S/C,r	AR,n	AR,r	Tmax/C	''',	Tet/O,n	Tet/O,r	O,n	O,r
0.2	1.3473	0.7803	1.6956	0.8899	0.7946	0.8768	0.6538	1.1788	0.1347	0.2096	0.0814	0.0809	0.4914	0.5439
0.3	1.3473	0.7803	1.7067	0.9041	0.7894	0.8631	0.6495	1.1603	0.135	0.2117	0.0829	0.0846	0.4824	0.5203
0.3	1.3473	0.7803	1.7149	0.919	0.7856	0.849	0.6464	1.1414	0.1352	0.2131	0.0841	0.0882	0.4758	0.4988
0.4	1.3473	0.7803	1.7207	0.9344	0.783	0.8351	0.6442	1.1227	0.1354	0.2138	0.0849	0.0918	0.4712	0.4795
0.5	1.3473	0.7803	1.7243	0.9501	0.7814	0.8212	0.6429	1.104	0.1355	0.2139	0.0854	0.0953	0.4684	0.4618
0.6	1.3473	0.7803	1.726	0.9663	0.7806	0.8075	0.6422	1.0856	0.1356	0.2133	0.0856	0.0987	0.467	0.4458
0.7	1.3473	0.7803	1.726	0.9829	0.7806	0.7938	0.6423	1.0672	0.1356	0.2121	0.0856	0.1021	0.4671	0.4311
0.8	1.3473	0.7803	1.7244	1.0003	0.7813	0.78	0.6428	1.0487	0.1355	0.2103	0.0854	0.1054	0.4683	0.4176
0.9	1.3473	0.7803	1.7215	1.0183	0.7826	0.7662	0.6439	1.0301	0.1354	0.2079	0.085	0.1086	0.4706	0.4052
0.9	1.3473	0.7803	1.7172	1.0372	0.7846	0.7523	0.6455	1.0114	0.1353	0.2048	0.0844	0.1118	0.474	0.3937
1	1.3473	0.7803	1.7112	1.057	0.7873	0.7382	0.6478	0.9925	0.1351	0.2009	0.0835	0.1148	0.4788	0.3832
1.1	1.3473	0.7803	1.7033	1.0778	0.791	0.7239	0.6508	0.9733	0.1349	0.1962	0.0825	0.1178	0.4851	0.3734
1.2	1.3473	0.7803	1.6934	1.0995	0.7956	0.7096	0.6546	0.954	0.1346	0.1907	0.0811	0.1207	0.4932	0.3645
1.3	1.3473	0.7803	1.6811	1.1219	0.8014	0.6955	0.6594	0.935	0.1342	0.1844	0.0795	0.1235	0.5032	0.3563
1.4	1.3473	0.7803	1.666	1.1446	0.8087	0.6817	0.6654	0.9165	0.1337	0.1772	0.0776	0.1261	0.5157	0.3489
1.4	1.3473	0.7803	1.6477	1.1674	0.8177	0.6684	0.6728	0.8986	0.1332	0.1693	0.0753	0.1285	0.531	0.3424

Appendix III

Result Curves of Efficiency with Reaction

Fig. III.1 Result Curves of Stage Efficiency with Reaction

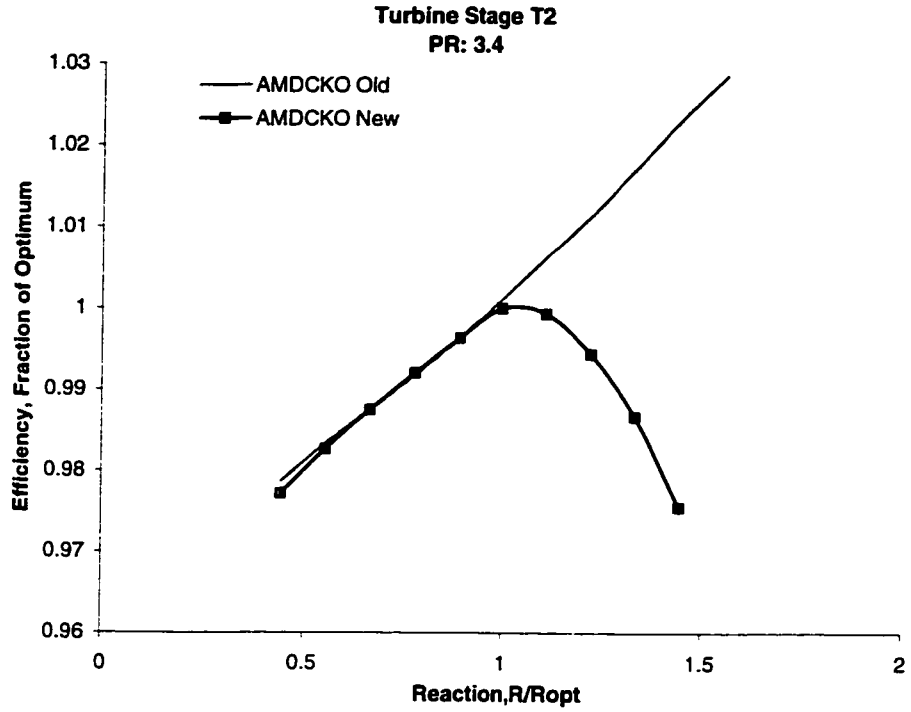

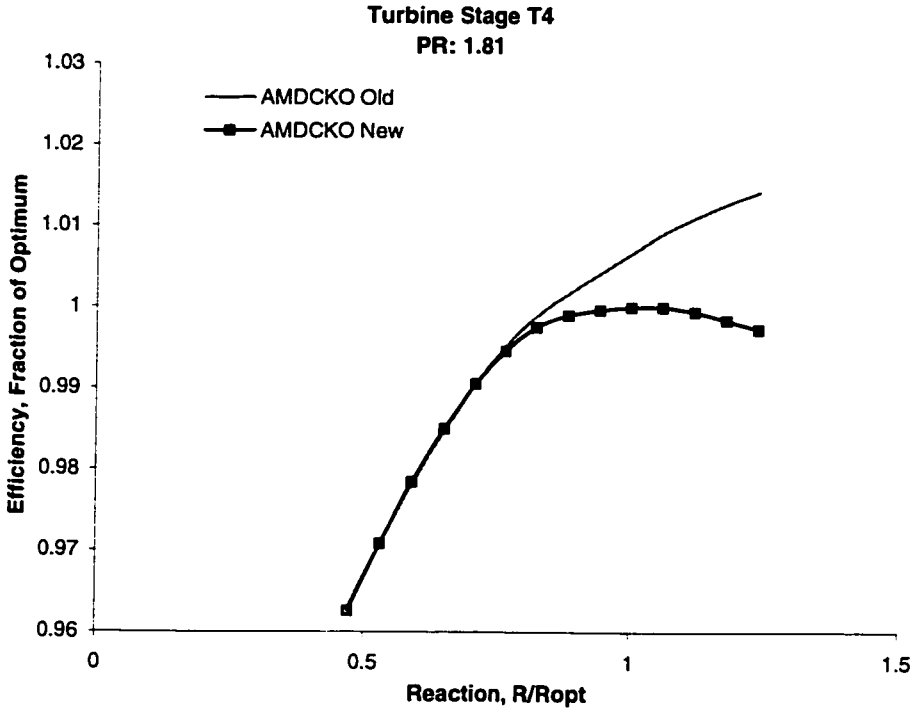

Fig. III.1 Result Curves of Stage Efficiency with Reaction (continued)

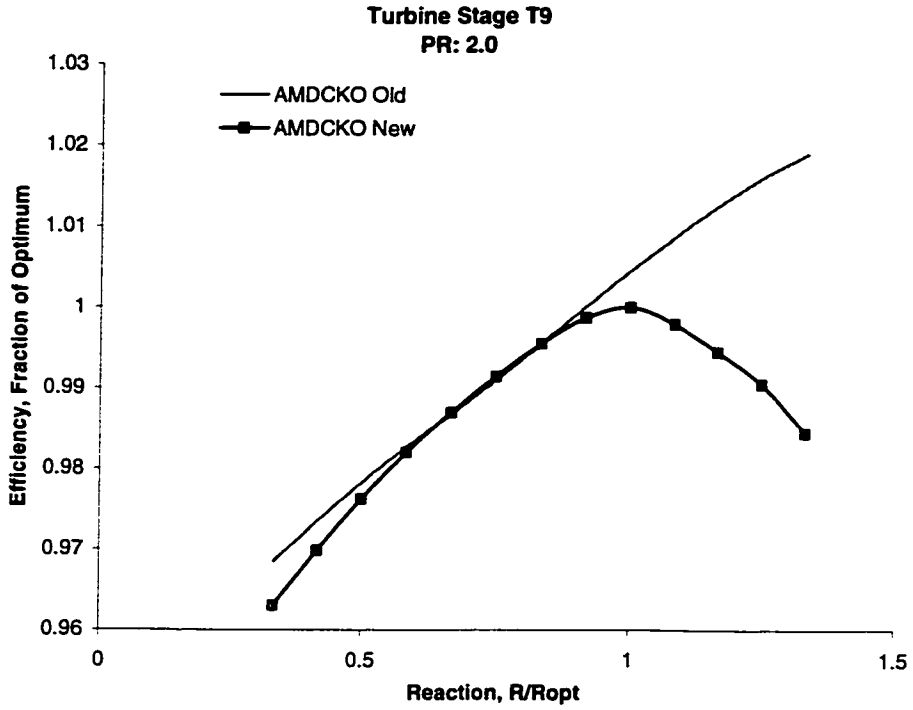

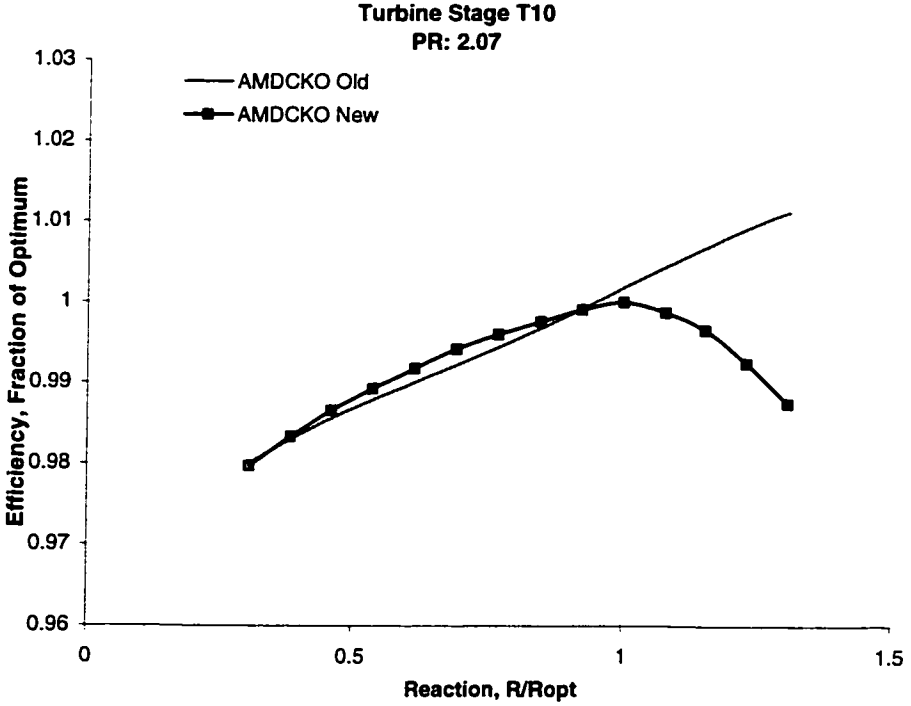

Fig. III.1 Result Curves of Stage Efficiency with Reaction (continued)

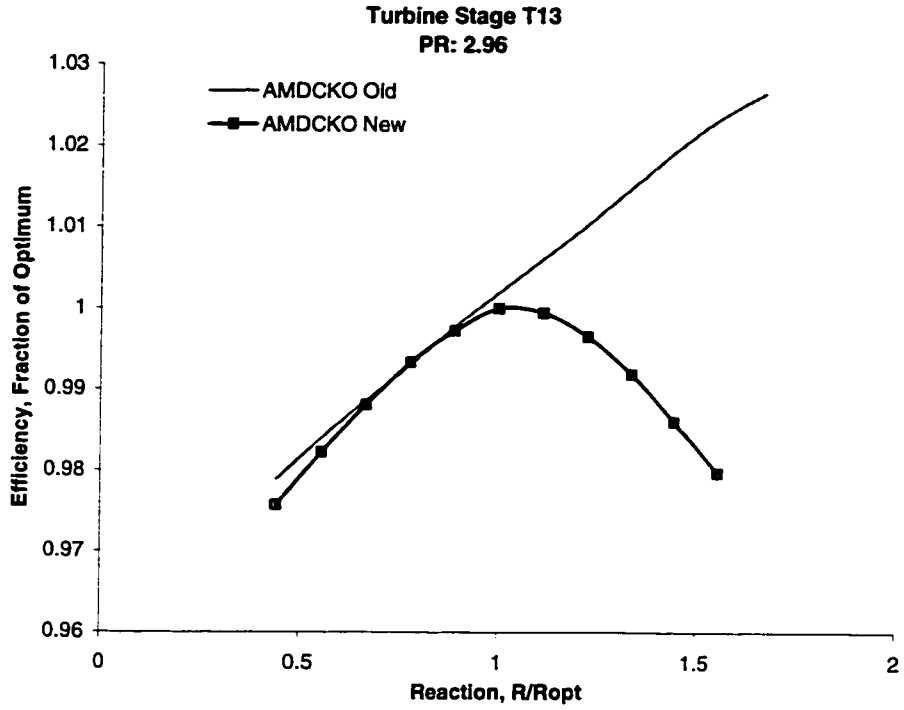

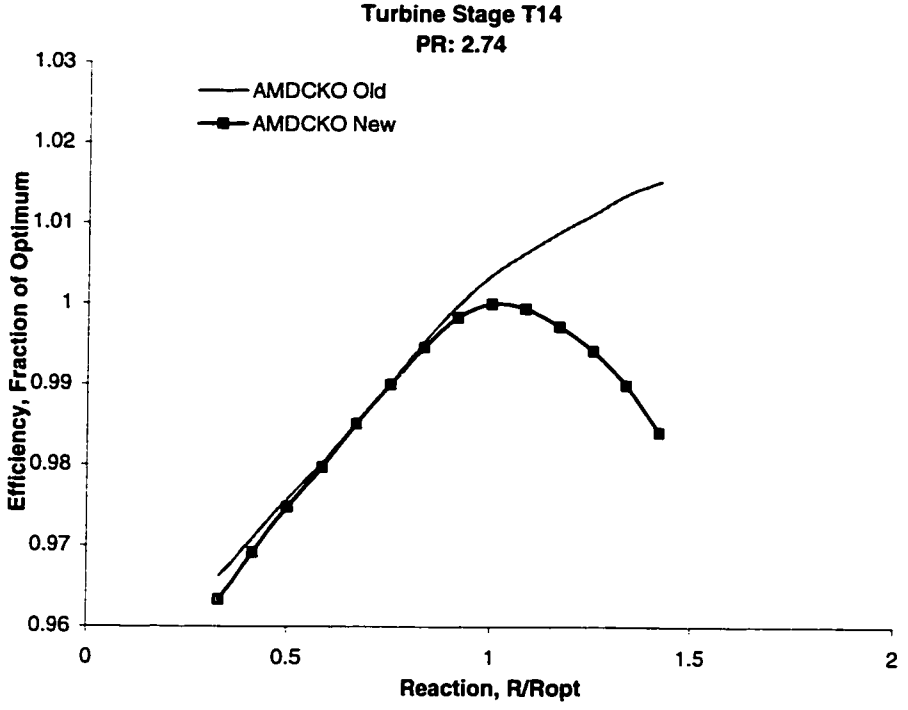

Fig. III.1 Result Curves of Stage Efficiency with Reaction (continued)

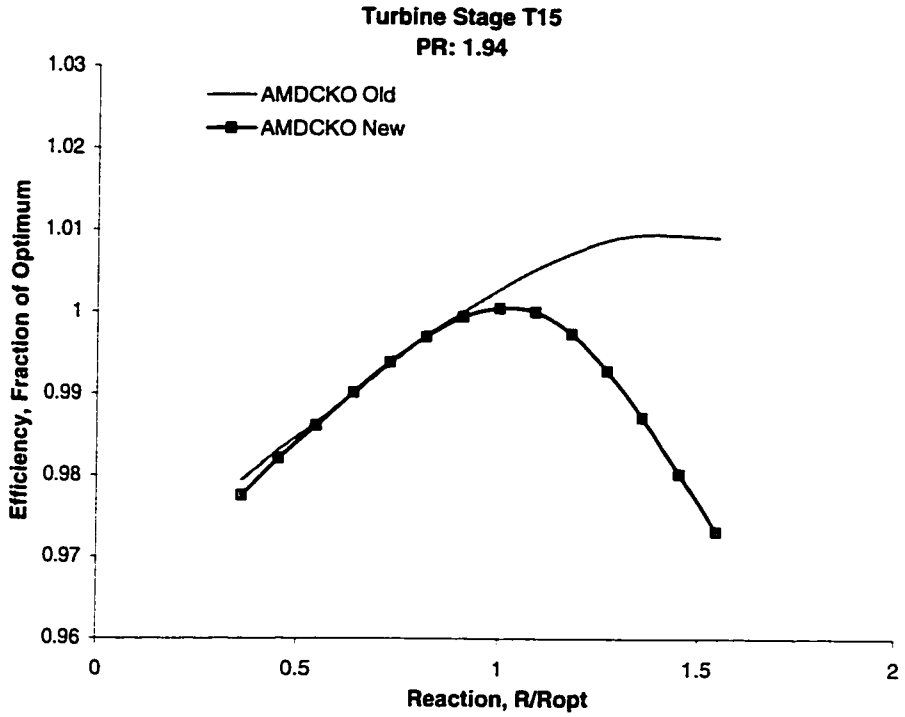

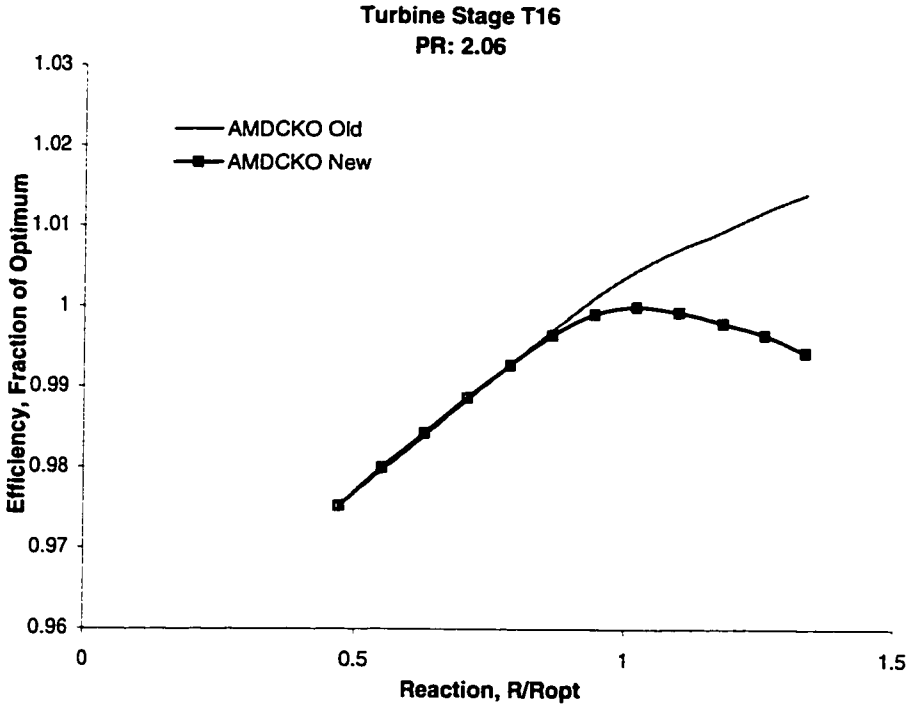

Fig. III.1 Result Curves of Stage Efficiency with Reaction (continued)

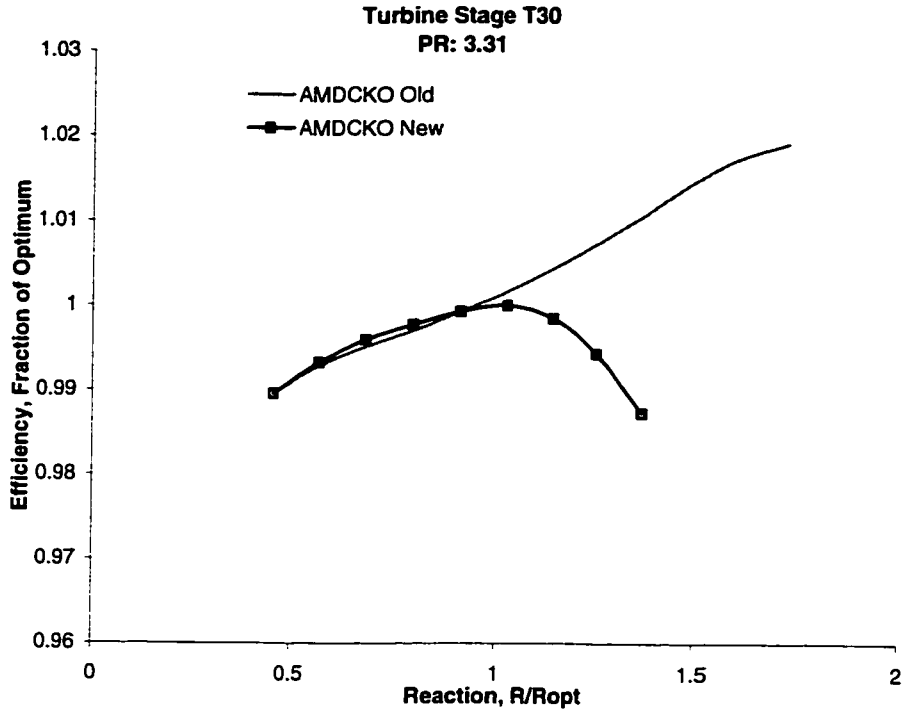

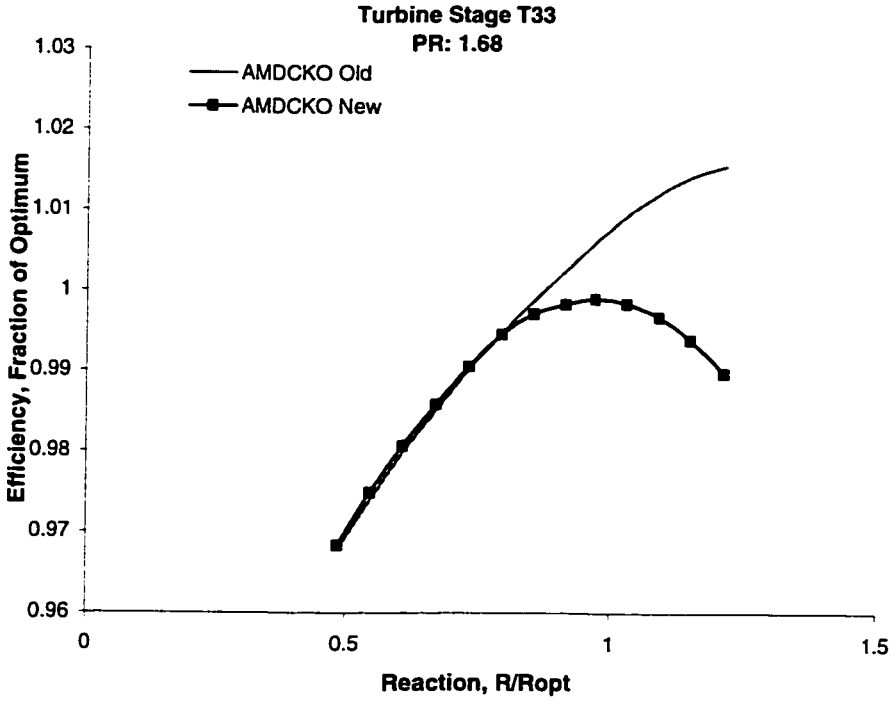

Fig. III.1 Result Curves of Stage Efficiency with Reaction (continued)

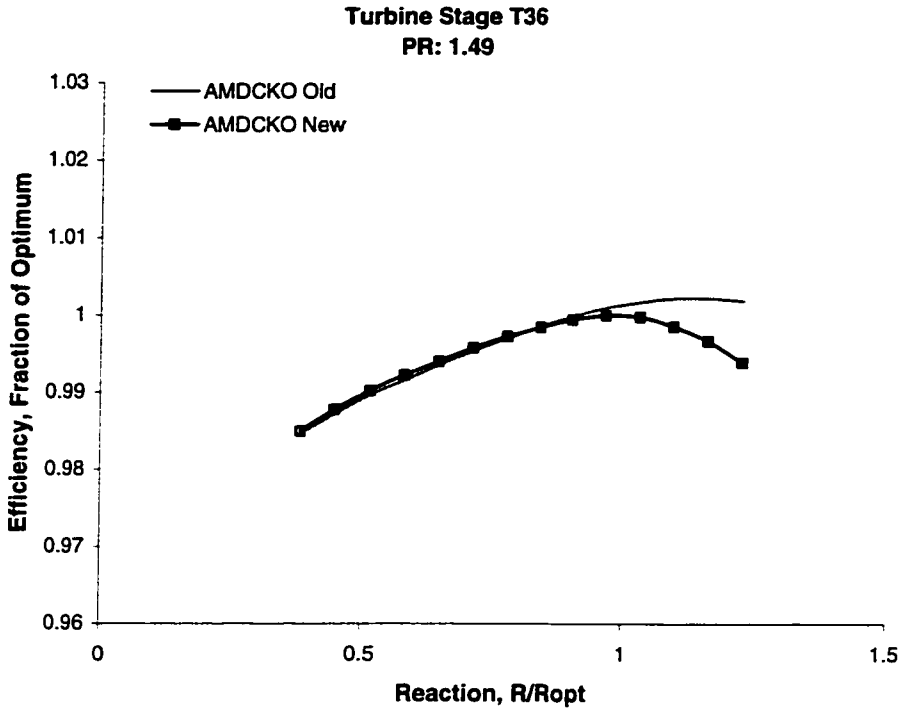

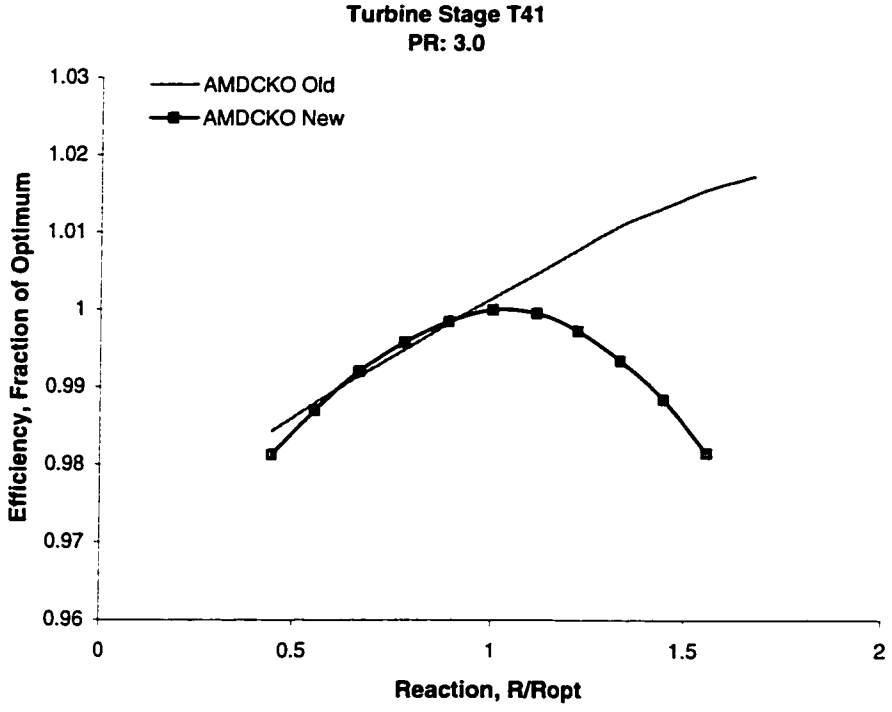

Fig. III.1 Result Curves of Stage Efficiency with Reaction (continued)

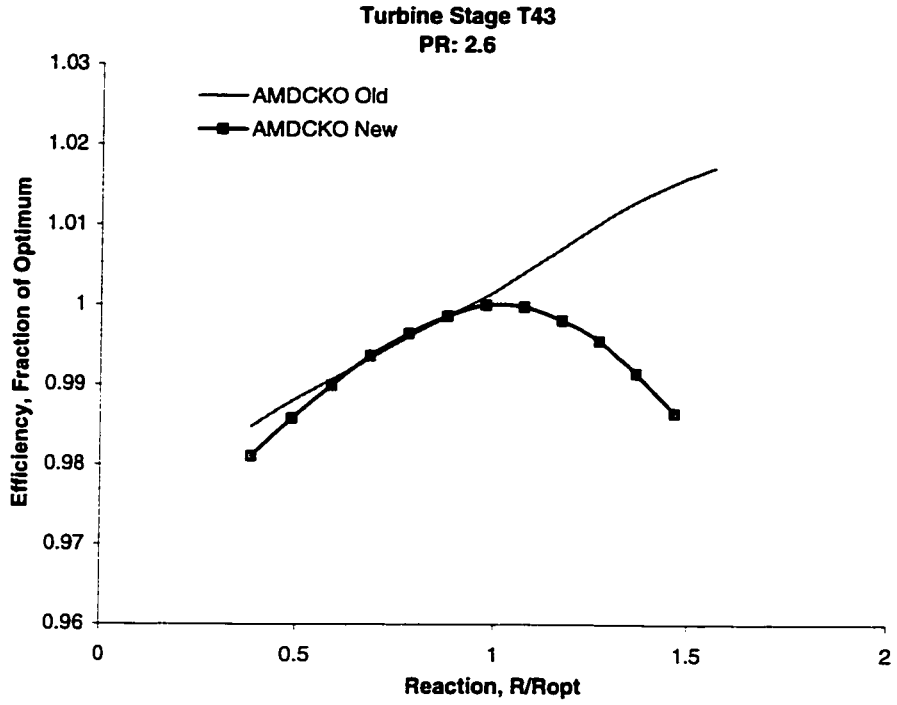

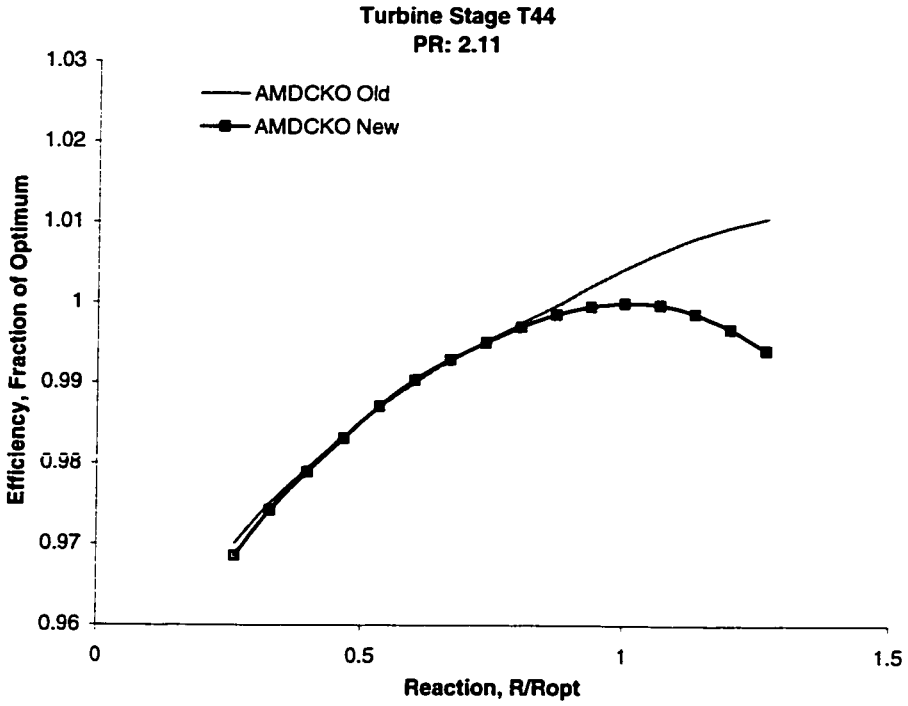

Fig. III.1 Result Curves of Stage Efficiency with Reaction (continued)